

**Modeling High Temperature Heat Pump with Thermal Storage for Process
Integration in Food and Beverage Processing Facilities**

by

Doran Mackowski

A dissertation submitted in partial fulfillment of
the requirements for the degree of

Master of Science

(Mechanical Engineering)

at the

UNIVERSITY OF WISCONSIN-MADISON

2024

Date of final oral examination: August 19, 2024

The thesis is approved by the following members of the Defense Committee:

Allison J. Mahvi, Assistant Professor, Mechanical Engineering

Gregory F. Nellis, Professor, Mechanical Engineering

Douglas T. Reindl, Professor, Mechanical Engineering

© Copyright by Doran Mackowski

ALL RIGHTS RESERVED

Dedication.

ACKNOWLEDGMENTS

TO BE COMPLETED

ABSTRACT

Food processing facilities are energy intensive, requiring both electricity as an energy source to power process equipment and refrigeration systems as well as fossil fuels supplied to boilers for process heating. As end-user food companies search for options to reduce their energy intensity and operating carbon footprint, there is a need to identify viable alternative to traditional fossil fuel fired boilers to supply process heating. This project explores various heat pumps systems, both with and without thermal storage, to heat hot water used for sanitation purposes in an example poultry processing harvest facility. As a harvest facility, its heating needs are modest since there are no cooking processes present or higher temperature heating requirements; thereby, establishing heat requirements that would be favorable to electrification using heat pumps to achieve greater efficiency compared to an electric boiler.

A computer model of both single stage and two stage heat pump configurations utilizing anhydrous ammonia as the working fluid was developed to simulate the heating performance of the various heat pump options and to quantify the power required to meet various loads as well as to compare the energy used and subsequent CO₂ emissions of these heat pump systems. In addition, the energy and operating CO₂ emissions for a gas-fired boiler and electric boilers were quantified for comparative purposes. The operating CO₂ emissions utilized emission factors from the US EPA with the electric region being the upper Midwest (MROW).

The findings show all heat pump models simulated had lower CO₂ emissions than a natural gas fired boiler in the MROW electrical grid subregion where the food processing plant being modeled was located. Break-even electricity emission factors for each heating option were

identified to determine the potential deployment of industrial heat pumping technologies beyond the MROW region. The results from this study support a further technoeconomic analysis to quantify the capital and operating costs associated with the deployment of electrically-driving heat pumps as an alternative to natural gas-fired boilers in industrial food and beverage processing facilities.

TABLE OF CONTENTS

TABLE OF CONTENTS.....	v
LIST OF TABLES	vii
LIST OF FIGURES	viii
LIST OF SYMBOLS AND ABBREVIATIONS	xi
CHAPTER 1: INTRODUCTION	1
1.1 Greenhouse Gas Emissions and Climate Change	1
1.2 Decarbonization Initiatives	4
1.3 Food and Beverage Industry Energy Consumption and Emissions.....	5
1.4 Heat Pumps	8
1.5 Project Objectives	11
CHAPTER 2: MODEL	13
1.1 System models	13
1.2 Component Models.....	20
1.3 Compressor Model.....	21
1.3.2 Refrigeration Capacity	26
1.3.3 Power Consumption.....	29
1.3.4 Compressor Discharge Temperature.....	32
1.4 Condenser	35
CHAPTER 3: Results and Discussion	58
CHAPTER 4: Conclusions and Recommendations for Further Work	70
REFERENCES	76
APPENDIX A.....	79

A.1 Compressor selection software performance data **Error! Bookmark not defined.**

APPENDIX B 88

LIST OF TABLES

Table 1:Geometry and Materials of Condenser	37
Table 2: Parameters for superheated refrigerant heat transfer coefficient correlation in Equation 26.....	46
Table 3: Design Parameters of Heat pump Systems.	60
Table 4: Simulation results.	65
Table 5: Maximum EF for CO2 emissions savings by technology.	69
Table 6: Frick Coolware selection data for SGC 2313 at 55°F evaporation temperature and 160°F condensing temperature.	79
Table 7: Frick Coolware selection data for SGC 2313 at 55°F evaporation temperature and 150°F condensing temperature. [OBJ]	80
Table 8:Frick Coolware selection data for SGC 2313 at 55°F evaporation temperature and 140°F condensing temperature	81
Table 9:Frick Coolware selection data for SGC 2313 at 55°F ammonia evaporation temperature and 130°F ammonia condensing temperature.....	82
Table 10:Frick Cookware selection data for SGC 2313 at 55°F ammonia evaporation temperature and 120°F ammonia condensing temperature. [OBJ].....	83
Table 11:Frick Cookware selection data for SGC 2313 at 55°F ammonia evaporation temperature and 110°F ammonia condensing temperature.....	84
Table 12:Frick Cookware selection data for SGC 2313 at 55°F ammonia evaporation temperature and 100°F ammonia condensing temperature. [OBJ].....	85
Table 13:Frick Cookware selection data for SGC 2313 at 55°F ammonia evaporation temperature and 90°F ammonia condensing temperature.....	86
Table 14:Frick Cookware selection data for SGC 2313 at 55°F ammonia evaporation temperature and 80°F ammonia condensing temperature. [OBJ].....	87
Table 15: Load profile of hot water need at subject plant.	88

LIST OF FIGURES

Figure 1: Difference in mean global surface temperature vs the 1901-2000 average. The red bars indicate above average global mean temperature, the blue bars indicate below average [7].	2
Figure 2: Sea level rise from 1993 through June 2023. The error of ± 4 mm (about 0.16 in) is shown in the shaded region [8].	3
Figure 3: Energy use and carbon footprint of food and beverage processing facilities in the US [22].	6
Figure 4: Separate cooling/refrigeration and heating is current industry standard.	7
Figure 5: Diagram of a basic heat pump with energy flows.	8
Figure 6: Integrated refrigeration/heat pump system of one heat pump without thermal storage.	11
Figure 7: Integrated refrigeration/heat pump system with one heat pump and thermal storage... ..	13
Figure 8: Integrated refrigeration/heat pump system with two heat pumps in series and no thermal storage.	15
Figure 9: Integrated refrigeration/heat pump system with two heat pumps and thermal storage.	16
Figure 10: US EPA eGRID 2022 map showing lbs./MWh of CO ₂ emissions by subregion. Note MROW ¹	17
Figure 11: Oil cooling load curve and Coolware selection data vs slide valve position [%] for a 150°F condenser saturation temperature [24].	24
Figure 12: Oil discharge temperature vs slide valve percentage. Note a similar curve could be made in terms of condenser saturation temperature and PLF.	26
Figure 13: Maximum evaporator capacity vs condenser saturation temperature.	28
Figure 14: FFLP vs PLF for lower-pressure curves and higher-pressure curves. Note the line of ideal unloading where FFLP/PLF=1 [24]	30
Figure 15: Power to the compressor at full load vs condenser saturation temperature.	31
Figure 16: Compressor discharge temperature vs condenser heat rejection at 140°F condenser saturation temperature. Note the slight difference at the extremes of condenser heat rejection [24].	33

Figure 17: Compressor discharge temperature vs condenser heat rejection utilizing the lower-pressure coefficient at 100°F condenser saturation temperature. Note the largest difference is 1.2°F at maximum capacity [24].	34
Figure 18: Basic illustration of a shell and tube heat exchanger. Note the change in shell side fluid direction at the end of baffling spaces [25].	36
Figure 19: Diagram of the sub-heat exchanger model showing fluid flow direction, heat flows, and resistance networks.	38
Figure 20: Resistance network at node j including constituent resistances, node temperatures, and heat transfer through sub-heat exchanger j.	43
Figure 21: Layout of staggered tube bank model showing orientation of pitches.	46
Figure 22: Resistance network at node j including constituent resistances, node temperatures, and heat transfer through sub-heat exchanger j.	49
Figure 23: Plot showing curve fit of the conductivity of water compared to the EES material property function values. Note the two sets align.	51
Figure 24: Plot of water conductivity versus the temperature range of water in these simulations.	53
Figure 25: The conductivity of the tube, as reported by EES material property function, over the range of temperatures experienced by the tube wall in the simulations.	54
Figure 26: Condenser temperature profiles of refrigerant and water for a single heat pump at maximum load, 410 gal/min. Note the pinch at node 7.	56
Figure 27: Condenser temperature profiles of refrigerant and water. Note the inset which shows the pinch at node 7.	56
Figure 28: Volumetric flow rate of the example plant load (water) vs time [hours]. Note the three-hour period of peak or near peak load.	58
Figure 29: Constant rate of change load profile.	59
Figure 30: COP vs volumetric flow rate for a single heap pump with no thermal storage meeting the constant rate of increase load profile. Note the maximum between 290 gpm and 368 gpm.	61
Figure 31: COP of two heat pump system without thermal storage meeting the constant rate of change load profile.	62

Figure 32: COP heating of the single heat pump system and high stage of the two-heat pump system vs volumetric flow rate. Note the similarity.	64
Figure 33: Condenser saturation temperature [F] vs volumetric flow rate. Note the divergence from full load (410gpm) to minimum load (80gpm).	64
Figure 34: Annual CO ₂ emissions [tons] by simulation.....	66
Figure 35: The single heat pump system without thermal storage, COP and volumetric flow rate vs simulation time.	67
.Figure 36: Two heat pump system without storage COP vs time.....	68
Figure 37: COP vs PLF for heat pumps simulation from minimum load to maximum load. Note the rate of change is greater with PLF below 0.5.	71

LIST OF SYMBOLS AND ABBREVIATIONS

A	area [m ²]
AAD	absolute average deviation [%]
Br	Brinkman Number ($\mu u^2/k\Delta T$) [-]
\dot{C}	capacitance rate [W kg K ⁻¹]
c_p	specific heat [J kg ⁻¹ K ⁻¹]
D	diameter [mm]

Greek Symbols

α	void fraction [-]
β	eigenvalue [-]

Subscripts

cs	cross section
exp	expected

TO BE COMPLETED

CHAPTER 1: INTRODUCTION

1.1 Greenhouse Gas Emissions and Climate Change

Thoughtful action ought to be taken to reduce greenhouse gas (GHG) emissions to mitigate the disruptive effects of anthropogenic climate change. According to NASA, “The effects of human-caused global warming are happening now, are irreversible for people alive today, and will worsen as long as humans add greenhouse gases to the atmosphere” [1]. Measures to reduce the emissions of greenhouse gases need to proceed without delay because the magnitude and rate of climate change and its associated risks depend on near-term mitigation [2]. Therefore, an immediate effort must be made to identify areas where reductions in GHG emissions are possible and environmentally prudent.

Scientists overwhelmingly agree that human fossil fuel use is playing a significant role in climate change [3]. According to the American Meteorological Society, “evidence indicates that the leading cause of climate change in the most recent half century is the anthropogenic increase in the concentration of atmospheric greenhouse gases, including carbon dioxide (CO₂), chlorofluorocarbons, methane, tropospheric ozone, and nitrous oxide” [4]. The American Chemical Society’s position statement on global climate change states increasing GHG emissions are changing the Earth’s climate, and that “human activity is the primary cause” [5]. The American Association for the Advancement of Science states that about 97% of climate scientists conclude, based upon well-established evidence, that human driven climate change is occurring. These conclusions are not based upon a single study, rather numerous studies in many

disciplines over several decades and has been publicly expressed by almost every membership organization of experts in climate science [6].

The Earth is warming. 2010-2020 was the hottest decade ever recorded and nine of the ten hottest years on record happened between 2012 and 2022 [5][7]. **Figure 1**, below, shows the difference in mean global temperature between the 1901-2000

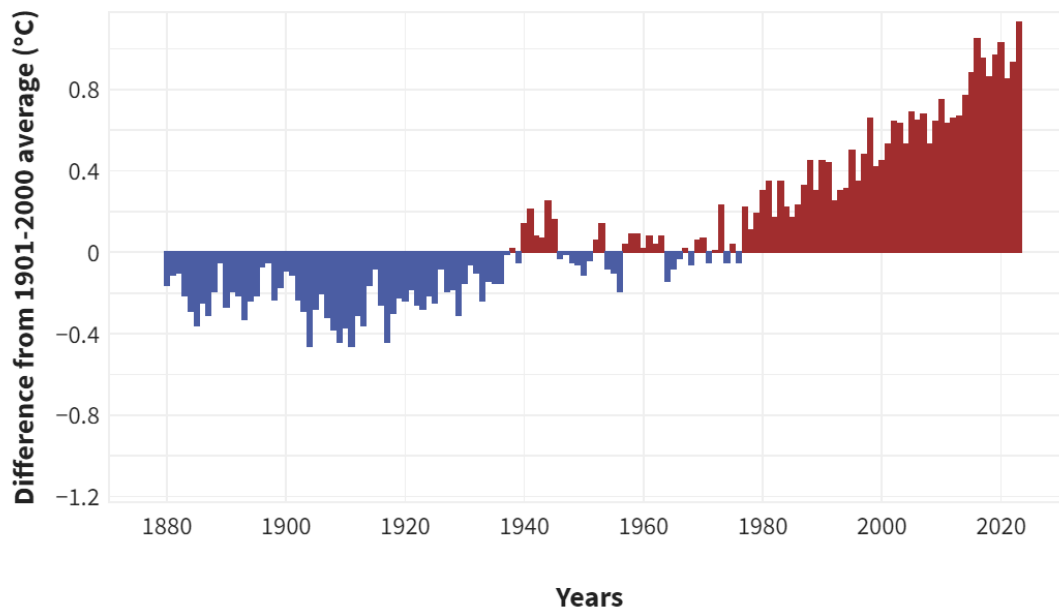


Figure 1: Difference in mean global surface temperature vs the 1901-2000 average. The red bars indicate above average global mean temperature, the blue bars indicate below average [7].

average and the global mean for the years 1880-2020. This illustrates a trend of temperature rise over that time span. Global average surface temperatures have risen an average rate of 0.17°F per decade since 1901, and the rate of temperature rise has increased since the 1970's [5]. The evidence shows Earth warming at an ever-increasing rate.

Global mean sea levels have been rising at an accelerating rate. Seas rose an estimated 4-5 inches from 1900 to 1990 based upon tidal gauge data. From 1990 to 2015 the global mean sea level rose 3 inches, a measurement that agrees with modern satellite altimeters. **Figure 2** shows

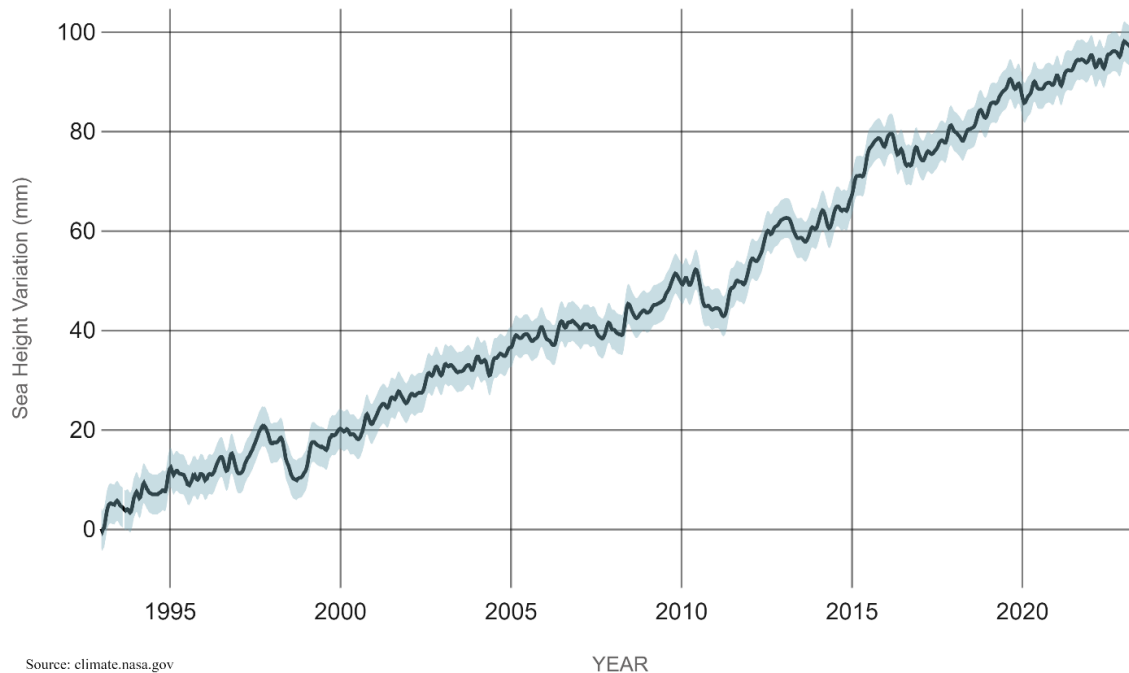


Figure 2: Sea level rise from 1993 through June 2023. The error of ± 4 mm (about 0.16 in) is shown in the shaded region [8].

sea level rise from 1993 through June 2023. NOAA states, “On a pathway with high greenhouse gas emissions and rapid ice sheet collapse, models project that average sea level rise for the contiguous United States could be 2.2 meters (7.2 feet) by 2100 and 3.9 meters (13 feet) by 2150”. This sea level rise is already impacting densely populated coastal regions.

The increase in global temperature has a large economic impact. It has been estimated that “\$143 billion per year of the cost of extreme weather events is attributable to climate change” [2]. The US alone could incur over \$1 trillion (about \$3,100 per person in the US) in

sea level rise and storm surge damages through the year 2100 [9]. It is believed the negative economic impacts of climate change will increase with rising temperatures [10]. Due to the increase in negative economic impact associated with rising temperature, it is important to quickly reduce GHG emissions.

The negative impact of climate change on human well-being is also significant. The World Health Organization estimates, “between 2030 and 2050, climate change is expected to cause approximately 250,000 additional deaths per year from undernutrition, malaria, diarrhea and heat stress alone” [11]. The incidence of malaria is expected to increase because the parasite is more vigorous in warmer climates [10]. Changes in agricultural production are predicted to adversely affect poorer regions of the globe more severely, leading to increased hunger and food insecurity [12]. Avoiding large scale human suffering is a strong motivation to reduce the effects of anthropogenic climate change.

1.2 Decarbonization Initiatives

Decarbonization initiatives are underway in many sectors with the goal of reducing GHG emissions and reducing the effects of climate change. The push for decarbonization comes from mandates with penalties for non-compliance, government investment and subsidies, and/or public pressure on industry to act. The decarbonization drive includes buildings, transportation, and industry, including the food and beverage processing industry. Governmental policies are dependent upon the party/parties in power, but the public desire for action has been steadily increasing [13].

Examples of legislation promoting decarbonization are New York City Local Law 97 (LL97) and the Building Emissions Reduction and Disclosure Act (BERDO) in Boston. In 2019 New York city passed LL97 enacting limits on emissions from buildings over 25,000 square feet (about four times the area of a basketball court). Failure to reduce emissions will result in fines [13]. Similarly, Boston's BERCO requires emissions reductions in large buildings, requiring third party verification of compliance [14]. Although these laws do not specifically target the food and beverage processing industry, they show the motivation for establishing and enforcing emission standards.

In March of 2024, the US Department of Energy announced a \$6 billion investment to decarbonize energy intensive industries including the food and beverage industry funded by the Infrastructure Law and Inflation Reduction Act. The investment funds 33 projects including 3 projects at 16 food and beverage processing sites to demonstrate energy efficiency and electrification of process heat [15]. In September 2022, the U.S. Department of Energy (DOE) announced the "Industrial Efficiency and Decarbonization" funding opportunity [16]. This program funds up to \$104 million-dollar industrial decarbonization projects. With more investment highlighting the ability to efficiently transition to electrification, more decarbonization initiatives are likely to proceed.

1.3 Food and Beverage Industry Energy Consumption and Emissions

The food and beverage industry is an opportunity to meaningfully contribute to decarbonization through technology shifting while simultaneously achieving reductions in energy consumption. Agriculture, food processing, and distribution are responsible for about

30% of global energy consumption [17]. Annually, the US consumes 1,262 TBtu of primary energy for food and beverage processing as of 2018, with the largest share used for process heating, cooling and refrigeration as shown in **Figure 3**. Many food and beverage processing facilities have both large refrigeration loads and heating requirements . A wide range of food

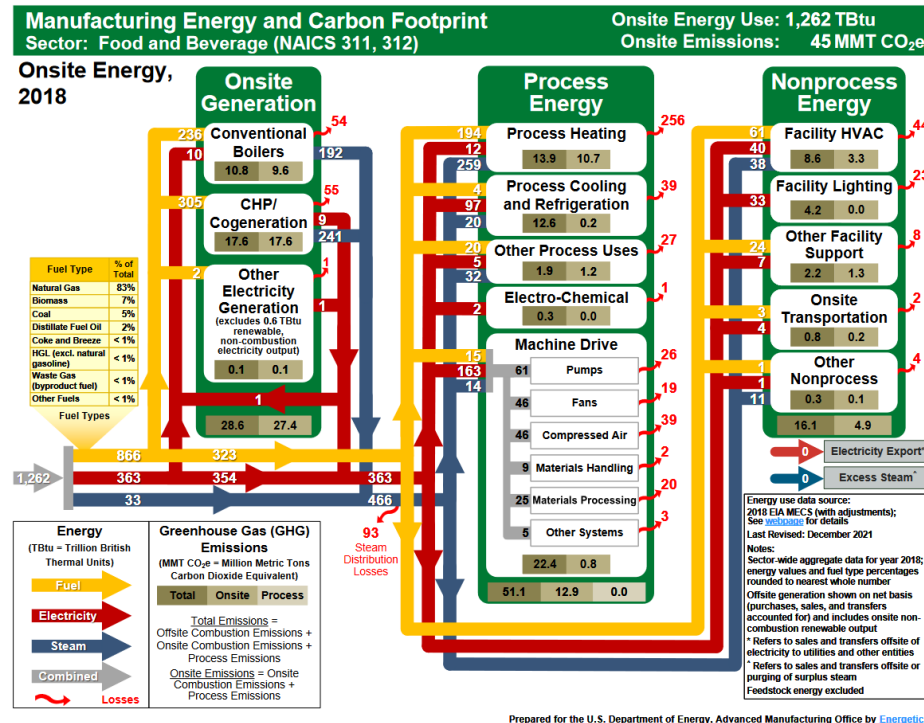


Figure 3: Energy use and carbon footprint of food and beverage processing facilities in the US [22].

processing food processing facilities can reduce their energy intensity by improvements in process integration, through the recovery and use of waste heat, and transitioning from on-site combustion to heat pumping for process heating to reduce site energy consumption and scope 1 & 2 CO₂ emissions, respectively.

Most of the food and beverage processing facilities today have separate, unintegrated, cooling and heating, **Figure 4**. Facilities utilize electricity to power the refrigeration system,

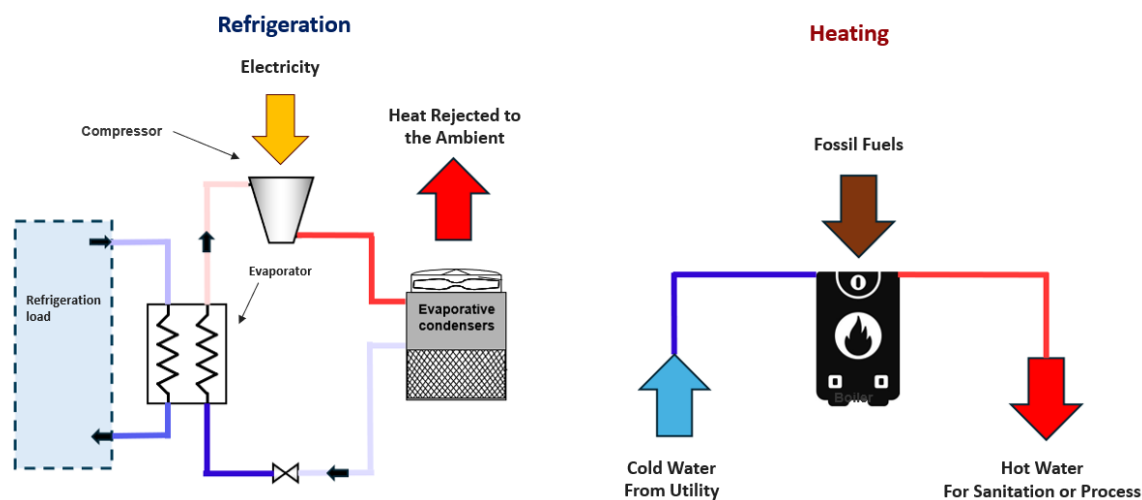


Figure 4: Separate cooling/refrigeration and heating is current industry standard.

which reject the heat to the ambient as a waste stream. The same facility will then have a separate fossil fuel-fired boiler for process heating and sanitation. Although on-site boilers can be powered with electricity to reduce Scope 1 emissions, most boilers utilize fossil fuels [19] as the energy input. These fossil fuel boilers significantly contribute to the 45 million metric tons of CO₂ equivalent released each year as part of the overall emissions from this sector.

Energy savings and reductions in on site emission can be achieved through improved thermal process integration to utilize energy inputs more efficiently and through various decarbonization strategies. One strategy for decarbonization of food processing facilities involves deploying heat pumps that can simultaneously support refrigeration and heating demands of a facility. For example, the Mohrenbrauerei brewery in Austria utilizes a 370-kW heat pump with heat storage to reduce the on-site burning of 1.8 GWh of fossil fuels annually. The Arla Videbæk dairy in Denmark's heat pumping saves the burning of 4.6 GWh of fossil fuels onsite, along with the corresponding 1,400 metric tons of CO₂ per year utilizing waste heat

[19]. The benefits in carbon emissions and energy efficiency are different from facility to facility, therefore understanding the various processes and their required thermal streams is essential followed by detailed transient modeling of the processes and utility systems intended to support the processes is essential.

1.4 Heat Pumps

Heat pumps are a technology that can be used to increase energy efficiency and reduce onsite carbon emissions by replacing fossil fuel boilers for process heat and sanitation. As used in this research, a heat pump is a vapor compression cycle whose primary output of interest is heat as shown in **Figure 5**. Fundamentally different from heat pumps used in other applications.

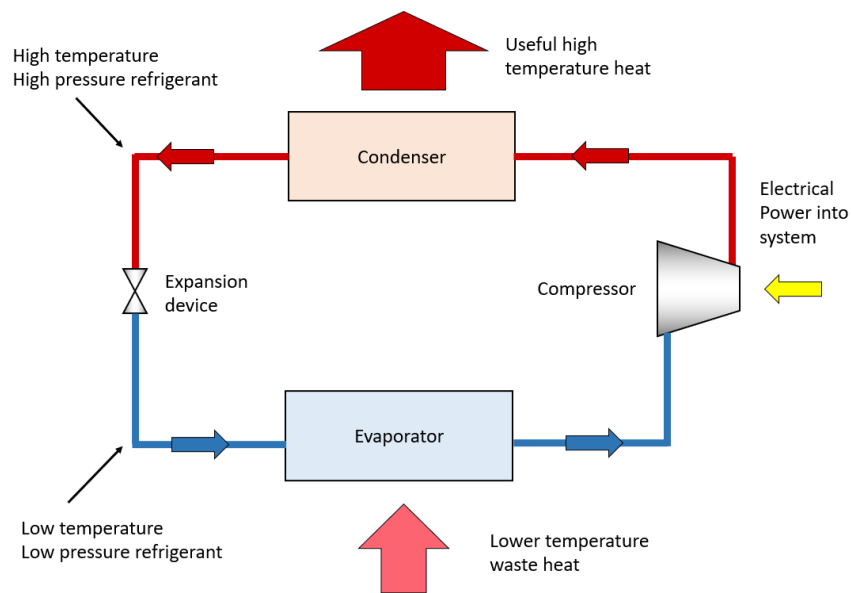


Figure 5: Diagram of a basic heat pump with energy flows.

such as building space conditioning, a heat pump applied to a food processing facility can leverage removal of heat as part of process refrigeration rather than drawing heat from the ambient environment as is the case for heat pumps applied in building space conditioning. Heat pumps require heat addition into the evaporator where cold, low-pressure, two-phase refrigerant in the evaporator experiences an increase in its enthalpy by absorbing heat from a low temperature condition space or a process requiring cooling. The refrigerant leaves the evaporator as a vapor and is lifted to a higher temperature and pressure through the compressor. The energy used by the compressor is added to the refrigerant discharged as a superheated gas. This high pressure, high temperature superheated gas is passed through the condenser where it gives up heat to meet a terminal heating demand and changes phase to a liquid before exiting the condenser. The high-pressure liquid refrigerant leaves the condenser in a saturated or subcooled liquid condition where it is throttled through an isenthalpic expansive device back into the evaporator to continue the cycle.

Heat pumps are a promising technology for decarbonization because they often use many times less energy than a resistance heater to produce the same amount of useful heat. The metric used to describe heat pump performance is the coefficient of performance (COP_H). The COP_H of a heat pump is a dimensionless number defined as the useful heat output divided by the energy consumed, in a consistent set of units, as shown in **Equation 1**. High temperature heat pumps have been recorded with a COP_H up to 8 when the temperature lift is as low as 36°F, but most heat pumps operate with a COP_H between 2 and 5 [19]. Comparing a heat pump to a resistance heater which has a COP_H of 1, it is clear why the technology is being pursued. Heat pumps can outperform resistance heaters in COP_H because they are not simply producing heat, but rather moving heat from a source to a load.

$$COP = \frac{\text{useful heat}}{\text{Power used}}$$

Equation 1

Where:

COP = coefficient of performance [–]

useful heat = heat rejected by condenser $[\frac{kbtu}{hr}]$

Power used = work into system as electricity $[\frac{kbtu}{hr}]$

Heat pumps are ideal for use in food and beverage processing facilities because there are almost always refrigeration loads within the facilities that provide thermal energy input to the heat pump. The heat pump is then able to operate at a suitable temperature to deliver higher temperature thermal energy to meet heating demands. This integration, shown in **Figure 6** can also improve efficiency on the refrigeration side, but those advantages are outside of the scope of this paper. One of the challenges in the application of heat pumps in food processing facilities is matching the time-coincidence of heating and cooling (refrigeration) since the heat pump itself is not configured to store thermal energy. Food and beverage processing facilities are also positioned well for transition to heat pumps because the infrastructure and expertise for running industrial compressors and heat exchangers already exist for the refrigeration. There are currently mature heat pump technologies that can meet applications up to 212°F [19]. There is a need for heat at these temperatures for applications including sanitation.

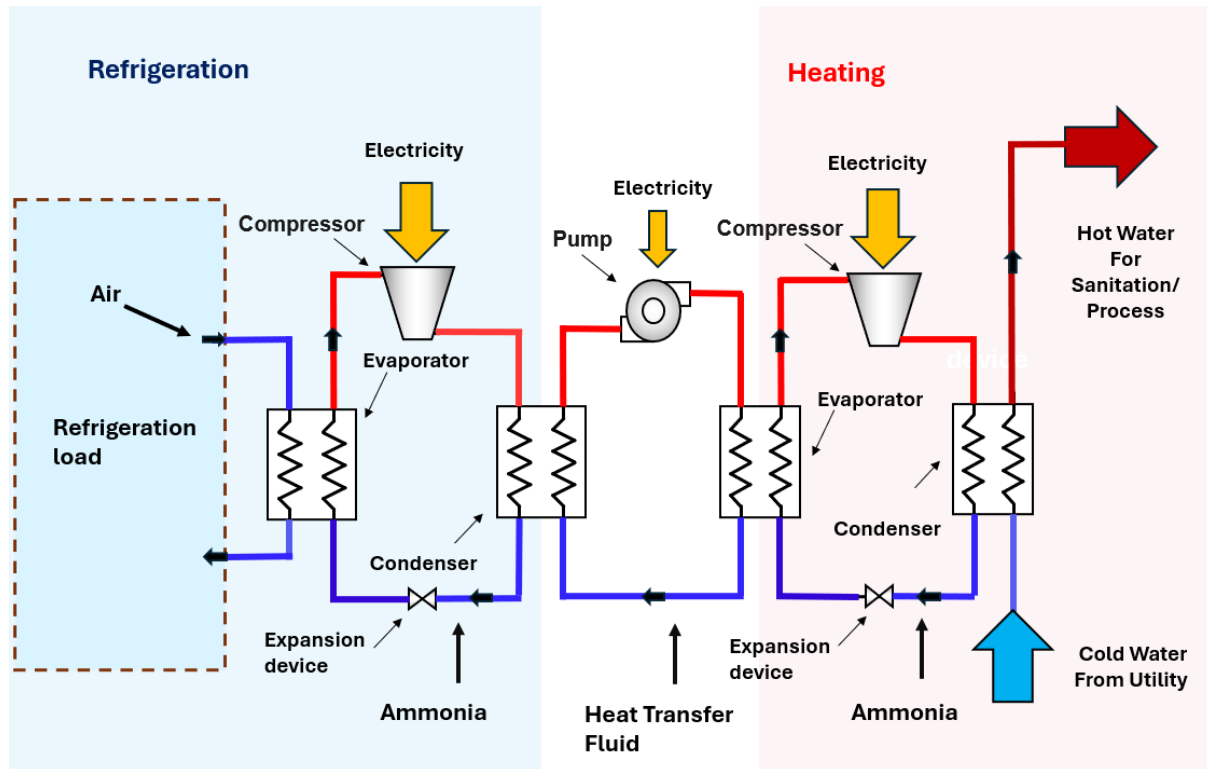


Figure 6: Integrated refrigeration/heat pump system of one heat pump without thermal storage.

1.5 Project Objectives

The objective of this project is to evaluate the feasibility of various high temperature heat pumping system configurations to produce 140°F hot water for sanitation at an industrial poultry processing facility. The feasibility will rely on the development of a detailed model to simulate the heat pump's performance and quantify **the** total energy required to meet the facilities hot water load, the COP_H of the heat pump system, the total carbon emissions of the heat pump systems, as well as how these systems compare to a fossil fuel-fired boiler. The project is only concerned with determining the energy consumption and carbon footprint of the heat pump systems and does not quantify capital or operating economics. The goal is to

determine if any of the heat pump system configurations yield energy savings or reductions in Scope 1 and Scope 2 CO₂ emissions versus the current standard. This project will focus on the heat pump side of the system, as shown in **Figure 7**, neglecting the refrigeration side and the

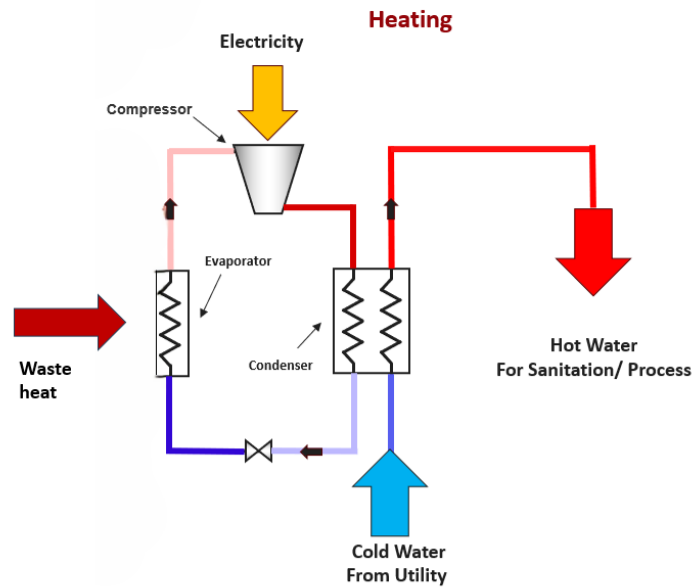


Figure 7: The heat pump side of an integrated system without storage

intermediate loop used to deliver the waste heat to the heat pump's evaporator. The evaporator is assumed to have an ample source of waste heat.

CHAPTER 2: MODEL

1.1 System models

Four heat pump systems were modeled. Systems containing one heat pump, both with and without a thermal storage system, are modeled as previously shown in **Figure 6** and below in **Figure 7**. Thermal storage provides two major benefits, first, it allows for smaller heat

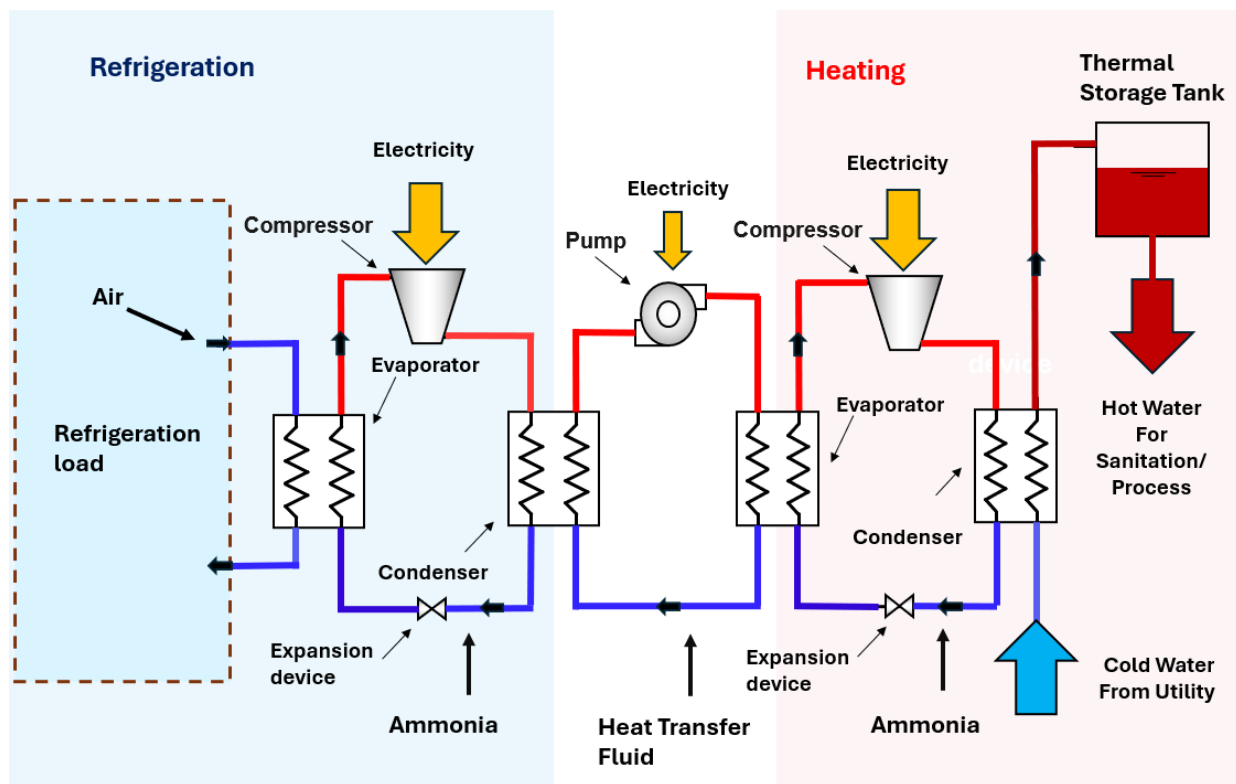


Figure 7: Integrated refrigeration/heat pump system with one heat pump and thermal storage.

pump since it needs to operate and meet an average heating load rather than a peak load. Second, the heat pump can be sized and controlled to operate at a best or near best efficiency point since

the thermal storage system provides a means to supplement the heat pump by discharging when instantaneous heating demands exceed the heat pump's capacity or charge when the heating demand is less. In contrast, a direct heat pump system without storage must be sized to meet the peak heating demand and subsequently operate at lower heating capacity which requires the compressor to unload resulting in lower operating efficiency. Thermal storage can also provide the opportunity to use energy during off-peak hours or when renewable energy is most prevalent. This operating flexibility allows the end-user to leverage both economic and environmental concerns, for example, to support decarb goals. This project will only consider the energy consumption benefits of thermal storage due to running a smaller compressor at full capacity to meet the average load, versus a larger heat pump that must meet both the maximum and minimum load.

Systems with two heat pumps in series both with and without thermal storage systems will also be modeled as seen in **Figure 8** and **Figure 9**. A system comprised of two heat pumps in series can have a higher COP_H due to the lower lift needed for each individual heat pump and maintaining a closer match in refrigerant condensing pressure/temperature to generate the hot fluid stream in two steps rather than a single step. In these simulations, the refrigerant sides of the heat pump are modeled as separate, and only the water passes through both heat pumps. The two heat pumps in series can be optimized by finding the intermediate water temperature, meaning the temperature of the water leaving the first condenser and entering the second, that maximizes the system COP_H .

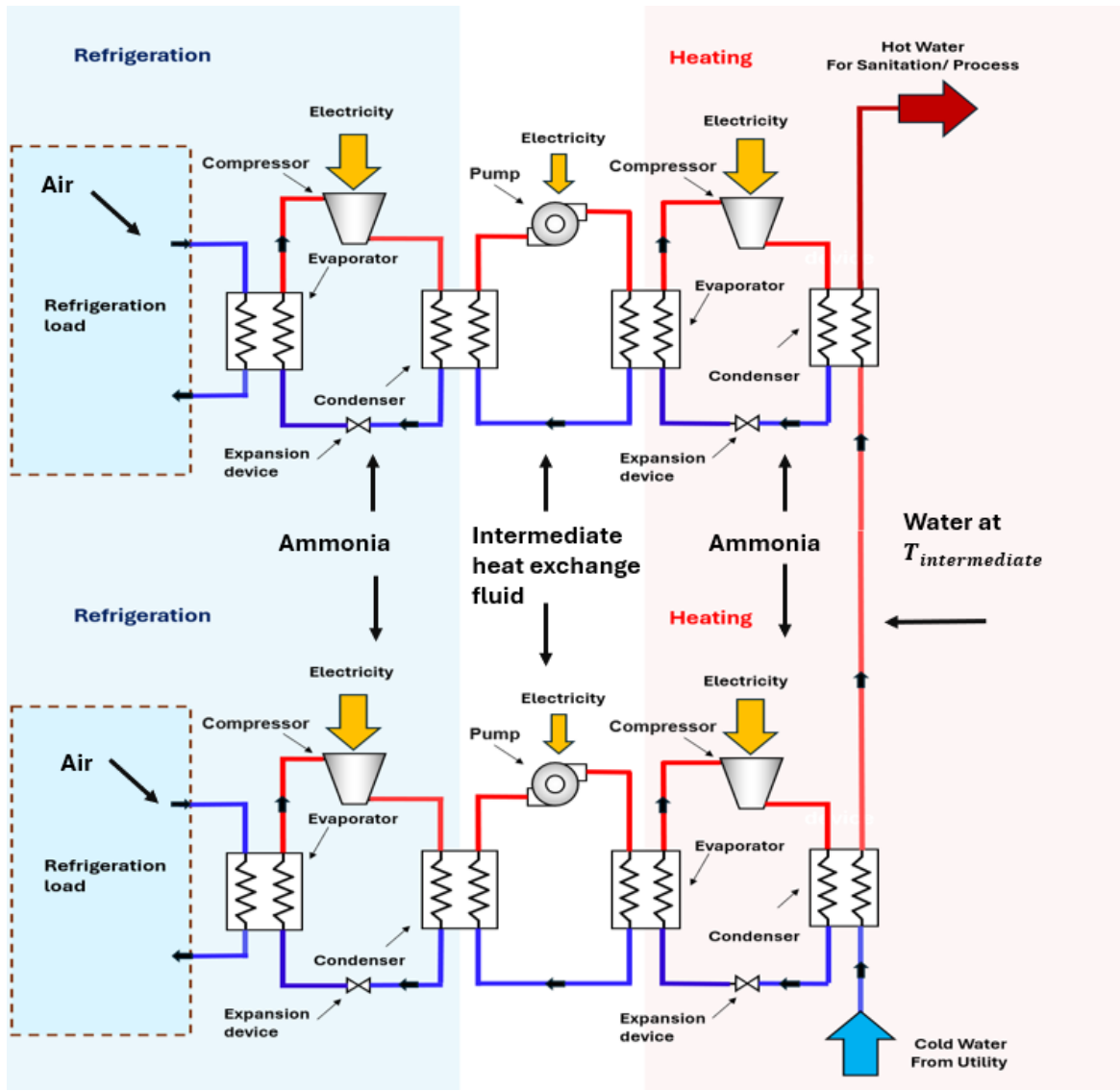


Figure 8: Integrated refrigeration/heat pump system with two heat pumps in series and no thermal storage.

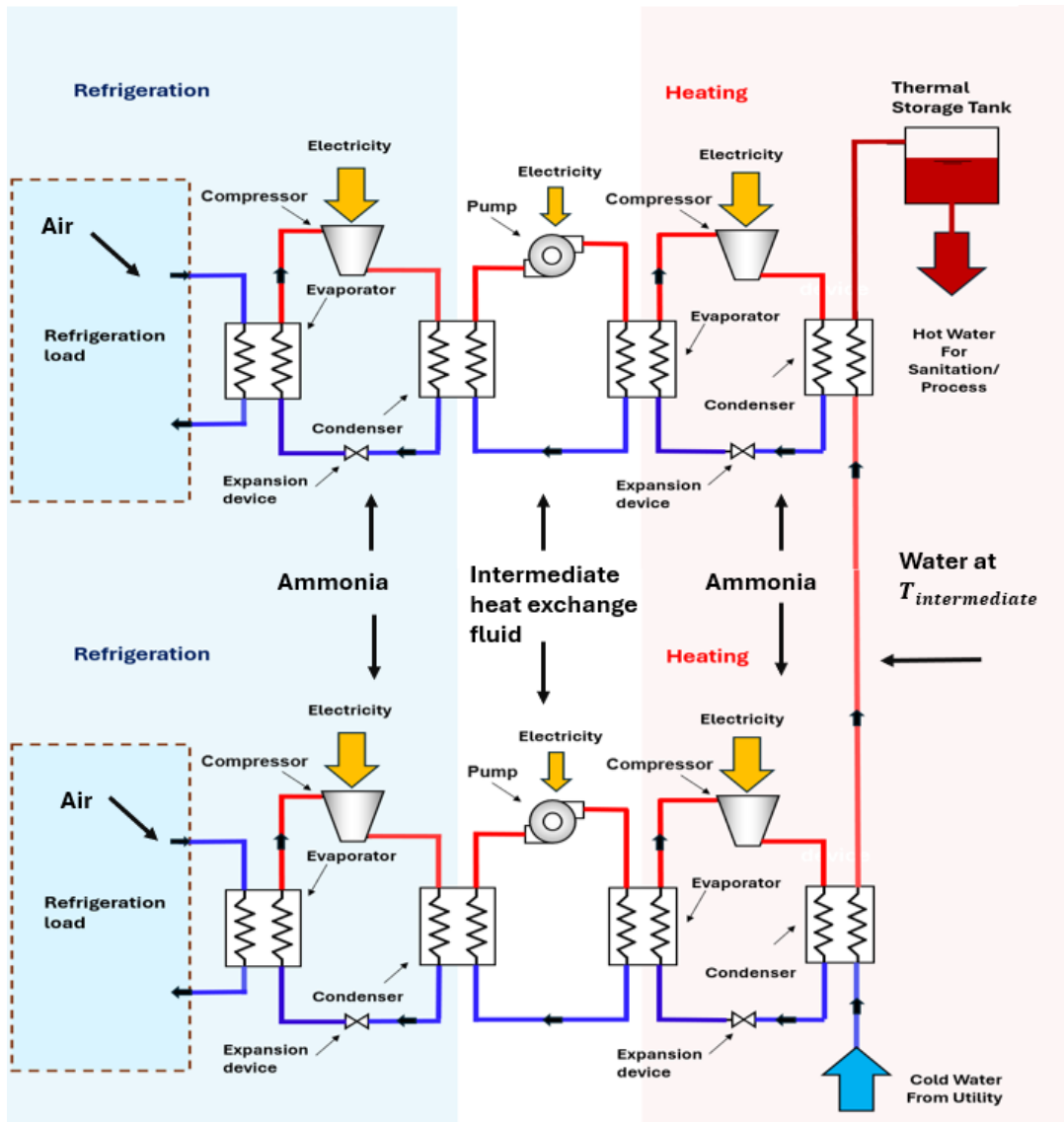


Figure 9: Integrated refrigeration/heat pump system with two heat pumps and thermal storage.

The refrigerant used in these simulations, ammonia, was chosen for several reasons.

Ammonia is an efficient refrigerant with a high latent heat of vaporization, $522.4 \frac{\text{btu}}{\text{lbm}}$ at the 98.12 psi evaporator saturation pressure used in these simulations. Ammonia is used extensively as a

refrigerant in the food and beverage processing industry, therefore the infrastructure and proficiency with ammonia refrigeration already exists in this sector. Ammonia has a Global Warming Potential (GWP) of zero and an ozone depletion potential (ODP) of zero, both are important considerations when choosing a refrigerant with the intention of reducing GHG emissions.

To accurately compare the Scope 2 CO₂ emissions of the heat pump simulations with the Scope 1 emissions of a fossil fuel fired boiler, the emission factor (pounds of CO₂ per megawatt hour of electricity produced) in the proposed geographic location of the heat pump must be known. Electric utility-generated emissions of CO₂ vary geographically based on the primary energy sources as shown in **Figure 10**. The location of interest for this project is in the MROW

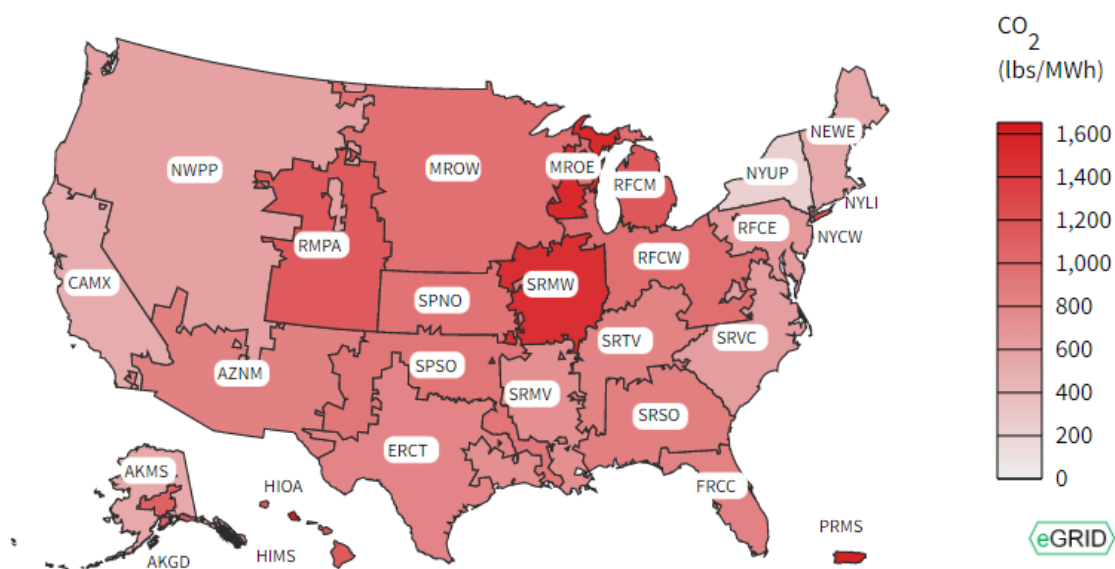


Figure 10: US EPA eGRID 2022 map showing lbs./MWh of CO₂ emissions by subregion. Note MROW¹.

subregion which has emission levels of 936.29 lbs/MWh of electricity produced. The baseline heating plant to generate hot water is a boiler with an assumed combustion efficiency of 0.95 and

operating with natural gas as the fuel. This efficiency is the upper limit of industrial boiler efficiency estimates [21]. Noting these differences in CO₂ per megawatt hour of electricity produced across the US shows how important having a low carbon electrical grid is to the goal of decarbonization through electrification.

To determine the total energy consumption required to meet the facility's needs with a fossil fuel fired boiler, the expected daily sanitation water needs of the plant were simulated and summarized in **Table 12** in Appendix B. The hot water load profile quantifies the plant's water flow rate requirement (in gallons per minute) at 10-minute increments over a 24-hour daily period. The total flow mass flow rate of water for each 10-minute increment can then be calculated using the density found in material property functions. The total energy required can be found using **Equation 2** and **Equation 3**. The ground water to be heated enters the heat pump at a constant temperature of 55°F and is set to exit the heat pump at 140°F. The enthalpies are found using material property functions. Using an emission factor of natural gas of 1.1665×10^{-4} pounds of CO₂ per Btu [22] and **Equation 4**, the total CO₂ emissions using a natural gas boiler, $Emmissions_{total,CO_2,gas}$ boiler, $Emmissions_{total,CO_2,gas}$ can be found. The total CO₂ emissions generated by using a boiler burning natural gas onsite can then be compared to the Class 2 emissions associated with the heat pump options meeting the same aggregate quantity of hot water supplied to the plant.

$$Q_{increment} = m_{water,increment} \cdot (i_{water,set} - i_{water,utility}) \quad \text{Equation 2}$$

Where:

$Q_{increment}$ = Total energy transfered to water in time increment [kBtu]

$m_{water,increment}$ = Total mass flow of water [lbm]

$i_{water,utility}$ = Enthalpy of cold utility water entering condenser $[\frac{kBtu}{lbm}]$

$i_{water,set}$ = Enthalpy of water exiting condenser $[\frac{kBtu}{lbm}]$

$$Q_{total} = \sum_{n=1}^{144} Q_{increment}$$

Equation 3

Where:

Q_{Total} = Total energy transfered to water in 24 hours [kBtu]

$$Emmissions_{total,CO_2,gas} = \frac{Q_{total}}{\eta_{boiler}} \cdot EF_{ng}$$

Equation 4

Where:

$Emmissions_{total,CO_2,gas}$ = Total CO2 emission with natural gas boiler [lbm]

η_{boiler} = Boiler efficiency [–]

EF_{ng} = Emission factor natural gas $[\frac{lbm}{Btu}]$

The simulations were run using TRNSYS: Transient System Simulation Tool [23]. Heat pump models are developed in Fortran to create components for TRNSYS project simulations. TRNSYS reads the load profile data and determines operation of the heat pump for each time step. Since the hot water load profile data is provided in ten-minute increments, the TRNSYS time steps are likewise set to 10 minutes. Material properties are obtained using TRNSYS and EES property functions.

1.2 Component Models

A computer model was developed to simulate and quantify the performance of the various heat pump systems options introduced above in Section 2.1, with or without storage, for heating 55°F utility water to 140°F hot water for plant sanitation that occurs over a limited period of time each day. This required the creation of an overall system model comprised of compressor model sufficiently detailed to determine operating conditions at various loads, and a condenser model sufficient to determine the appropriate condensing pressure for each load condition to produce the desired leaving water temperature. The evaporator is simply modeled as a black box with a 55°F evaporating temperature, as this production plant being used as the focal point for this research has constant refrigeration loads well in excess of the heat that can be absorbed into the heat pump's evaporator (waste heat). The expansion valve is modeled as isenthalpic. Thermal storage is assumed ideal with no losses, it is sized to ensure it can accumulate a sufficient volume of hot water so the heat pump can operate with an average load of 180.4 gallons per minute over 24 hours instead of the having to operate the heat pump to meet the instantaneous hot water demands as they occur. The modeling of the compressor and condenser is explored in further detail in this chapter.

The model's purpose is to simulate the operation of the heat pump. The main values of interest include COP_H , the COP_H of the heat pump system seen in **Equation 5** which is a function of both \dot{W}_{comp} , the power into the compressor, and $\dot{q}_{required}$, the total heat rejected from the refrigerant to the water in the condenser, are discussed in detail in section 2.4.

Calculating the power required to run the compressor is discussed in section 2.3.3. Other values of interest include total heat transferred from the refrigerant to the water, the total power consumed by the compressor, the maximum heat transfer rate, and the maximum power consumption.

$$COP_{hp} = \frac{\dot{q}_{required}}{\dot{W}_{comp}} \quad \text{Equation 5}$$

Where:

COP_H = Coefficient of performance heat pump system [–]

$\dot{q}_{required}$ = Heat transfer rate from refrigerant to water required to meet load $[\frac{\text{Btu}}{\text{hr}}]$

\dot{W}_{comp} = Power consumed by the compressor $[\frac{\text{Btu}}{\text{hr}}]$

1.3 Compressor Model

A compressor model is required to determine power consumption, compressor discharge temperature, refrigeration capacity, maximum condenser heat rejection as well as the oil cooling load and oil discharge temperature over a range of loads as a function of the machine's operating suction pressure and discharge pressure. The compressor model is based on performance data from Coolware, the compressor selection software from Frick [24]. The SGC 2313 screw compressor was chosen, and performance data was taken at nine condensing temperatures, at 10°F intervals from 80°F to 160°F. There was data from 21 slide valve positions, that range from

100% slide valve to 0% slide valve at 5% intervals per condensing temperature as can be seen in Table 3 through Table 11 in Appendix A. The slide valve is the control which loads or unloads the compressor, 100% corresponding to full capacity (load) and 0% corresponding to the compressor's minimum operating capacity. Linear regression was used to find coefficients for performance curves of a range of suction and discharge conditions.

A scaling factor, SF, was introduced to appropriately size the compressor to meet the design heating load for the system configuration being considered. The assumption being that the performance curves are of similar shape within the SF range used in the simulations of 0.33 to 2.1. The appropriate SF is found by adjusting its value until the partial load ratio (PLR), discussed in section 2.3.2 approaches 1 at design condition. The scaling factor determined for each system option is then applied to the curve fits for evaporation capacity, condenser heat rejection, and power consumed by the compressor for all other operating conditions applicable to the system option being simulated.

1.3.1 Oil Cooling Load

Linear regression was used to obtain coefficients for an oil cooling load curve, **Equation 6**, which is shown graphically in **Figure 11**. The plot shows the oil cooling load curve at 150°F condenser saturation temperature. The oil cooling load curve was found as a function of slide valve percentage and $T_{sat,condenser}$ early in the project, but could be recalculated as a function of $T_{sat,condenser}$ and PLR and be applied to this or future models. The simulations for this project

assume the oil cooling load is rejected as waste heat to the ambient. The plot shows that the oil cooling load can be significant.

$$\begin{aligned} \dot{q}_{oil,cooling} = & a_{oil,cool} + b_{oil,cool} \cdot SV + c_{oil,cool} \cdot SV^2 \\ & + d_{oil,cool} \cdot T_{sat,condenser} + e_{oil,cool} \cdot T_{sat,condenser}^2 \\ & + f_{oil,cool} \cdot SV \cdot T_{sat,condenser} \end{aligned} \quad \text{Equation 6}$$

Where:

$$\dot{q}_{oil,cooling} = \text{Rate of heat transfer from compressor to oil} \left[\frac{kBtu}{hr} \right]$$

$$SV = \text{Slide valve position [\%]}$$

$$a_{oil,cool} = 707.96 \left[\frac{kBtu}{hr} \right]$$

$$b_{oil,cool} = -13.76 \left[\frac{kBtu}{hr} \right]$$

$$c_{oil,cool} = 0.013 \left[\frac{kBtu}{hr} \right]$$

$$d_{oil,cool} = -13.84 \left[\frac{kBtu}{hr \cdot F} \right]$$

$$e_{oil,cool} = 0.096 \left[\frac{kBtu}{hr \cdot F^2} \right]$$

$$f_{oil,cool} = \text{Condenser saturation temperature [F]}$$

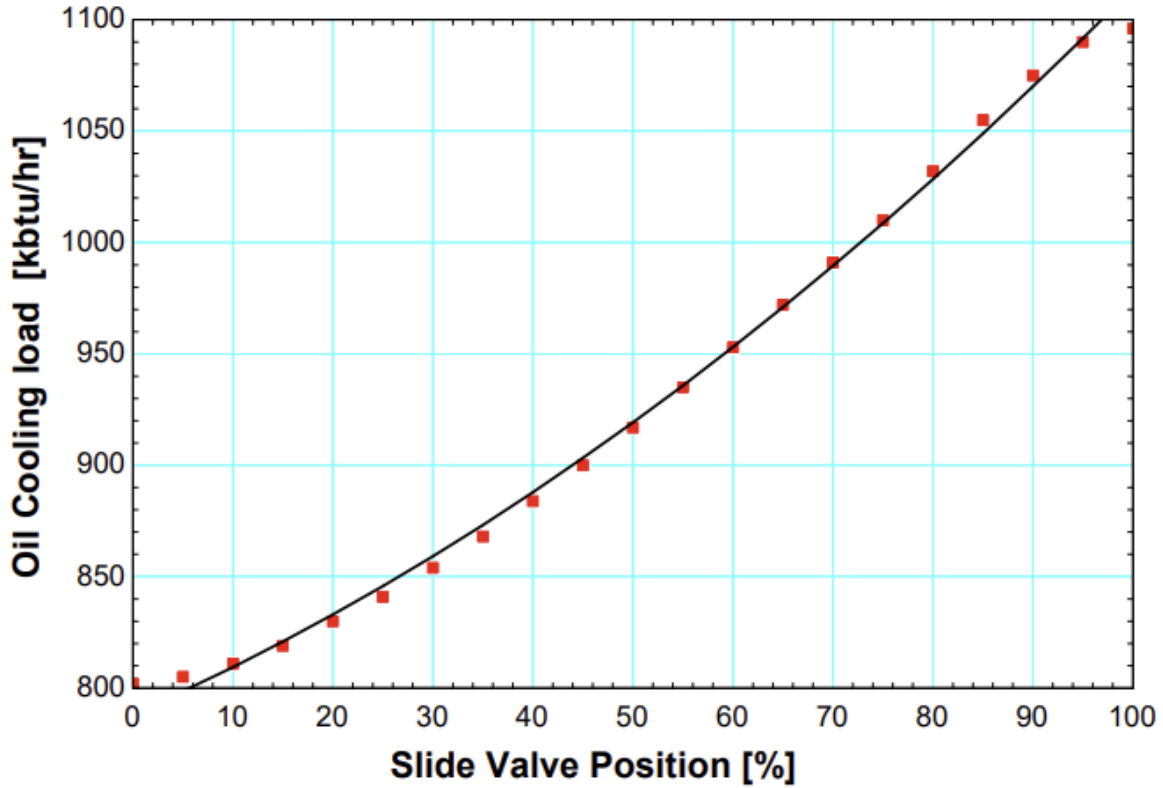


Figure 11: Oil cooling load curve and Coolware selection data vs slide valve position [%] for a 150°F condenser saturation temperature [24].

An equation of the oil flow rate as a function of slide valve position and condenser saturation temperature with coefficients found through linear regression was made **Equation 7**. This equation could also be cast in terms of $T_{sat,condenser}$ and PLR and be applied to future models. The material properties of the oil are available from Frick on the Coolware application [24]. The oil density, ρ_{oil} , was modeled as a constant of $8.4 \left[\frac{lbm}{gal} \right]$ as it varies from $8.2 \left[\frac{lbm}{gal} \right]$ to $8.6 \left[\frac{lbm}{gal} \right]$ over the temperature range of interest. The density can be used with \dot{V}_{oil} to find the mass flow rate of oil \dot{m}_{oil} . The oil specific heat, c_{oil} was likewise modeled as a constant of $0.49 \left[\frac{Btu}{lbm \cdot F} \right]$ and varies from $0.47 \left[\frac{Btu}{lbm \cdot F} \right]$ to $0.47 \left[\frac{Btu}{lbm \cdot F} \right]$. Having the oil cooling load, mass flow

rate, density and specific heat, and the oil return temperature, $T_{oil,return}$, which is found in Coolware, the oil discharge temperature $T_{oil,dis}$ can be found **Equation 8**, plotted in **Figure 12**. Viewing **Figure 11** and **Figure 12** a sizable amount of energy exists in the oil cooling load and exists at a high enough temperature to do useful heating can be seen.

$$\begin{aligned}\dot{V}_{oil} = & a_{oil,flow} + b_{oil,flow} \cdot SV + c_{oil,flow} \cdot SV^2 \\ & + d_{oil,flow} \cdot T_{sat,condenser} + e_{oil,flow} \cdot T_{sat,condenser}^2 \\ & + f_{oil,flow} \cdot SV \cdot T_{sat,condenser}\end{aligned}\tag{Equation 7}$$

Where:

$$\begin{aligned}\dot{V}_{oil} = & \left[\frac{gal}{min}\right] \\ a_{oil,flow} = & -20.3 \left[\frac{gal}{min}\right] \\ b_{oil,cool} = & 0.048 \left[\frac{gal}{min}\right] \\ c_{oil,cool} = & -8.61 \times 10^{-4} \left[\frac{gal}{min}\right] \\ d_{oil,cool} = & 0.44 \left[\frac{gal}{min \cdot F}\right] \\ e_{oil,cool} = & 1.02 \times 10^{-3} \left[\frac{kBtu}{min \cdot F^2}\right] \\ e_{foil,flow} = & 1.42 \times 10^{-3} \left[\frac{gal}{min \cdot F}\right]\end{aligned}$$

$$T_{oil,dis} = \frac{\dot{q}_{oil,cooling}}{\dot{m}_{oil} \cdot c_{oil}} + T_{oil,return}\tag{Equation 8}$$

Where:

$T_{oil,dis}$ = Compressor discharge temperature of oil [F]

\dot{m}_{oil} = Mass flow rate of oil $[\frac{lbm}{min}]$

c_{oil} = 0.048 Specific heat of oil $[\frac{Btu}{lbm \cdot F}]$

$T_{oil,return}$ = Oil return temperature 130°F [F]

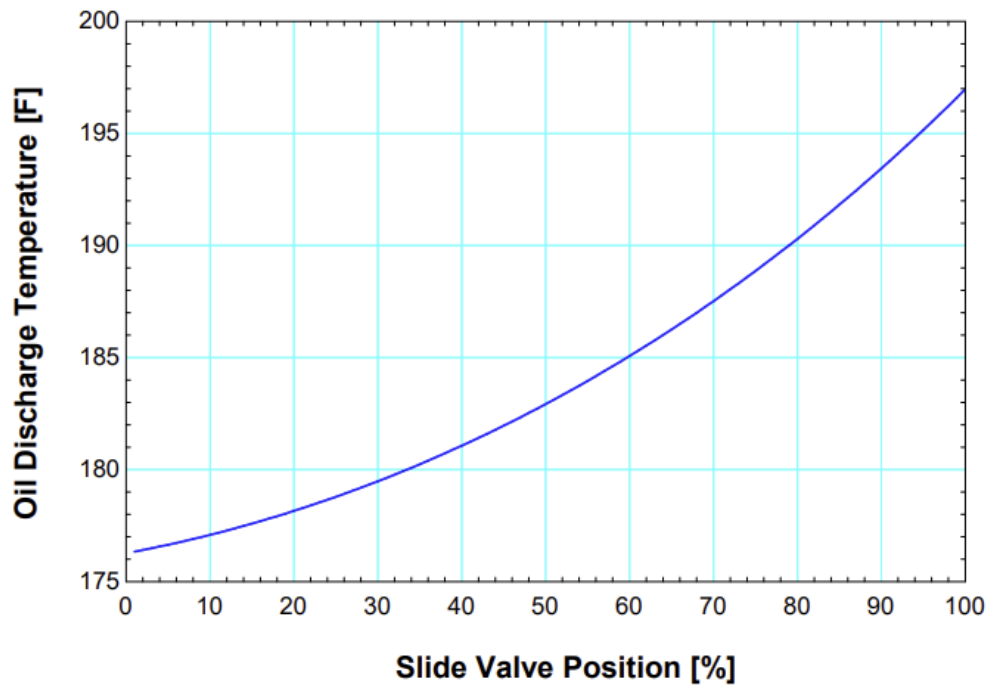


Figure 12: Oil discharge temperature vs slide valve percentage. Note a similar curve could be made in terms of condenser saturation temperature and PLF.

1.3.2 Refrigeration Capacity

The maximum refrigeration capacity at each condenser saturation temperature was used to find the Part Load Ratio (PLR) that corresponds to the hot water load at any given time. The

refrigeration capacity was used, even though condenser heat rejection is the main interest with heat pumping because manufacturers cast PLR in terms of evaporator capacity. As such, Coolware has the evaporator capacity percentage as an output of the selection software. Linear regression was used to determine the coefficients of **Equation 9**. The coefficients are based on the evaporator refrigeration capacity at full load over the 9 condensing saturation temperatures in **Table 6** through **Table 14** in Appendix A. A plot of $\dot{q}_{evap,max}$ vs $T_{sat,condenser}$, **Figure 13**, shows a close fit between the curve and the compressor selection data with an R^2 value of 99.94. The maximum evaporator capacity allows for the calculation of the PLF, **Equation 10** at each slide valve position recorded in the selection data tables. The PLF will be used to determine the power into the compressor as discussed in chapter 2.3.3.

$$\dot{q}_{evap,max} = SF \cdot (a_{evap,max} + b_{evap,max} \cdot T_{sat,condenser} + c_{evap,max,dis} \cdot T_{sat,condenser}^2) \quad \text{Equation 9}$$

Where:

$$\dot{q}_{evap,max} = \text{Maximum refrigeration capacity} \left[\frac{\text{kBtu}}{\text{hr}} \right]$$

$$SF = \text{Scaling factor} [-]$$

$$T_{sat,condenser} = \text{Condenser Saturation Temperature [F]}$$

$$a_{evap,max} = 1.0996 \times 10^4 \left[\frac{\text{kBtu}}{\text{hr}} \right]$$

$$b_{evap,max} = -5.5244 \left[\frac{\text{kBtu}}{\text{hr} \cdot \text{F}} \right]$$

$$c_{evap,max} = -1.1867 \times 10^1 \left[\frac{\text{kBtu}}{\text{hr} \cdot \text{F}^2} \right]$$

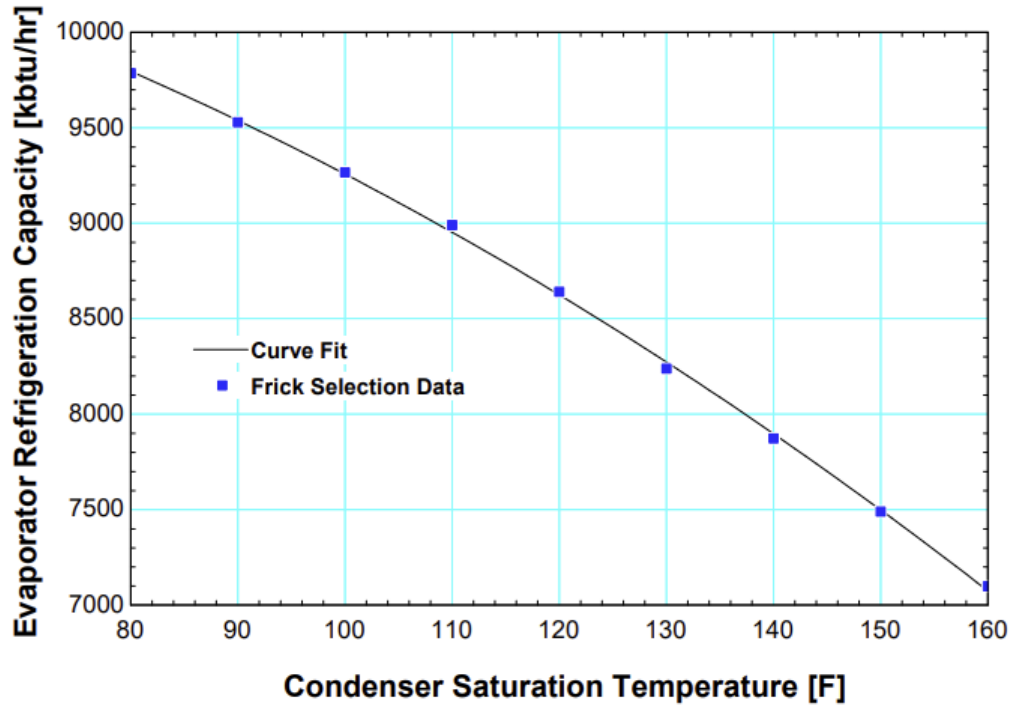


Figure 13: Maximum evaporator capacity vs condenser saturation temperature.

$$PLF = \frac{\dot{q}_{evap}}{\dot{q}_{evap,max}} \quad \text{Equation 10}$$

Where:

$$\dot{q}_{evap} = \text{Evaporator refrigeration capacity} \left[\frac{\text{kBtu}}{\text{hr}} \right]$$

$$\dot{q}_{evap,max} = \text{Maximum evaporator capacity at } T_{\text{sat,condenser}} \left[\frac{\text{Btu}}{\text{hr}} \right]$$

The enthalpy and mass flow rate of the refrigerant entering and exiting the evaporator is used to determine \dot{q}_{evap} , **Equation 11**. The mass flow rate of refrigerant, $\dot{m}_{\text{refrigerant}}$, is determined as described in section 2.4. The enthalpy of refrigerant leaving the evaporator, $i_{\text{ref,evap,out}}$, is found through property functions at the evaporator saturation temperature,

$T_{sat,evap}$ and a quality = 1. The enthalpy of refrigerant entering the evaporator, $i_{ref,evap,in}$ is equal to $i_{ref,out}$, the enthalpy of the refrigerant leaving the condenser, due to the isenthalpic expansion process, and can be found through property functions at $T_{sat,condenser}$ and a quality = 0.

$$\dot{q}_{evap} = \dot{m}_{refrigerant} \cdot (i_{ref,evap,out} - i_{ref,evap,in}) \quad \text{Equation 11}$$

Where:

$$i_{ref,evap,out} = \text{Enthalpy of refrigerant exiting the evaporator} \left[\frac{\text{kBtu}}{\text{lbm}} \right]$$

$$i_{ref,evap,in} = \text{Enthalpy of refrigerant entering the evaporator} \left[\frac{\text{kBtu}}{\text{lbm}} \right]$$

$$\dot{m}_{refrigerant} = \text{Mass flow rate of refrigerant} \left[\frac{\text{lbm}}{\text{hr}} \right]$$

1.3.3 Power Consumption

The heat pump compressor electrical power demand is a key value of interest. It is determined by the Fraction of Full Load Power (FFLP) vs PLR curves as shown in **Figure 14**. The FFLP is the power into the compressor at the current load divided by the power into the compressor at full load at the same condensing and evaporating temperatures. The plot shows the screw compressor's efficiency is highest at full load, and lowest at the minimum load. The unloading is more efficient in the lower-pressure curve than the higher-pressure curve. The curves were calculated using **Equation 12**. The FFLP was used in **Equation 13** to find \dot{W}_{comp} ,

the power into the compressor. The maximum power into the compressor $\dot{W}_{comp,max}$ is calculated in **Equation 14**, from coefficients found using linear regression, **Figure 15**.

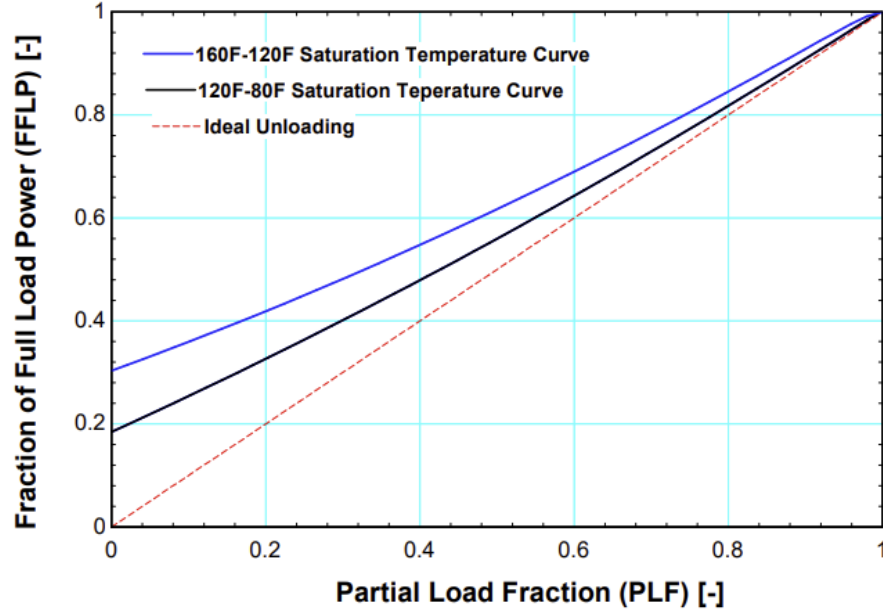


Figure 14: FFLP vs PLF for lower-pressure curves and higher-pressure curves. Note the line of ideal unloading where $FFLP/PLF=1$ [24]

$$FLFP = a_{FFLP} + b_{FFLP} \cdot PLF + c_{FFLP} \cdot PLF^2$$

Equation 12

Where:

$FFLP$ = Fraction of Full Load Power [-]

a_{FFLP} = Higherpressure: 0.3034 [-], Lower – pressure: 0.1846 [-]

b_{FFLP} = Higherpressure: 0.5439 [-], Lower – pressure: 0.6814 [-]

c_{FFLP} = Higherpressure: 0.1670 [-], Lower – pressure: 0.1375 [-]

$$\dot{W}_{comp} = \dot{W}_{comp,max} \cdot FFLP$$

Equation 13

Where:

$$\dot{W}_{comp,max} = \text{Power into compressor at maximum load at } T_{sat,condenser} \left[\frac{kbtu}{hr} \right]$$

$$\dot{W}_{comp,max} = a_{pow,max} + b_{pow,max} \cdot T_{sat,condenser} + c_{pow,max} \cdot T_{sat,condenser}^2 \quad \text{Equation 14}$$

Where:

$$a_{pow,max} = -3.3828 \times 10^2 \left[\frac{kbtu}{hr} \right]$$

$$b_{pow,max} = 7.6349 \left[\frac{kbtu}{hr \cdot F} \right]$$

$$c_{pow,max} = 6.7114 \times 10^2 \left[\frac{kbtu}{hr \cdot F^2} \right]$$

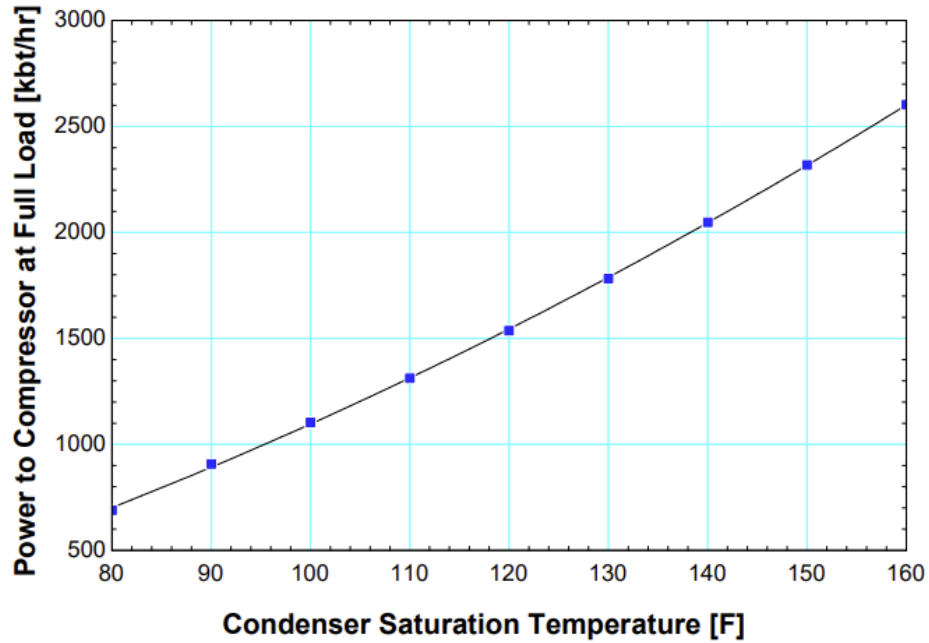


Figure 15: Power to the compressor at full load vs condenser saturation temperature.

1.3.4 Compressor Discharge Temperature

The screw compressor's discharge temperature, $T_{ref,comp,dis}$, will vary based on its operating suction pressure, discharge pressure, and slide valve position. The compressor's discharge temperature was required to find the enthalpy of refrigerant entering the condenser. Linear regression was used to obtain **Equation 15** that can predict $T_{ref,comp,dis}$ as a function of $\dot{q}_{required}$ and $T_{sat,condenser}$. Two sets of coefficients were obtained, one for the higher-pressure heat pumps with condenser saturation temperatures of 150°F to 120°F and one for the lower-pressure heat pumps with condenser saturation temperatures of 120°F to 80°F. The higher-pressure curve and lower-pressure curve are plotted vs the selection data in **Figure 16** and **Figure 17** respectively.

$$\begin{aligned}
 T_{ref,comp,dis} = & a_{comp,dis} + b_{comp,dis} \cdot \dot{q}_{required} + c_{comp,dis} \cdot \dot{q}_{required}^2 \\
 & + d_{comp,dis} \cdot T_{sat,condenser} + e_{comp,dis} \cdot T_{sat,condenser}^2 \\
 & + f_{comp,dis} \cdot \dot{q}_{required} \cdot T_{sat,condenser}
 \end{aligned}
 \tag{Equation 15}$$

Where:

$T_{ref,comp,dis}$ = Compressor discharge temperature [F]

$T_{sat,condenser}$ = Condenser saturation temperature [F]

$a_{comp,dis}$ = High Pressure: -38.449 [F], low pressure: -126.03 [F]

$b_{comp,dis}$ = High Pressure: $-2.3115 \times 10^{-4} \left[\frac{F \cdot hr}{kBtu} \right]$, low pressure: $-9.0829 \times 10^{-3} \left[\frac{F \cdot hr}{kBtu} \right]$

$c_{comp,dis}$ = High Pressure: $1.3816 \times 10^{-7} \left[\frac{F \cdot hr^2}{kBtu^2} \right]$, low pressure: $1.5396 \times 10^{-7} \left[\frac{F \cdot hr^2}{kBtu^2} \right]$

$d_{comp,dis}$ = High Pressure: 1.9828 [–], low pressure: 3.8801 [–]

$$e_{comp,dis} = \text{High Pressure: } -2.0432 \times 10^{-3} \left[\frac{1}{F} \right], \text{low pressure: } -1.1752 \times 10^{-2} \left[\frac{1}{F} \right]$$

$$f_{comp,dis} = \text{High Pressure: } 2.1574 \times 10^{-6} \left[\frac{\text{hr}}{\text{Btu}} \right], \text{low pressure: } 7.5133 \times 10^{-5} \left[\frac{\text{hr}}{\text{Btu}} \right]$$

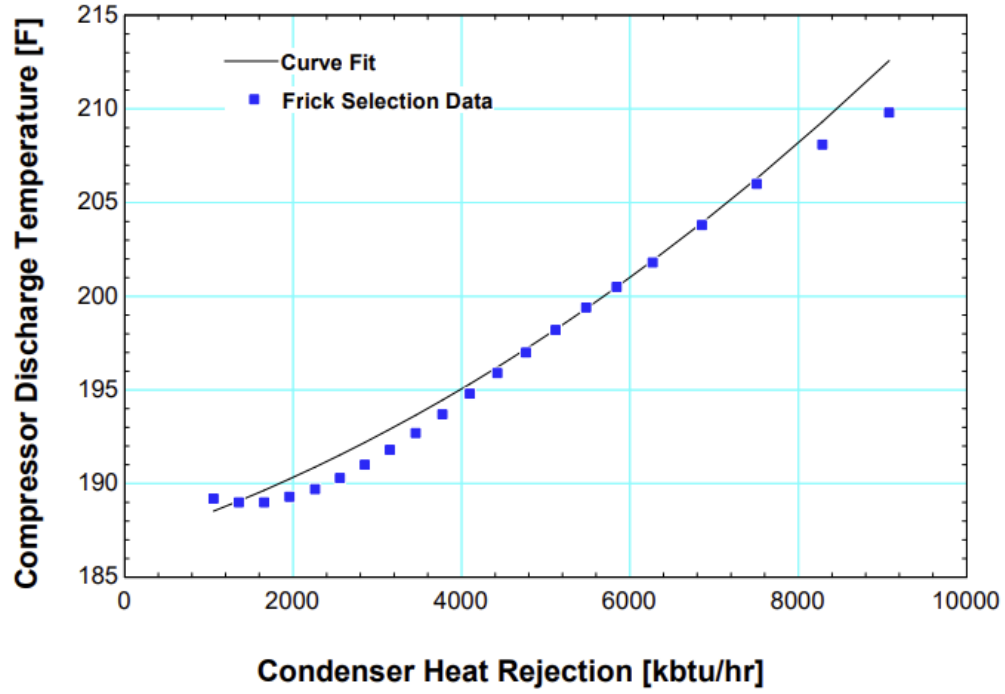


Figure 16: Compressor discharge temperature vs condenser heat rejection at 140°F condenser saturation temperature. Note the slight difference at the extremes of condenser heat rejection [24].

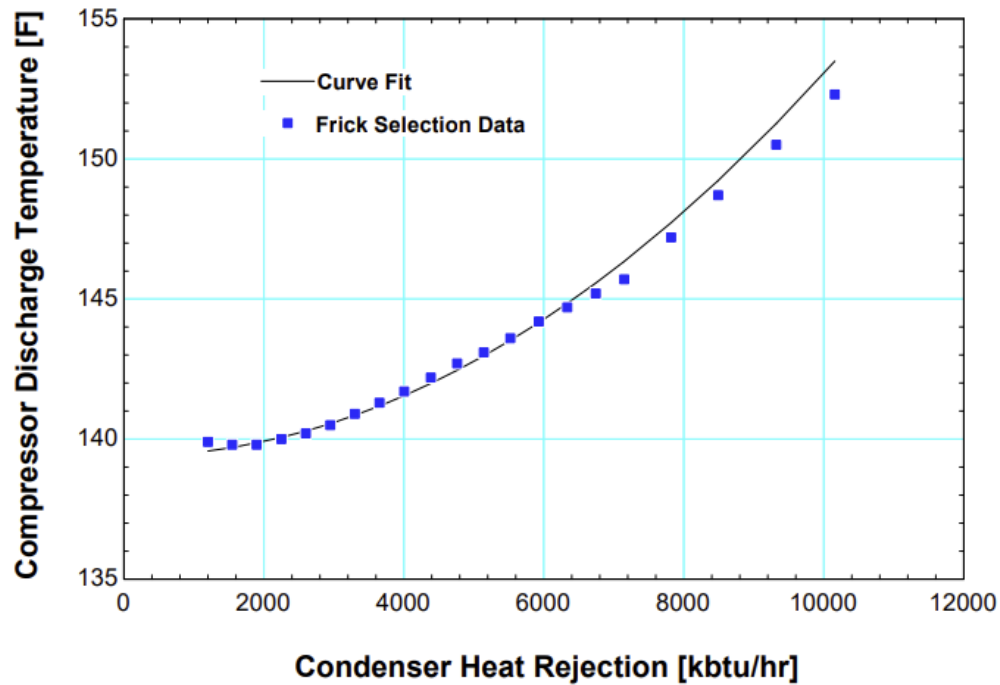


Figure 17: Compressor discharge temperature vs condenser heat rejection utilizing the lower-pressure coefficient at 100°F condenser saturation temperature. Note the largest difference is 1.2°F at maximum capacity [24].

The higher-pressure plot was calculated at 140°F condenser saturation temperature and shows a maximum difference of 2.8°F between the curve fit, 212.6°F and the selection data value of 209.8°F, which is only 4.0% of the superheat at this condensing temperature. The lower-pressure plot was calculated at 100°F condenser saturation temperature and shows a maximum difference of 1.26°F between the curve fit at 153.5°F and the selection data value of 152.3°F, which is only 2.3% of the superheat at this condensing temperature. Since the superheat represents less than 15% of the total heat transfer in all simulations the variation is acceptable.

1.4 Condenser

A condenser model was needed to determine operating conditions that couple the refrigerant and heating of water at all load conditions. Hot water heating loads below the design condition result in a smaller temperature difference between the refrigerant and the water to achieve the desired water outlet temperature compared to full-load conditions. The reduced temperature difference allows for a slightly lower refrigerant condensing pressure. Lower condensing pressures are advantageous because they require less power for the compressor compared to higher pressures, mitigating some of the reduced efficiency associated with running screw compressors at part load as discussed in section (2.3.3). This condenser model calculates an appropriate refrigerant saturation pressure, thus providing a more accurate heat pump system simulation at part load.

The condenser was modeled as a simplified shell-and-tube heat exchanger as shown in **Figure 18** where water is the tube side fluid and ammonia the shell side fluid. The figure shows a shell-and-tube heat exchanger has flow characteristics of both counterflow, where the refrigerant traverses laterally flows through the shell from inlet to outlet and cross-flow as it is redirected vertically across the tube bundle by the internal baffles. The condenser in this project was modeled as a counterflow heat exchanger that uses crossflow correlations for determining the heat transfer coefficient of the refrigerant over the tubes. Shell-and-tube heat exchangers often have multiple passes of each tube; this project's condenser was modeled as a single pass on the tube-side (water-side). The heat transfer for a single tube was modeled and the results scaled up based on the total number of tubes in the condenser.

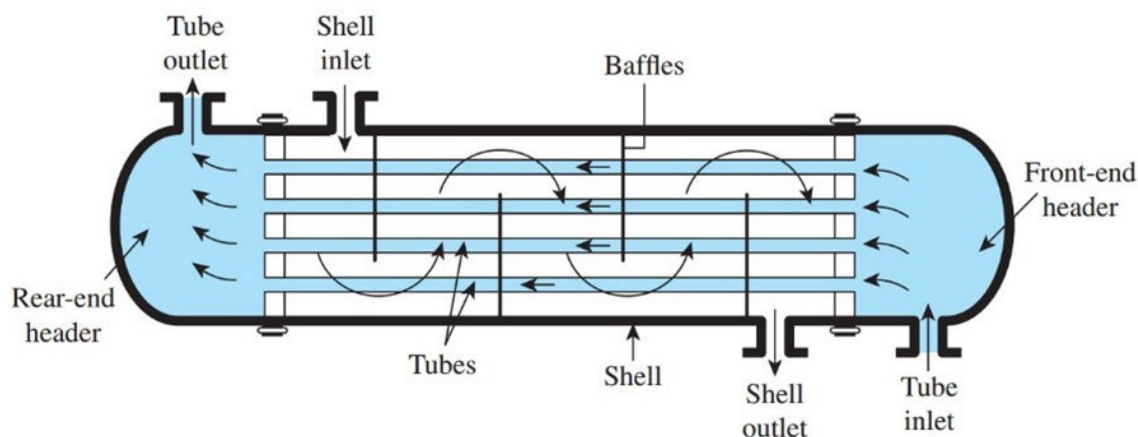


Figure 18: Basic illustration of a shell and tube heat exchanger. Note the change in shell side fluid direction at the end of baffling spaces [25].

The physical design (sizing) of the condenser varies between simulations. The number of tubes was selected to keep the maximum velocity of water to approximately 5 ft/sec, for the fixed tube diameter used in all cases, and depends on the volumetric flow rate of the maximum load. The length of each tube is also dependent on the maximum load and is determined to ensure the design condenser saturation temperature is near 150°F. The shell-and-tube condenser was modeled with the specifications in **Table 1**. The condenser designs were informed by detailed performance data and physical specifications provided by Isotherm. Condenser geometry such as shell diameter, tube diameter and thickness, and the number of baffles was chosen directly from this data.

Table 1: Geometry and Materials of Condenser

Configuration	One heat pump no thermal storage	One heat pump with thermal storage	Two heat pump no storage high stage	Two heat pump no storage low stage	Two heat pump with storage high stage	Two heat pump with storage low stage
Material	SA214-ERW	SA214-ERW	SA214-ERW	SA214-ERW	SA214-ERW	SA214-ERW
Outside diameter [in]	0.75	0.75	0.75	0.75	0.75	0.75
Inside diameter [in]	0.62	0.62	0.62	0.62	0.62	0.62
Thickness [in]	0.065	0.065	0.065	0.065	0.065	0.065
Length [in]	705	718	565	577	575	585
Cross-sectional inner tube area [in ²]	0.302	0.302	0.302	0.302	0.302	0.302
Outside tube area [in ²] Single tube	1639	1669	1313	1341	1337	1360
Inside tube area [in ²] Single tube	1373	1399	1100	1124	1120	1139
Total outside tube surface area [ft ²]	1092.67	486.80	875.33	391.13	389.96	396.67
Total inside tube surface area [in ²]	915.33	408.04	733.33	749.33	326.67	332.21
Shell inner diameter [in]	24	16	24	24	16	16
Number of baffles	7	7	7	7	7	7

The model utilizes a finite difference method where the condenser tube is discretized into n connected sub-heat exchangers with $n+1$ nodes on both the water-side and refrigerant-side of

the condenser, as shown in **Figure 19**. The number of sub-heat exchangers used was chosen to reduce simulation computation times while providing a solution that converges within the tolerance chosen. The temperature of water at the first node, $j=1$ is equal to $T_{\text{water,set}}$, the load setpoint of 140°F. The temperature of the refrigerant at the first node, $j=1$ is equal to the discharge temperature of the compressor $T_{\text{ref,comp,dis}}$, and is dependent upon the saturation pressure and capacity ratio. This discharge temperature was calculated from the curve-fit discussed in section 2.3.4. The temperature of the water at the last node, $j=n+1$ is equal to $T_{\text{water,utility}}$, which is set to 55°F in these simulations. The refrigerant at the last node, $j=n+1$ is equal to $T_{\text{sat,condenser}}$ which is determined by closing a mass and energy balance the water-side and refrigerant-side of the heat exchanger coupled into the heat pump with the further assumption that the condensed high-pressure refrigerant leaves the shell with a quality of 0.

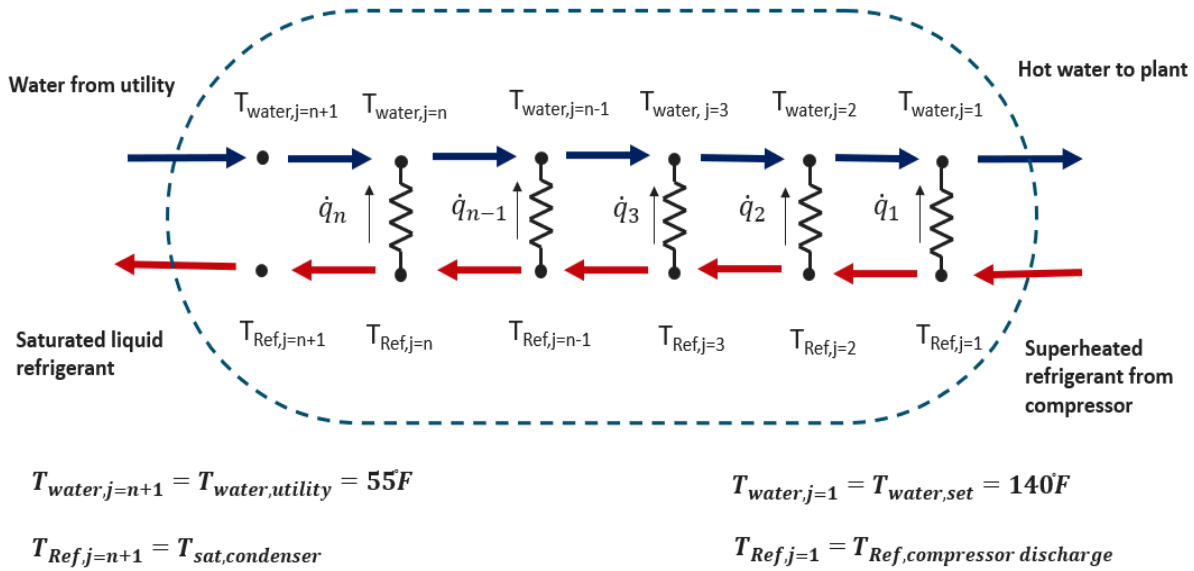


Figure 19: Diagram of the sub-heat exchanger model showing fluid flow direction, heat flows, and resistance networks.

The total heat transfer required to meet the given load, $\dot{q}_{required}$, is determined by **Equation 16**, where $i_{water,utility}$ equals the enthalpy at $j=n+1$, and $i_{water,set}$ equals the enthalpy of water at node $j=1$. The enthalpies are determined by the pressure and temperature of the water, which are known on the intake side, and are the setpoints of the water for the outlet side. Since the flow rate and temperatures are known, the total heat transfer required for a given heating load condition is also known.

$$\dot{q}_{required} = \dot{m}_{water} \cdot (i_{water,set} - i_{water,utility}) \quad \text{Equation 16}$$

Where:

$$\dot{q}_{required} = \text{total heat transfer rate from the refrigerant to the water} \left[\frac{\text{Btu}}{\text{hr}} \right]$$

$$\dot{m}_{water} = \text{mass flow rate of water} \left[\frac{\text{lbm}}{\text{hr}} \right]$$

$$i_{water,set} = \text{enthalpy of the water leaving the condenser} \left[\frac{\text{Btu}}{\text{lbm}} \right]$$

$$i_{water,utility} = \text{enthalpy of water entering the condenser from the utility} \left[\frac{\text{Btu}}{\text{lbm}} \right]$$

The heat transfer rate to the water found in **Equation 16** must balance with the heat transfer rate from the refrigerant **Equation 17**. The enthalpy at node $j=1$, $i_{ref,j=1}$, equals $i_{ref,comp,discharge}$, and the enthalpy at node $j=n+1$, $i_{ref,j=n+1}$, equals $i_{ref,out}$.

$$\dot{q}_{required} = \dot{m}_{refrigerant} \cdot (i_{ref,comp,discharge} - i_{ref,out}) \quad \text{Equation 17}$$

Where:

$$\dot{m}_{refrigerant} = \text{mass flow rate of refrigerant} \left[\frac{\text{lbm}}{\text{hr}} \right]$$

$$i_{ref,comp,discharge} = \text{enthalpy of the refrigerant leaving the compressor} \left[\frac{\text{Btu}}{\text{lbm}} \right]$$

$$i_{ref,out} = \text{enthalpy of refrigerant leaving the condenser} \left[\frac{\text{Btu}}{\text{lbm}} \right]$$

The model begins with a guess value for the condenser saturation temperature, $T_{sat,condenser,guess}$, and uses that guess value to determine $i_{ref,comp,discharge}$ and $i_{ref,out}$. Rearranging Equation 2 to solve for $\dot{m}_{refrigerant}$ makes it easy to determine the refrigerant mass flow rate at $T_{sat,condenser,guess}$ that satisfies the required heat transfer rate to the water. The model takes this refrigerant mass flow rate and these enthalpies to determine if the refrigerant condenser outlet condition, $i_{ref,out}$ is a saturated liquid. If the exit state enthalpy is within tolerance of the enthalpy of saturated liquid refrigerant at the guess condensing pressure, the condenser model has converged, and the appropriate condensing pressure has been found. If the exit enthalpy does not fall within the tolerance of the enthalpy of saturated liquid, the program iterates between a maximum and minimum saturation temperatures until the correct condensing pressure is found.

The process of determining if the refrigerant exiting condition is that of a saturated liquid is multistep. The model uses the compressor discharge temperature, $T_{ref,compressor discharge}$, determined from the curve fit using the guess condensing value, $T_{sat,condenser,guess}$, and the water outlet set point, $T_{water,set}$, as the temperatures at $T_{ref,j=1}$ and $T_{water,j=1}$, respectively. Using Equation 18, the

heat transfer rate from the refrigerant to the water in sub-heat exchanger j, \dot{q}_j , can be determined. The total resistance between the refrigerant and the water, $R_{total,j}$, is discussed in detail later in this chapter. Knowing the value of \dot{q}_j , $R_{total,j}$, and the mass flow rates allows for the calculation of the enthalpies for both water and the refrigerant at node j+1 by rearranging equations **Equation 19** and **Equation 20** to solve for the enthalpies of interest. Once the enthalpies $i_{Ref,j+1}$ and $i_{water,j+1}$ have been calculated, the temperatures of water and refrigerant at node j+1, $T_{water,j+1}$ and $T_{ref,j+1}$ respectively, can be determined from TRNSYS property functions. This process is repeated n times until all the heat transfer rates through, $\dot{q}_{j=n}$ and the enthalpies of both the water and refrigerant through node j=n+1 are determined.

$$\dot{q}_j = \frac{T_{ref,j} - T_{water,j}}{R_{total,j}} \quad \text{Equation 18}$$

Where:

\dot{q}_j = Heat transfered to water from refrigerant at node j [$\frac{\text{Btu}}{\text{hr}}$]

$T_{ref,j}$ = Temperature of refrigerant at node j [F]

$T_{water,j}$ = Temperature of water at node j [F]

$R_{total,j}$ = Total resistance between refrigerant and water at node j [$\frac{\text{F} \cdot \text{hr}}{\text{Btu}}$]

$$\dot{q}_j = \dot{m}_{water} \cdot (i_{water,j} - i_{water,j+1}) \quad \text{Equation 19}$$

$$\dot{q}_j = \dot{m}_{refrigerant} \cdot (i_{ref,j} - i_{ref,j+1}) \quad \text{Equation 20}$$

Where:

$i_{Ref,j+1}$ = Enthalpy of refrigerant at node $j + 1$ [F]

$i_{water,j+1}$ = Enthalpy of water at node $j + 1$ [F]

Because the mass flow rate of refrigerant, $\dot{m}_{refrigerant}$, was chosen specifically to meet load $\dot{q}_{required}$ as per **Equation 17** then the summation of the heat transfer in all sub-heat exchangers equals the required heat transfer as seen in **Equation 21**. Therefore, the water is entering the condenser at $T_{water,utility}$, and is exiting at $T_{water,set}$. Since $T_{ref, compressor discharge}$ was imposed as the refrigerant entering temperature, only the refrigerant outlet enthalpy, $i_{ref,j=n+1}$ needs to be checked to see if it falls within tolerance of the enthalpy of $i_{ref,out}$, the refrigerant at $T_{sat,condenser,guess}$ and quality of 0, **Equation 22**. As previously stated, if the exit refrigerant's enthalpy is within tolerance of the enthalpy of saturated liquid then $T_{sat,condenser,guess}$ is considered the appropriate condensing temperature to model. If not, the model iterates using the bisection method to converge upon the appropriate value of $T_{sat,condenser,guess}$.

$$\dot{q}_{required} = \sum_{j=1}^n \dot{q}_j \quad \text{Equation 21}$$

Where:

n = Number of sub-heat exchangers [-]

$$|i_{ref,out} - i_{ref,j=n+1}| \leq Tolerance_{enthalpy}$$

Equation 22

Where:

$$Tolerance_{enthalpy} = \text{Allowed difference between } i_{ref,out} \text{ and } i_{ref,j=n+1} \left[\frac{\text{Btu}}{\text{lbm}} \right]$$

A resistance network was modeled to find the value of $R_{total,j}$ in **Equation 18**. The resistance network contains four constituent resistances, $R_{conv,ref,j}$ the convective resistance of the refrigerant at node j , $R_{tube,j}$ the conductive resistance of the tube at node j , $R_{foul,j}$ the fouling resistance at node j , and $R_{conv,water,j}$ the convective resistance of water at node j . These resistances are connected in series as shown in **Figure 20** with the heat transfer rate, \dot{q}_j shown flowing from the refrigerant to the water. The total resistance, $R_{total,j}$ was calculated using the **Equation 23** for resistances in series, equaling the sum of the individual resistances [26]. The individual resistances must be determined before being summed into an equivalent total resistance.

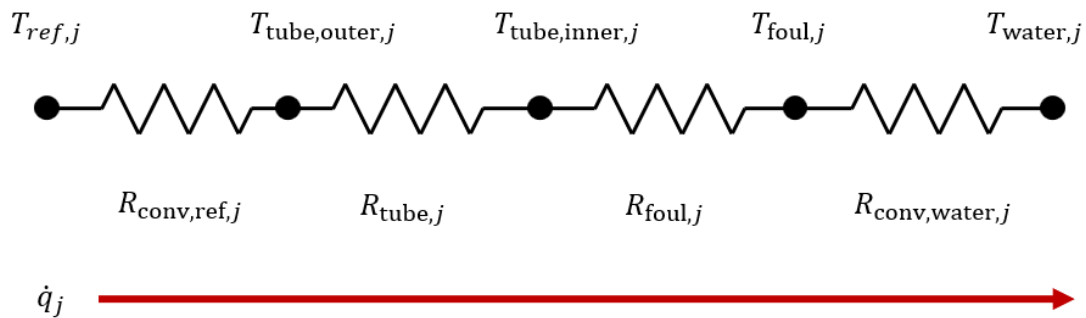


Figure 20: Resistance network at node j including constituent resistances, node temperatures, and heat transfer through sub-heat exchanger j .

$$R_{total,j} = R_{conv,ref,j} + R_{tube,j} + R_{foul,j} + R_{conv,water,j} \quad \text{Equation 23}$$

Where:

$$R_{conv,ref,j} = \text{Convective resistance of refrigerant at node } j \left[\frac{\text{F} \cdot \text{hr}}{\text{Btu}} \right]$$

$$R_{tube,j} = R = \text{Conductive resistance of tube at node } j \left[\frac{\text{F} \cdot \text{hr}}{\text{Btu}} \right]$$

$$R_{foul,j} = \text{Fouling resistance at node } j \left[\frac{\text{F} \cdot \text{hr}}{\text{Btu}} \right]$$

$$R_{conv,water,j} = \text{Convective resistance of water at node } j \left[\frac{\text{F} \cdot \text{hr}}{\text{Btu}} \right]$$

The convective resistance of refrigerant at node j , $R_{conv,ref,j}$, was calculated utilizing **Equation 24 [26]**. The outer area of the tube segment, $A_{tube\ seg,outer}$ was calculated by dividing the total outer tube area of a single tube found in **Table 1**, by the total number of sub-heat exchangers, n , in the condenser model. The heat transfer coefficient of the refrigerant, $h_{ref,j}$, was calculated with two different methods depending upon whether the node falls into the superheated or saturated region of the heat exchanger. The condenser model checks the enthalpy of refrigerant at each node, $i_{ref,j}$, versus $i_{ref,x=1}$, the enthalpy of the refrigerant at the guess condensing pressure with a quality of 1. If $i_{ref,j} > i_{ref,x=1}$ the model uses a superheated correlation to determine the heat transfer coefficient of the refrigerant, $h_{ref,j}$. If $i_{ref,j} \leq i_{ref,x=1}$ the model uses a condensing correlation to determine the heat transfer coefficient. As noted above, when $i_{ref,j} > i_{ref,x=1}$, the refrigerant is in the superheated regime. The correlation used

to determine the heat transfer coefficient of refrigerant is one of external flow over a staggered bank of tubes in **Equation 25**, **Equation 26**, and **Table 2** [27].

$$R_{conv,ref,j} = \frac{1}{h_{ref,j} \cdot A_{tube\ seg,outer}} \quad \text{Equation 24}$$

Where:

$$h_{ref,j} = \text{Heat transfer coefficient at node } j \left[\frac{\text{Btu}}{\text{F} \cdot \text{hr} \cdot \text{in}^2} \right]$$

$$A_{tube\ seg,outer} = \text{Outer area of single tube segment [in}^2\text{]}$$

$$h_{ref,j} = \frac{Nu_{ref,j} \cdot k_{ref,j}}{D_{tube,outer}} \quad \text{Equation 25}$$

Where:

$$Nu_{ref,j} = \text{Nusselt number of refrigerant at node } j [-]$$

$$k_{ref,j} = \text{Conductivity of refrigerant at node } j \left[\frac{\text{btu}}{\text{F} \cdot \text{hr} \cdot \text{in}} \right]$$

$$D_{tube,outer} = \text{Outer diameter of tube [in]}$$

$$Nu_{ref,i} = c \cdot \left(\frac{a}{b} \right)^p \cdot Re_{ref,sh,j}^m \cdot Pr_{ref,sh,j}^n \cdot \left(\frac{Pr_{ref,sh,j}}{Pr_{ref,sh,i}} \right)^{0.25} \quad \text{Equation 26}$$

Where:

$Re_{ref,sh,j}$ = Reynolds number of superheated refrigerant at node j [–]

$Pr_{ref,sh,j}$ = Free stream Prandlt number of refrigerant at node j [–]

$Pr_{ref,sh,s,j}$ = Tube surface Prandlt number of refrigerant at node j [–]

S_T = Transverse pitch

S_L = Lateral pitch

$$a = \frac{S_T}{D_{outer,tube}}$$

$$b = \frac{S_L}{D_{outer,tube}}$$

And:

Table 2: Parameters for superheated refrigerant heat transfer coefficient correlation in Equation 26

$Re_{ref,sh,j}$	c	P	m	N
1-500	1.04	0	0.4	0.36
500-1000	0.71	0	0.5	0.36
1000 - 2×10^5	0.35	0.2	0.6	0.36
$2 \times 10^5 - 2 \times 10^6$	0.031	0.2	0.8	0.36

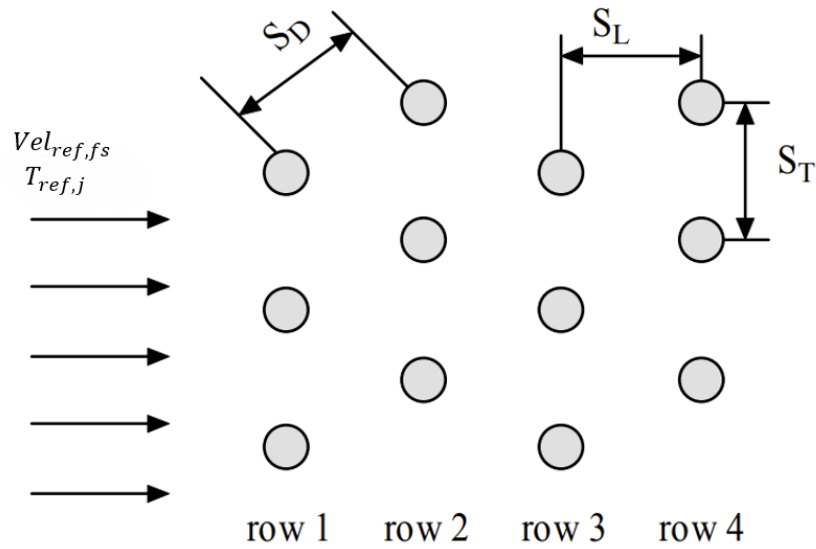


Figure 21: Layout of staggered tube bank model showing orientation of pitches.

The conductivity of the refrigerant was found using internal TRNSYS material property functions. The average free stream velocity of the refrigerant, $Vel_{ref,fs}$, was calculated by dividing the refrigerant volumetric flow rate, \dot{V}_{ref} , by the average cross-sectional area of the baffling spaces. The velocity, $Vel_{ref,max}$, used to find the Reynolds number, $Re_{ref,sh,j}$, is found in **Equation 12** and **Equation 13**. The geometry of this model has $S_D > \frac{S_T + D_{tube,outer}}{2}$ as both S_T and $S_T = 0.9975$ [in]. Therefore, **Equation 27** was used in these simulations.

$$\text{If:} \quad S_D > \frac{S_T + D_{tube,outer}}{2}$$

$$\text{Then} \quad \therefore Vel_{ref,max} = \frac{S_T}{S_T - D_{tube,outer}} \cdot Vel_{ref,fs} \quad \text{Equation 27}$$

$$\text{If not, then:} \quad \therefore Vel_{ref,max} = \frac{0.5 \cdot S_T}{S_D - D_{tube,outer}} \cdot Vel_{ref,fs} \quad \text{Equation 28}$$

$$\text{Where:} \quad S_D = S_L^2 + \left[\left(\frac{S_T}{2}\right)^2\right]^{1/2}$$

When $i_{ref,j} \leq i_{ref,x=1}$, the given node is in the condensing regime. The correlation used to determine the heat transfer coefficient of refrigerant is film condensation on a bank of cylinders shown in **Equation 29** [28]. Note the correlation is formatted in SI units, all inputs are converted into SI, the heat transfer coefficient, $h_{ref,j}$ is then converted into $\left[\frac{\text{Btu}}{\text{F}\cdot\text{hr}\cdot\text{in}^2}\right]$ after calculation. The correlation for $h_{ref,j}$ in the condensing region requires a value for $T_{wall,i}$, but $T_{wall,i}$ is not known without a value for $h_{ref,j}$. Therefore, a guess value for $T_{wall,i}$ is made. This guess value is used to calculate \dot{q}_j using **Equation 30** and $R_{wall,j}$, the resistance network between the water and tube wall, found in **Figure 22** and **Equation 31**. The heat transfer rate,

$\dot{q}_{wall,j}$ found in **Equation 30** must fall within tolerance of heat transfer rate found in Equation 15, \dot{q}_j , as seen in **Equation 32**. If the values are within tolerance, $T_{wall,j}$ is considered the appropriate tube wall temperature. If the values are not within tolerance, the model uses the bisection method to iterate between the maximum and minimum wall temperature until the appropriate value is found.

$$h_{ref,j} = 0.728 \cdot \frac{k_l}{n_{rows} \cdot D_{tube,outer}} \cdot \left[\frac{g \cdot (\rho_l - \rho_v) (n_{rows} \cdot D_{tube,outer})^3 \cdot h_{ref,lv}}{k_l \cdot \nu_l (T_{sat,condenser} - T_{wall,i})} \right]^{1/4} \quad \text{Equation 29}$$

g = gravitational acceleration $[\frac{m}{s^2}]$

ρ_l = Density of saturated liquid refrigerant $[\frac{kg}{m^3}]$

ρ_v = Density of saturated vapor refrigerant $[\frac{kg}{m^3}]$

$h_{ref,lv}$ = latent heat of vaporization of refrigerant $[\frac{J}{kg}]$

ν_l = Dynamic viscosity of refrigerant $[\frac{J}{kg}]$

$T_{wall,i}$ = Temperature of tube wall at node j [K]

$$\dot{q}_{wall,j} = \frac{T_{wall,j} - T_{water,j}}{R_{wall,j}} \quad \text{Equation 30}$$

Where:

$\dot{q}_{wall,j}$ = Heat transferred to water from wall at node j $[\frac{Btu}{hr}]$

$T_{wall,j}$ = Temperature of refrigerant side tube wall at node j [F]

$R_{wall,j}$ = Total resistance between water and refrigerant side tube wall at node j [—]

$$R_{wall,j} = R_{wall,j} + R_{foul,j} + R_{conv,water,j} \quad \text{Equation 31}$$

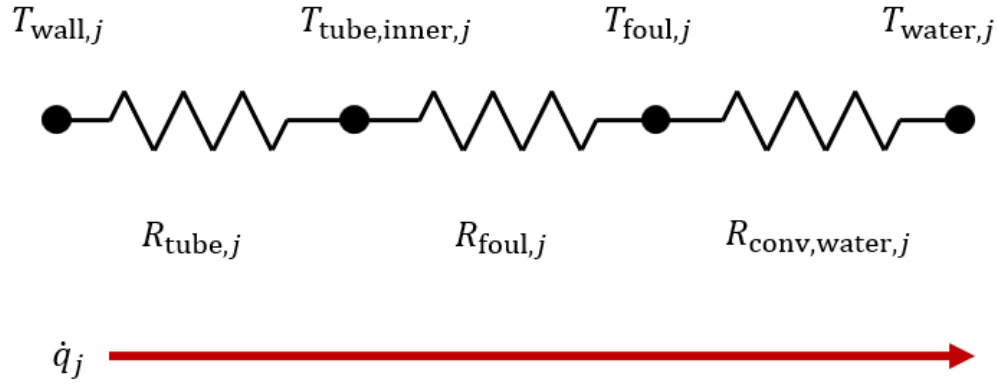


Figure 22: Resistance network at node j including constituent resistances, node temperatures, and heat transfer through sub-heat exchanger j

$$|\dot{q}_{wall,j} - \dot{q}_j| \leq Tolerance_{wall,temp} \quad \text{Equation 32}$$

Where:

$Tolerance_{wall,temp} =$ Allowed difference between $\dot{q}_{wall,j}$ and \dot{q}_j $\left[\frac{\text{Btu}}{\text{hr}}\right]$

The convective resistance of the water is calculated using **Equation 33**. The inner surface area of the tube is calculated by dividing the total inner surface area of the tube from **Table 1** by n , the number of sub-heat exchangers. The heat transfer coefficient, $h_{water,j}$, is calculated using **Equation 34**. The conductivity of the water, $k_{water,j}$, is determined using a curve fit in the form of the below **Equation 35**. The curve fit was created using material property functions in EES

and is compared to the EES material property values in **Figure 23**. The Nusselt number is calculated using **Equation 36** and is dependent on both the Reynold's number and the Prandtl number at node j, shown in **Equation 37** and **Equation 38** respectively [29][30].

$$R_{conv,water} = 1/(h_{water,j} \cdot A_{tube\ seg,inner}) \quad \text{Equation 33}$$

Where:

$h_{water,j}$ = Convective heat transfer coefficient of water at node j [$\frac{\text{Btu}}{\text{F} \cdot \text{hr} \cdot \text{in}^2}$]

$A_{tube\ seg,inner}$ = Inner area of tube segment [in]

.

$$h_{water,j} = \frac{Nu_{water,j} \cdot k_{water,j}}{D_{tube,inner}} \quad \text{Equation 34}$$

Where:

$Nu_{water,j}$ = Nusselt number of water at node j [–]

$k_{water,j}$ = conductivity of water at node j [$\frac{\text{Btu}}{\text{F} \cdot \text{hr} \cdot \text{in}}$]

$D_{tube,inner}$ = Inner diameter of tube [in]

$$k_{water,j} = k_{w,a} + k_{w,b} \cdot T_{water,j} + k_{w,c} \cdot T_{water,j}^2 \quad \text{Equation 35}$$

Where:

$$k_{w,b} = 0.02491135 \left[\frac{\text{Btu}}{\text{F} \cdot \text{hr} \cdot \text{in}} \right]$$

$$k_{w,b} = 0.00006783361 \left[\frac{\text{Btu}}{\text{F}^2 \cdot \text{hr} \cdot \text{in}} \right]$$

$$k_{w,c} = 0.00006783361 \left[\frac{\text{Btu}}{\text{F}^3 \cdot \text{hr} \cdot \text{in}} \right]$$

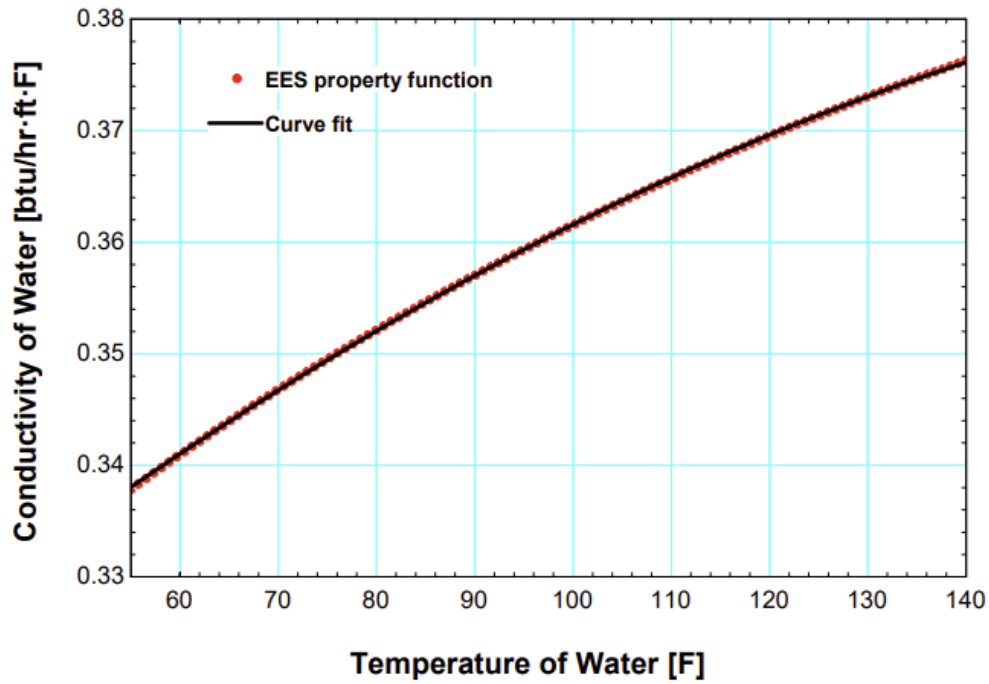


Figure 23: Plot showing curve fit of the conductivity of water compared to the EES material property function values. Note the two sets align.

$$Nu_{water,j} = 0.023 \cdot Re_{water,j}^{0.8} \cdot Pr_{water,j}^{0.3} \quad \text{Equation 36}$$

Where:

$Nus_{water,j}$ = Nusselt number of water at node j [–]

$Re_{water,j}$ = Reynolds number of water at node j [–]

$PR_{water,j}$ = Prandlt number of water at node j [–]

$$Re_{water,j} = \frac{\rho_{water,j} \cdot Vel_{water} \cdot D_{tube,inner}}{\mu_{water,j}}$$

Equation 37

Where:

$\rho_{water,j}$ = density of water at node j [$\frac{lbm}{ft^3}$]

Vel_{water} = Velocity of water at node j [$\frac{ft}{s}$]

$\mu_{water,j}$ = Kinematic viscosity of water at node j [$\frac{ft^2}{s}$]

$$PR_{water,j} = \frac{\nu_{water,j}}{\alpha_{water,j}}$$

Equation 38

Where:

$\nu_{water,j}$ = Dynamic viscosity of water at node j [$\frac{lbm}{ft \cdot s}$]

$\alpha_{water,j}$ = Thermal diffusivity of water at node j [$\frac{ft^2}{s}$]

The density of water is modeled as a constant at 62 [$\frac{lbm}{ft^3}$] due to the negligible change over the temperature range of 55°F to 140°F the water experiences in this simulation, as shown in **Figure**

24. The kinematic viscosity of water at node j , $\mu_{water,j}$ is determined through an internal TRNSYS material property function and the velocity are found by dividing the volumetric flow rate of water, \dot{V}_{water} , based on the load, by the inner cross-sectional area of the tube found in **Table 1**.

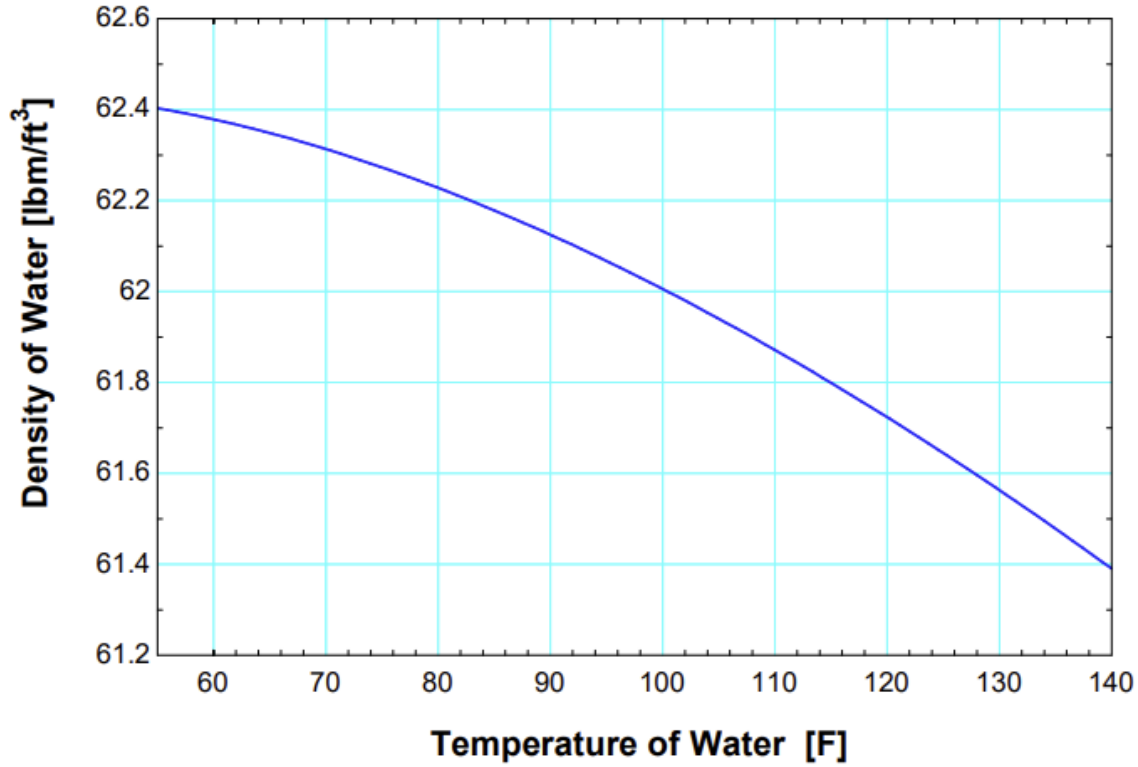


Figure 24: Plot of water conductivity versus the temperature range of water in these simulations.

The conduction resistance through the tube, $R_{tube,j}$, is determined using **Equation 16** [26]. The length of the tube segment, $L_{tube,seg}$, is calculated by dividing the tube length found in Table 1 by n , the number of sub-heat exchangers. The tube is modeled as SA214-ERW steel and its conductivity a constant at $9.15 \left[\frac{\text{Btu}}{\text{F}\cdot\text{hr}\cdot\text{ft}} \right]$ due to its change being less than 0.5%, from 9.171

$\left[\frac{\text{Btu}}{\text{F}\cdot\text{hr}\cdot\text{ft}}\right]$ to $9.117 \left[\frac{\text{Btu}}{\text{F}\cdot\text{hr}\cdot\text{ft}}\right]$, over the range of temperatures experienced by the tube in these simulations, 130°F through 138°F, as shown in **Figure 25**.

$$R_{tube,j} = \frac{\ln \frac{r_{out}}{r_{in}}}{2 \cdot \pi \cdot L_{tube,seg} \cdot k_{tube}} \quad \text{Equation 39}$$

Where:

r_{out} = Outer radius of tube [in]

r_{in} = Inner radius of tube [in]

$L_{tube,seg}$ = Length of sub – heat exchanger tube section [in]

k_{tube} = Conductivity of tube $\left[\frac{\text{btu}}{\text{F} \cdot \text{hr} \cdot \text{in}}\right]$

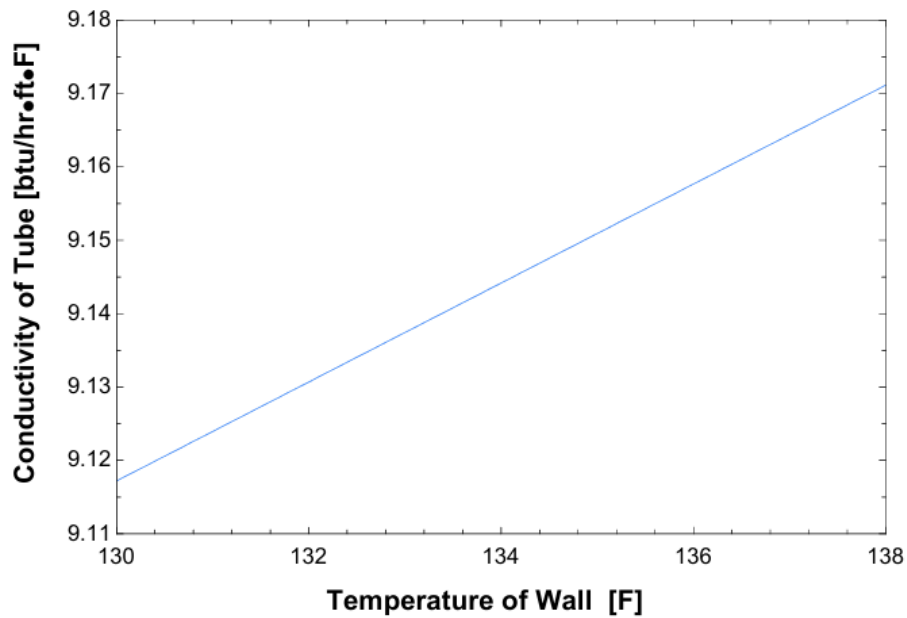


Figure 25: The conductivity of the tube, as reported by EES material property function, over the range of temperatures experienced by the tube wall in the simulations.

The fouling resistance, $R_{foul,j}$, is included to approximate the resistance caused by fouling on the water side of the tube and is calculated using **Equation 40**. The fouling factor that was chosen, $Factor_{foul}$, is the standard industry fouling value of $0.00025 \left[\frac{\text{ft}^2 \cdot \text{hr} \cdot \text{F}}{\text{Btu}} \right]$ [30]. The inner area of the tube segment is calculated by dividing the inner area of the tube found in **Table 1** by n , the number of sub-heat exchangers.

$$R_{foul,j} = \frac{Factor_{foul}}{A_{tube\ seg,inner}} \quad \text{Equation 40}$$

Where:

$$Factor_{foul} = \text{Fouling factor} \left[\frac{\text{in}^2 \cdot \text{hr} \cdot \text{F}}{\text{Btu}} \right]$$

$$A_{tube\ seg,inner} = \text{Inner area of tube} [\text{in}^2]$$

The code was written to ensure the operational conditions modeled were physically possible. The condenser must obey the 2nd law of thermodynamics, meaning the cold stream can never reach, nor exceed the temperature of the hot stream. Examples of the resulting temperature profiles for both the refrigerant and the water in the condenser are plotted by node for both the maximum and minimum loads in for a single heat pump without storage, **Figure 26 & Figure 27**.

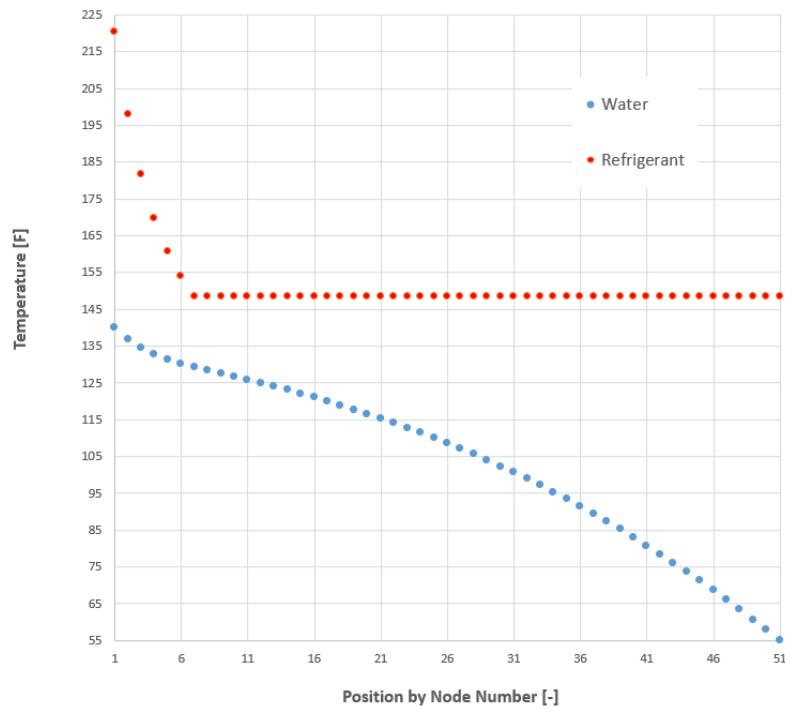


Figure 26: Condenser temperature profiles of refrigerant and water for a single heat pump at maximum load, 410 gal/min. Note the pinch at node 7.

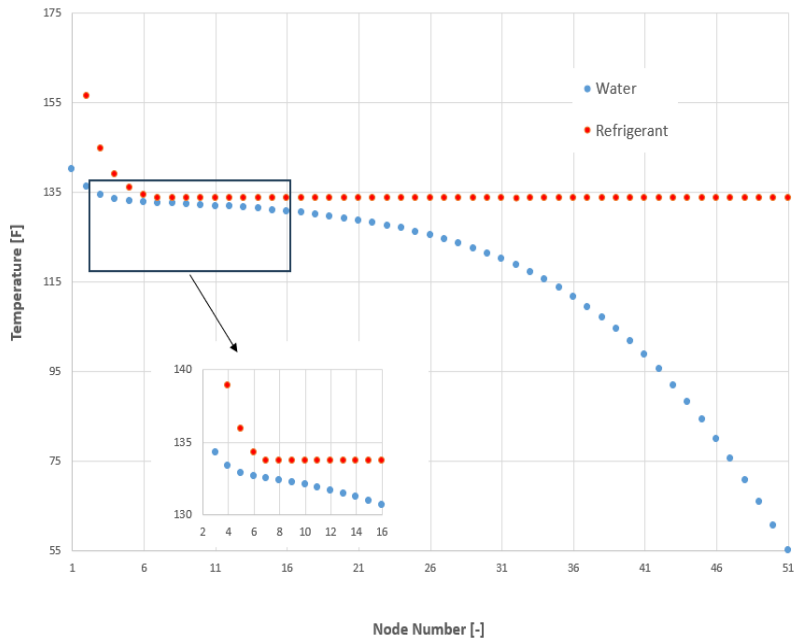


Figure 27: Condenser temperature profiles of refrigerant and water. Note the inset which shows the pinch at node 7.

As expected the difference in temperature required between the hot and cold streams (pinch point) decreases at part load conditions. At low load conditions, the saturation temperature of the refrigerant is often lower than the water's exit temperature and is lifted to its target in the superheated region. In all simulations, the pinch is at the node where the refrigerant first begins to condense.

Although the condenser model is simplified and approximate, it provides for a more accurate simulation of the entire system. The resistance network now complete, the model can iterate to the appropriate condensing pressure. This allows the model to predict the appropriate condensing pressure to gauge compressor power usage, which along with the condenser heat rejection, is required to determine COP_H . This model is used in the simulations detailed in the following chapter.

CHAPTER 3: Results and Discussion

The performances of the four heat pump systems and the natural gas-fired boiler designed to meet the daily hot water load profile given **Table 15** and shown graphically in **Figure 28**, were simulated. The single heat pump system pump and the two heat pump systems without storage were also simulated for a comparative condition with a minimum flow rate of 80 [gal/min] that increases linearly over a 24 hour period reaching a peak flow of 410 [gal/min] at the end of the period, as seen in **Figure 29**. The example plant load profile allows for comparison of the heat pump systems and a natural gas fired boiler. The constant rate of change profile allows for comparison of the systems across the entire range of loads simulated in the example plant load profile.

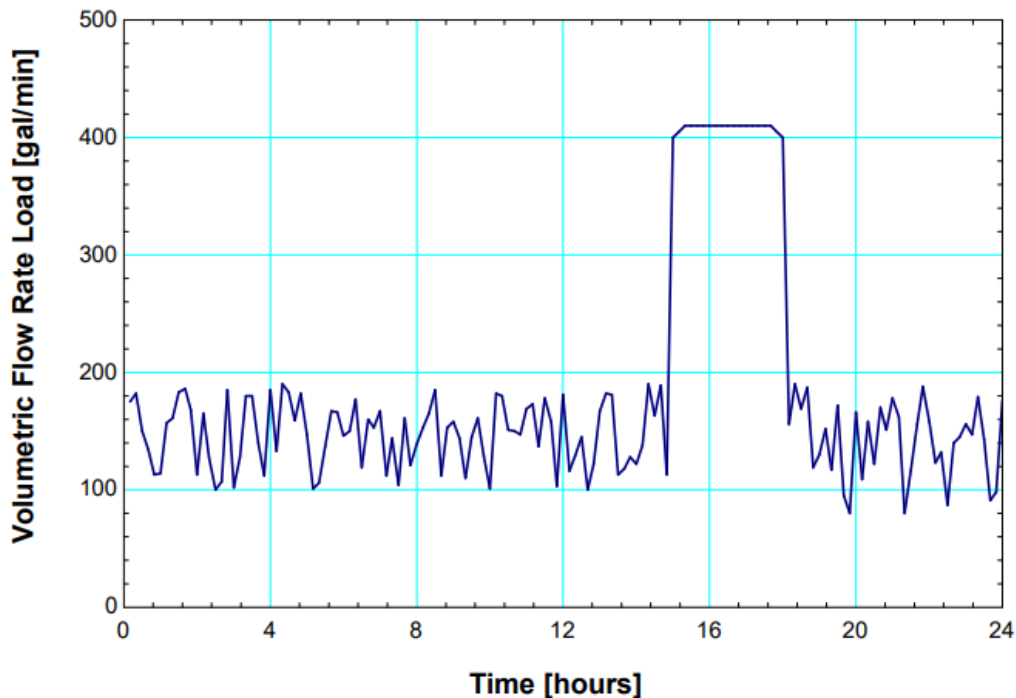


Figure 28: Volumetric flow rate of the example plant load (water) vs time [hours]. Note the three-hour period of peak or near peak load.

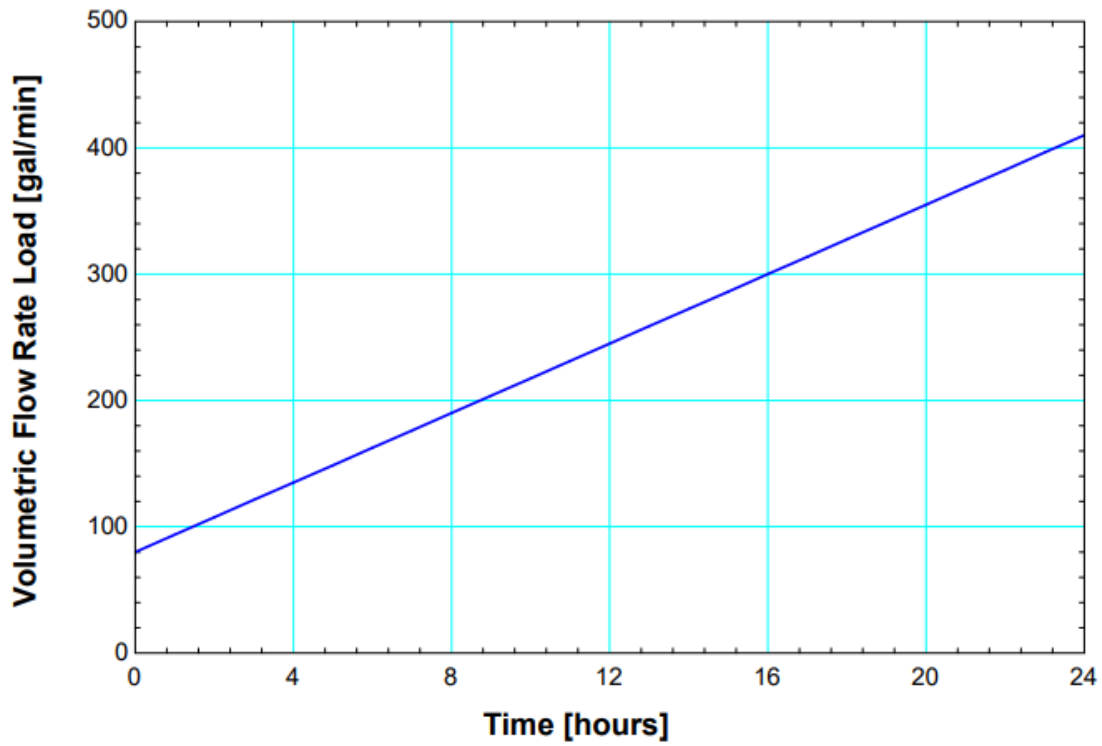


Figure 29: Constant rate of change load profile.

The parameters of each system at design condition are reported in **Table 3**. The design condenser saturation temperature targets were 10°F above the hot water temperature exiting the condenser. The scaling factor was adjusted to achieve a heat pump PLF at design conditions of one for the maximum heating load required for each respective case.

Table 3: Design Parameters of Heat pump Systems.

Heat Pump System	Scaling Factor [-]	Saturation Temperature at Design Conditions [F]
One Pump No Storage	2.10	149.82
One Pump with Storage	0.92	149.88
Two Heat Pumps in Series, no Storage: Low Stage Compressor	0.73	99.51
Two Heat Pumps in Series, no Storage: High Stage Compressor	1.23	149.56
Two Heat Pumps with Storage Low Stage Compressor	0.33	99.70
Two Heat Pumps in Series, with Storage High Stage Compressor	0.54	149.74

The COP_H versus volumetric flow rate of the single heat pump system without storage meeting the constant rate of change (linear) profile is shown in **Figure 30**. The COP_H ranges from a low of 2.17 to a high of 3.67. The plot shows the COP_H remains stable above 3.6 between 400 gpm and 235 gpm, then the COP_H begins to drop at an accelerating rate at lower load (flow) conditions. It is interesting to note the COP_H is at its maximum between 290 gpm and 368 gpm, showing that the increased efficiency of operating at a pressure below design pressure outweighed penalty caused by operating the compressor a part load for that range of flow rate or heat load conditions.

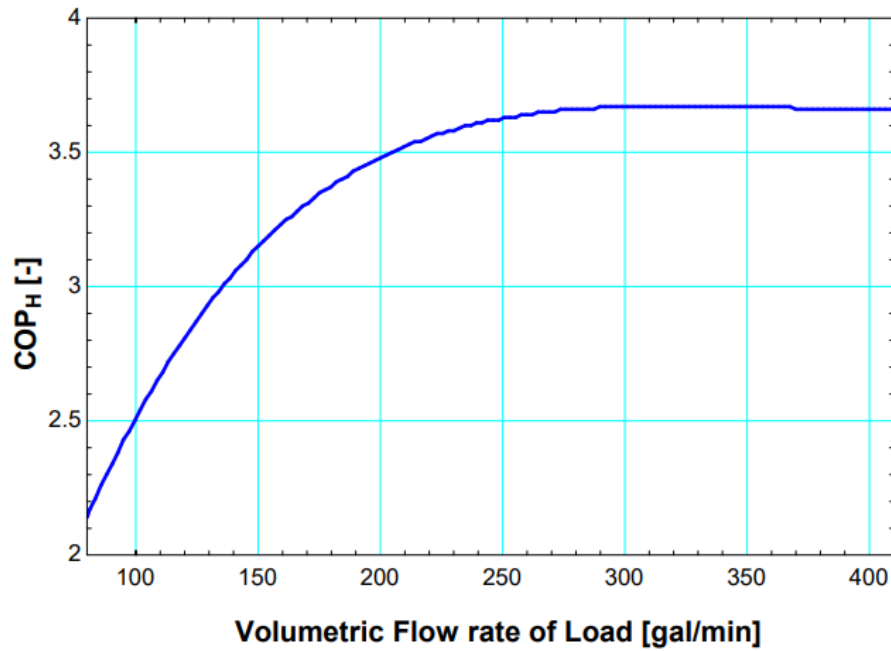


Figure 30: COP vs volumetric flow rate for a single heap pump with no thermal storage meeting the constant rate of increase load profile. Note the maximum between 290 gpm and 368 gpm.

The COP_H versus volumetric flow rate for the two-heat pumps in series system without thermal storage meeting the constant rate of change profile is shown in **Figure 31**. There are three COP_H values shown, the high-pressure stage, the low-pressure stage, and the combined COP_H of the entire system which is obtained using **Equation 41**. The low-pressure stage heat pump COP_H ranges from a high of 8.96 to a low of 5.37. The high-pressure stage heat pump COP_H ranges from a high of 3.72 to a low of 2.14. The combined COP_H ranges from a high of 4.90 to a low of 2.84. The intermediate water temperature between the two condensers is set to 90°F.

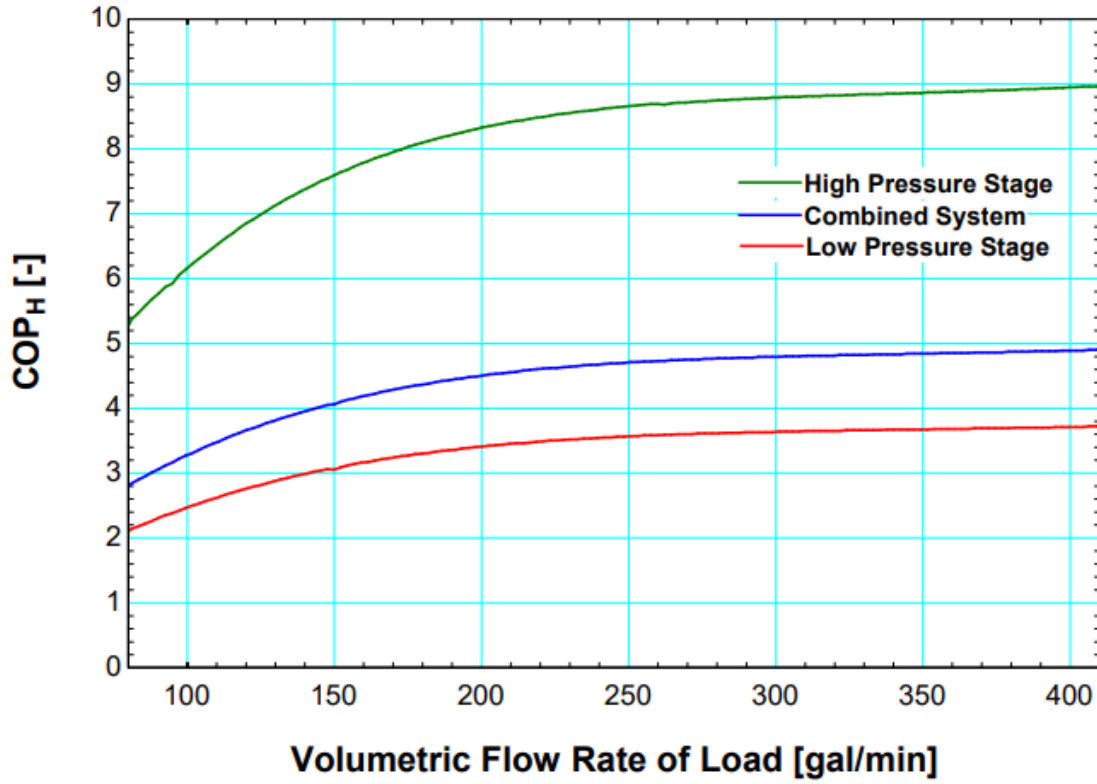


Figure 31: COP of two heat pump system without thermal storage meeting the constant rate of change load profile.

$$COP_{H,total} = \frac{Q_{total}}{W_{comp,low} + W_{comp,low}} \quad \text{Equation 41}$$

Where:

$COP_{H,total}$ = Total heating coefficient of performance high and low stages [-]

Q_{total} = Energy transfered to load from both condensers [Btu]

$W_{comp,low}$ = Work into low – pressure stage compressor [Btu]

$W_{comp,high}$ = Work into high – pressure stage compressor [Btu]

As expected, the performance curve of the single heat pump and the high-pressure stage of the two-heat pump system are similar, Figure 32 as they share the similar design conditions, condensing saturation temperature of approximately 150°F and meeting a load of 410 gpm. The difference between the curves is in part due to the slight difference in actual design conditions seen in **Table 3** of 149.82°F versus 149.56°F, but the major difference is due to the condenser geometry and load temperature through the condenser as shown in **Figure 26**. The single heat pump system has

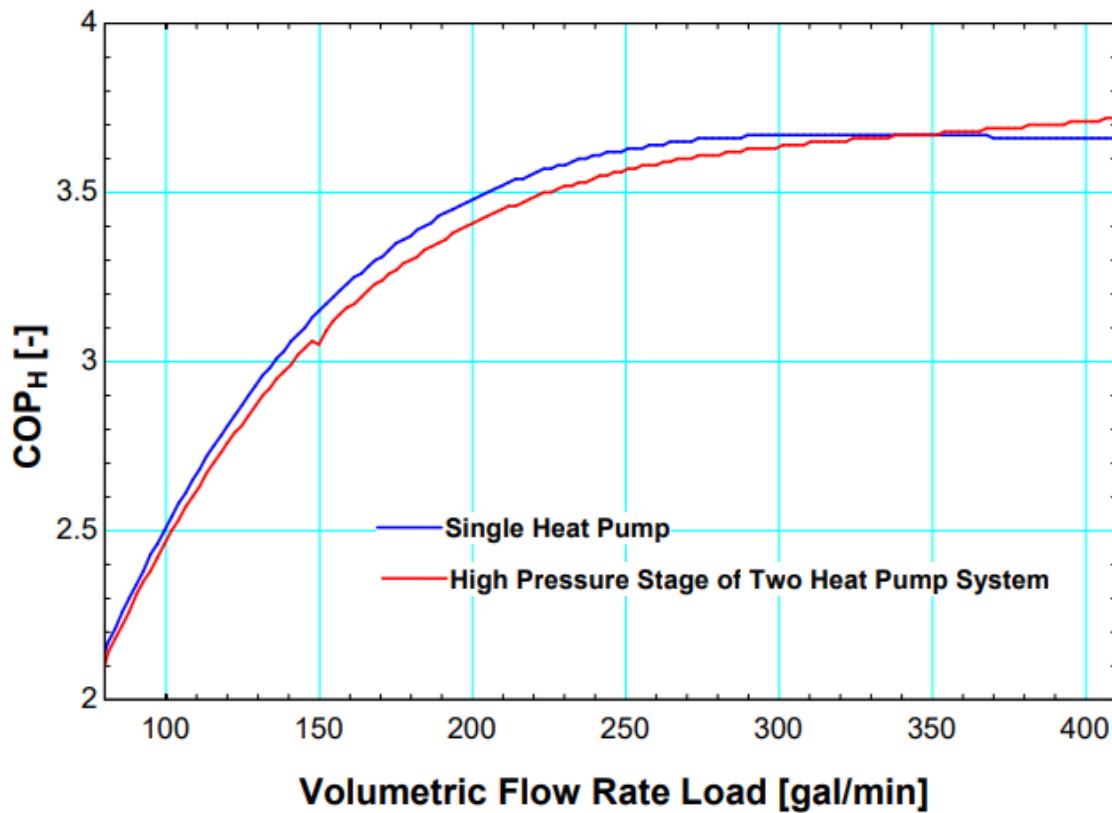


Figure 32: COP heating of the single heat pump system and high stage of the two-heat pump system vs volumetric flow rate. Note the similarity.

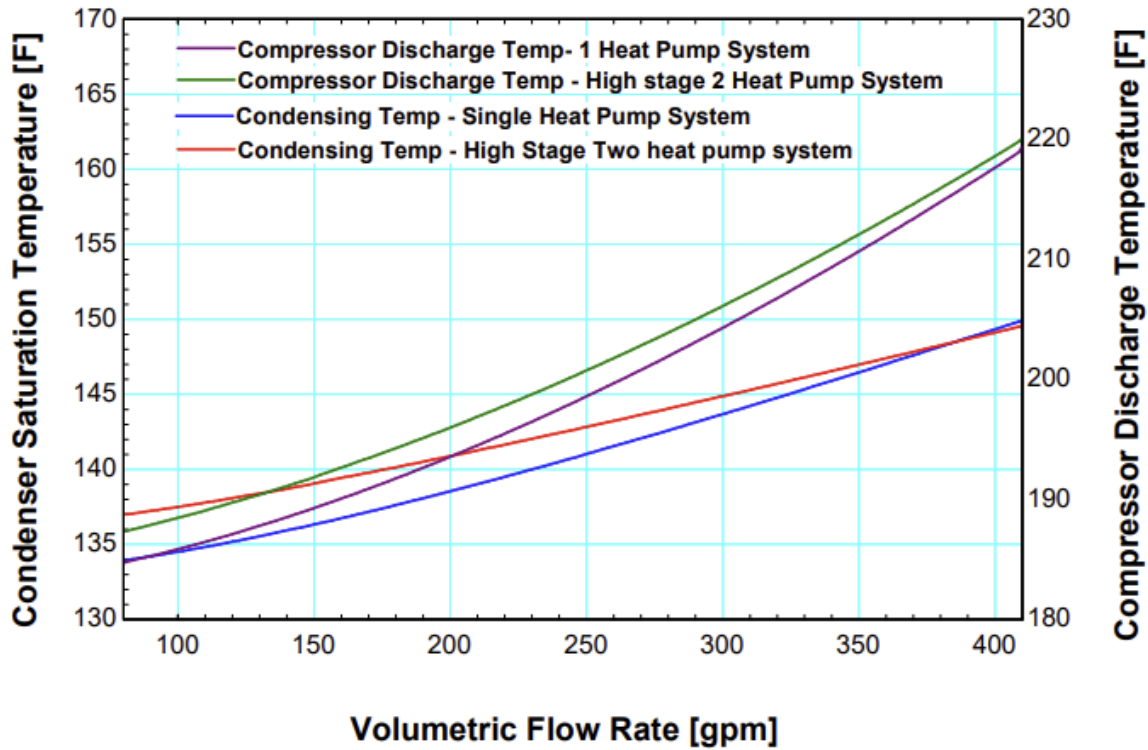


Figure 33: Condenser saturation temperature [F] vs volumetric flow rate. Note the divergence from full load (410gpm) to minimum load (80gpm).

a condenser tube length of 705 inches, compared to 565 inches for the high-pressure stage of the two-pump system. The two heat pump systems outperformed the single heat pump system in terms of COP_H at all loads.

Simulating the heat pump systems meeting the sample plant load profile, **Table 14**, over a year period by multiply a single day by 365, allows for comparing total energy consumption, COP_H , and CO_2 emissions between various heat pump systems and the natural gas fired boiler

Table 4. The heat pump system with the highest COP_H was the two heat pump system with thermal storage. This system had only 45.8% of the CO_2 annual emissions of the gas fired boiler, as shown graphically in **Figure 34**. The reduction in CO_2 emissions between the baseline natural

Table 4: Simulation results.

Water Heating System	COP_H	Total Electrical Power Consumed per Year [MWh]	CO_2 Emissions [ton]	Percentage of Baseline CO_2 Emissions [%]
Natural Gas Fired Boiler (Baseline)	N/A	N/A	4121	100
Electrical Resistance Boiler	1	8054	3799	92.2
One HP No Thermal Storage	3.24	6042	2851	69.2
One HP with Thermal Storage	3.70	5289	2497	60.6
Two HP No Thermal Storage	4.23	4621	2179	52.9
Two HP with Thermal Storage	4.89	4003	1887	45.8

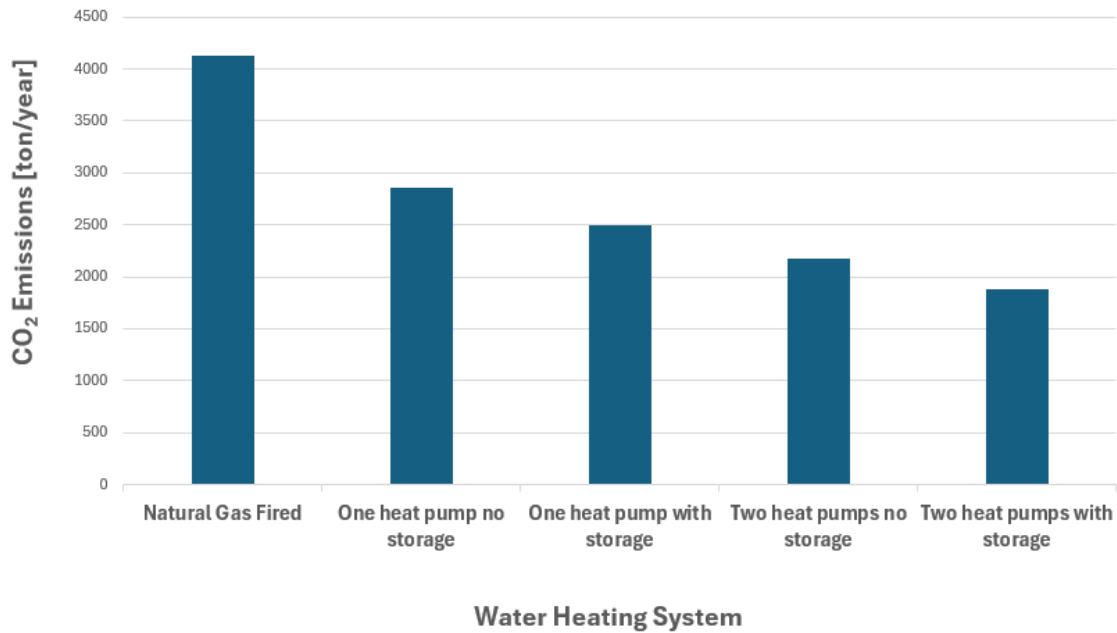


Figure 34: Annual CO₂ emissions [tons] by simulation.

gas fired boiler and the highest emission heat pump system, the single heat pump without thermal storage was 30.8%. The CO₂ emissions from each subsequent system are less than a 9% reduction than the next highest emitter. In other words, the marginal reduction in CO₂ emissions from the single heat pump system without storage to the single heat pump system with storage was 9%. The same marginal improvements were achieved with the series heat pumps both without and with storage.

The heat pump systems with storage were able to operate at their full rated capacity constantly as they simply had to meet the average load of 180.4 gpm, as such, this system option yielded a higher COP_H than their counterpart heat pump configuration with no storage. The COP_H for single heat pump system without thermal storage ranged from 2.19 to 3.70 as shown **Figure 35**, whereas the single heat pump with thermal storage ran at a constant COP_H of 3.70.

Figure 36 shows the two-heat pump system with no storage. The high-pressure stage COP_H ranges from 2.11 to 3.72, the low-pressure stage ranges from 5.32 to 8.97, and the combined COP_H ranges from 2.81 to 4.90.

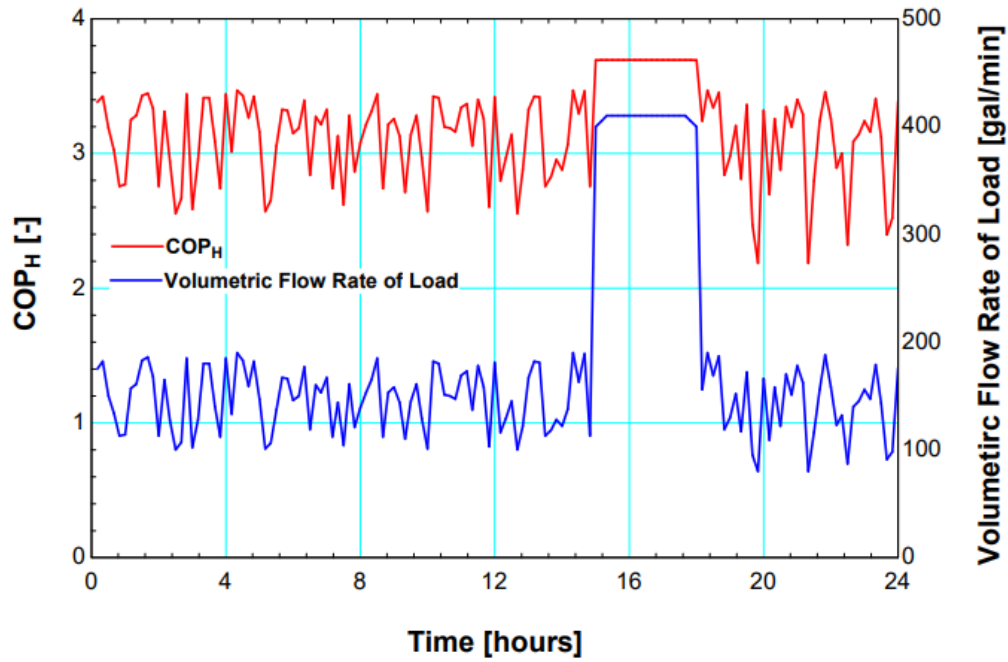
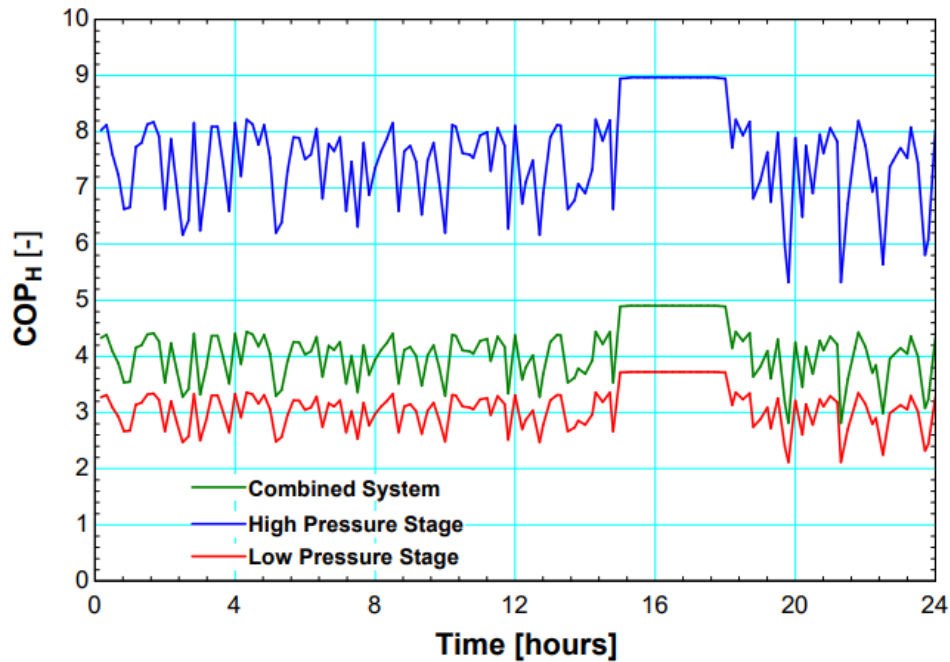


Figure 35: The single heat pump system without thermal storage, COP and volumetric flow rate vs simulation time.



.Figure 36: Two heat pump system without storage COP vs time

The simulations show that all the heat pump systems reduce CO₂ emissions vs the baseline system of a natural gas fired boiler in the MROW region. The heat pump systems did better than a boiler run with electrical resistance heating which has a COP_H of 1. The implementation of such systems in industry is dependent upon the economic situation, including natural gas vs electricity costs, the maintenance cost of running the systems, the capital expenses required to install the systems, interest rates, and any available subsidies. **Table 5** shows the electricity emission factors that would be required for each heat pump system option to have a “break even” in annual CO₂ emissions vs a natural gas fired boiler. Both of the two-heat pump in series systems would be beneficial in achieving reduction in annual CO₂ emissions anywhere in the US. The one heat pump system with thermal storage would reduce emission in all subregions other than the HIOA in Hawaii with an EF of 1575 lb./MWh and the PRMS in Puerto Rico with

an EF of 1593 lb/MWh Figure 10. The benefit of electrification of industrial heating will likely increase in the future as renewable energy use increases and coal use decreases as the primary energy source for our electrical grid.

Table 5: Maximum EF for CO₂ emissions savings by technology.

Water Heating System	Maximum Emission Factor of CO₂ Required for Emission Reductions vs Natural Gas Fired Boiler [lbm/Mwh]
Electrical Resistance Boiler	1023
One Heat Pump No Thermal Storage	1364
One Heat Pump with Thermal Storage	1557
Two Heat Pumps No Storage	1784
Two Heat Pumps with Storage	2061

CHAPTER 4: Conclusions and Recommendations for Further Work

Conclusions

Heat pumping can be an effective means of reducing energy consumption and carbon emissions. This project found potential GHG emissions reductions of 30.8% to 44.2%, but higher savings could likely be realized by system optimization and expanded process integration. All the heat pumps modeled have significant energy and emission savings versus electrical resistance heaters. There were also benefits found having two heat pumps in series as well as with thermal storage.

It was shown that COP_H remained high and stable until the PLF fell to around 0.5 as seen in **Figure 37**. This information helps to inform when utilizing a thermal storage system would be most beneficial. If the PLF would mostly remain above 0.5 with a particular load profile, the benefits of thermal storage will be small. Whereas load profiles that often have a PLF below 0.5 would benefit more from thermal storage.

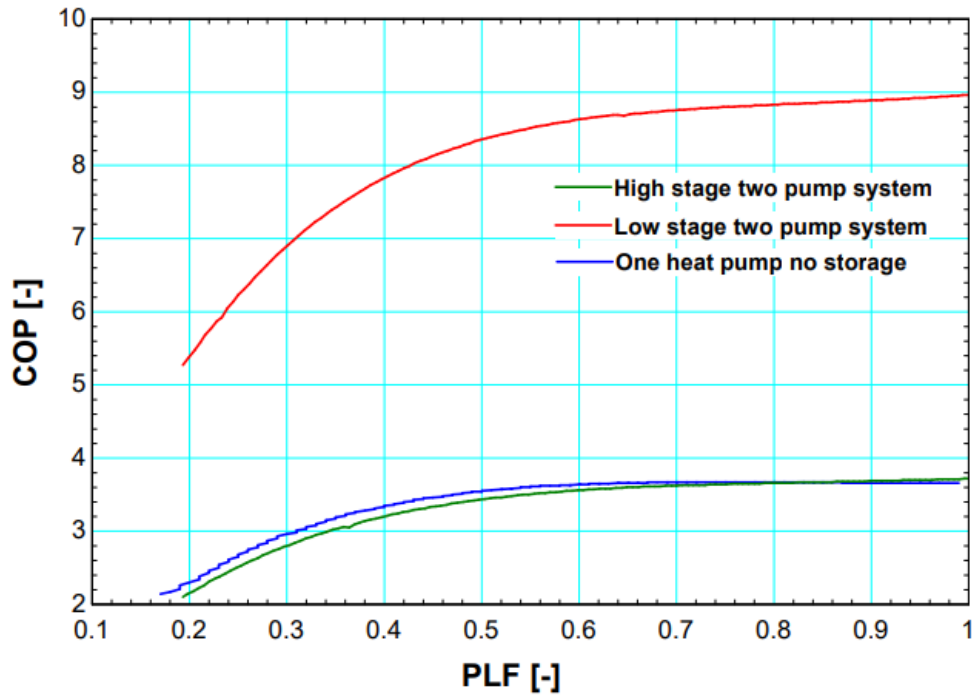


Figure 37: COP vs PLF for heat pumps simulation from minimum load to maximum load. Note the rate of change is greater with PLF below 0.5.

It was also shown that CO₂ emission reduction is very much dependent upon the EF of the electrical grid Figure 10 and Table 5. Therefore, it is important to continue to improve the EF of our electrical grid as the electrification of industrial heating expands as a means to decarbonization. The benefits of electrification diminish if more fossil fuel, particularly coal, is used as the primary energy source for electricity generation.

Recommendations

The application of heat pumps in food processing facilities has not yet taken a strong foothold. Consequently, there is a substantial body of work required to inform end-users and

practitioners on heat pump configurations that warrant further study and implementation. This is particularly the case when considering options that might integrate directly into existing “house” refrigeration systems as opposed to indirect system arrangements that do not share the house system’s refrigerant. Yet at this early stage, relatively simple heat pump models, such as the ones developed in the present project, can provide insights needed to set the future direction of the technology.

As an area for future work, there is clearly a need to refine some of the heat pump’s components in more detail. For example, the compressor model can be improved, including predicting oil cooling requirements. The current compressor model is a black box model entirely based on manufacturer’s selection software “data” [24] for one particular compressor size/model, the SG 2313. Because of the applied assumption of constant evaporating temperature in the present analysis, the compressor model only was required to resolve performance at a constant 55°F evaporator saturation temperature (**Table 5** through **Table 13**). An extension of the current approach should be expanded to include more compressor performance data points over a wider range of evaporator saturation temperatures to enable exploration of the effect of heat pump performance over varying low-side conditions. The performance curves of the SG 2313 screw compressor can also be compared to other models in Frick’s Coolware selection program (or data from other compressor manufacturers) with greater and/or lower capacity to confirm that the scaling factor produces acceptable results. A further compressor model refinement would be to pursue a semi-empirical or mechanistic model to enable a wider range of operating conditions to be reliably predicted.

The present components comprising the heat pump model are also steady state models and, given the nature of heating energy profiles in a plant that fluctuate, establishing a heat pump model with components that reflect the transient behavior can help answer questions about limits for “load following” as well as recommendations for minimum thermal storage requirements to provide sufficient thermal buffering or capacitance to meet time-varying heating loads.

A more detailed compressor model would also enable running simulations at different evaporation temperatures that can more accurately reflect the real-world conditions for a wider range of food and beverage processing facilities. It is also possible that the evaporators of the high stage and the low stage could be run at different evaporator saturation pressures depending on waste heat flows and plant conditions. The evaporator is currently modeled as a black box at a constant 55°F refrigerant saturation temperature for all evaporators in all simulations. Creating a more detailed, finite difference model of the evaporator would also allow for a more detailed simulation of plant loads using heat pump systems that lack thermal storage.

Parameters such as the intermediate water temperature of a two-heat pump system can be optimized. More detailed information on thermal streams for the plant or other plants can be analyzed to reflect operations more accurately. The intermediate water temperature between the outlet of the low-pressure stage condenser and the inlet of the high-pressure stage condenser of the two heat pump systems can be optimized. The 90°F intermediate temperature used in these simulations was chosen based on the optimized intermediate temperature of a relatively simple two stage heat pump model developed early in the project. The model had a black box condenser instead of a more detailed finite difference model. The simplified heat pump model also ran at

different saturation temperatures and maximum loads. Optimizing this intermediate temperature is important to assess series heat pumping more accurately.

Thermal storage systems can be modeled more effectively. Currently thermal storage is modeled simply as meeting an average load of 180.4 gallons per minute over 24 hours instead of having to operate the heat pump to meet the instantaneous hot water demands as they occur. Including thermal heat losses from the tank would aid in confirming the accuracy of the results. The storage model can report maximum storage required as well, helping to inform on the footprint and thus feasibility and cost of a thermal storage system.

A more detailed study of actual plant heat streams would be beneficial for quantifying the benefits of process integration. Pinch analysis can be used to find the minimum theoretical heating and cooling loads and can provide direction in the heat exchange system design needed to leverage these streams. This can assist in quantifying the benefits of the heat pump system on the refrigeration side of the plant as well as help identify the proper evaporator saturation temperatures of the heat pump systems. Exploring heating loads of various types of food processing facilities would help better understand the practical limits of electrification in the sector.

The oil cooling load can also be studied in detail to see if it could be used for water heating as the current model assumes it is rejected as a stream of waste heat to the ambient. As shown in **Figure 9** and **Figure 10**, there is a significant amount of energy in the oil cooling load, from 12.5% of the condenser heat rejection when PLF=1 with a 150°F condenser saturation

temperature, all the way to 52% at the minimum 12% PLF. Utilizing this heat could significantly save energy.

To achieve most of the future work, it would be best to improve the heat pump model itself to be more robust and stable. As written, the FORTRAN code for the heat pump requires time consuming, manual tuning of components to simulate different load conditions. The number of tubes in the condensers and the length of those tubes needs to be adjusted to achieve the desired load flow rates and for the saturation temperature of the condenser to meet design requirements. The scaling factor is manually adjusted to achieve a PLF close to 1 at design condition. Adding code to automate the setting of these parameters may be time beneficial if many different load profiles and conditions are to be simulated. The model is not stable between different load profiles and may not converge without time consuming, manual tuning of the bounds in the convergence loop. Improving the stability of the model or automating the tuning of the bound in the convergence loop would be time saving for future simulations.

The model, as written, simulates heat pump operation and quantifies its performance for a specific load profile. Creating a heat pump model that incorporates real compressor performance responsive to a broader range of evaporator saturation temperatures would allow for study of a broader range of load conditions. Creating a detailed thermal storage model and evaporator model can give more accurate simulations. Optimization of the intermediate temperature in the two heat pump systems and analysis of the oil cooling load allows for modeling of maximum energy and carbon savings.

REFERENCES

- (1) *Effects | Facts – Climate Change: Vital Signs of the Planet*. <https://climate.nasa.gov/effects/> (accessed 2023-12-18).
- (2) *WGII Summary for Policymakers Headline Statements*. <https://www.ipcc.ch/report/ar6/wg2/resources/spm-headline-statements/> (accessed 2023-12-18).
- (3) Mokhov, I. I. Climate Change: Causes, Risks, Consequences, and Problems of Adaptation and Regulation. *Her. Russ. Acad. Sci.* **2022**, 92 (1), 1–11. <https://doi.org/10.1134/S101933162201004X>.
- (4) Intergovernmental Panel On Climate Change. *Climate Change 2021 – The Physical Science Basis: Working Group I Contribution to the Sixth Assessment Report of the Intergovernmental Panel on Climate Change*, 1st ed.; Cambridge University Press, 2023. <https://doi.org/10.1017/9781009157896>.
- (5) US EPA, O. *Climate Change Indicators: U.S. and Global Temperature*. <https://www.epa.gov/climate-indicators/climate-change-indicators-us-and-global-temperature> (accessed 2023-12-18).
- (6) *What We Know*. What We Know. <https://whatweknow.aaas.org/get-the-facts/> (accessed 2023-12-18).
- (7) *Climate Change: Global Temperature | NOAA Climate.gov*. <http://www.climate.gov/news-features/understanding-climate/climate-change-global-temperature> (accessed 2023-12-18).
- (8) *Climate Change: Global Sea Level | NOAA Climate.gov*. <http://www.climate.gov/news-features/understanding-climate/climate-change-global-sea-level> (accessed 2023-12-19).
- (9) Neumann, J. E.; Emanuel, K.; Ravela, S.; Ludwig, L.; Kirshen, P.; Bosma, K.; Martinich, J. Joint Effects of Storm Surge and Sea-Level Rise on US Coasts: New Economic Estimates of Impacts, Adaptation, and Benefits of Mitigation Policy. *Clim. Change* **2015**, 129 (1), 337–349. <https://doi.org/10.1007/s10584-014-1304-z>.
- (10) Tol, R. S. J. The Economic Impacts of Climate Change. *Rev. Environ. Econ. Policy* **2018**, 12 (1), 4–25. <https://doi.org/10.1093/reep/rex027>.

- (11) *Climate Change*. American Meteorological Society.
<https://www.ametsoc.org/index.cfm/ams/about-ams/ams-statements/statements-of-the-ams-in-force/climate-change1/> (accessed 2023-12-18).
- (12) Intergovernmental Panel On Climate Change (Ipcc). *Climate Change 2022 – Impacts, Adaptation and Vulnerability: Working Group II Contribution to the Sixth Assessment Report of the Intergovernmental Panel on Climate Change*, 1st ed.; Cambridge University Press, 2023. <https://doi.org/10.1017/9781009325844>.
- (13) Curtis, N. *US decarbonization regulation and legislation*. Buro Happold.
<https://www.burohappold.com/articles/us-decarbonization-regulation-and-legislation/> (accessed 2024-07-31).
- (14) *Building Emissions Reduction and Disclosure* | *Boston.gov*.
<https://www.boston.gov/departments/environment/berdo> (accessed 2024-07-31).
- (15) *Biden-Harris Administration Announces \$6 Billion to Transform America’s Industrial Sector, Strengthen Domestic Manufacturing, and Slash Planet-Warming Emissions*. Energy.gov. <https://www.energy.gov/articles/biden-harris-administration-announces-6-billion-transform-americas-industrial-sector> (accessed 2024-07-31).
- (16) *Industrial Efficiency and Decarbonization Funding Opportunity Announcement*. Energy.gov. <https://www.energy.gov/eere/iedo/industrial-efficiency-and-decarbonization-funding-opportunity-announcement> (accessed 2024-07-31).
- (17) *Decarbonizing the food and beverages industry: A critical and systematic review of developments, sociotechnical systems and policy options* | *Elsevier Enhanced Reader*.
<https://doi.org/10.1016/j.rser.2021.110856>.
- (18) Manufacturing Energy and Carbon Footprint: Sector: Food and Beverage (NAICS 311, 312). **2018**.
- (19) *White paper: Strengthening Industrial Heat Pump Innovation - Decarbonizing Industrial Heat*. <https://hthp-symposium.org/high-temperature-heat-pumps/white-paper-strengthening-industrial-heat-pump-innovation/> (accessed 2023-01-29).
- (20) US EPA, O. *Data Explorer*. <https://www.epa.gov/egrid/data-explorer> (accessed 2024-08-12).
- (21) *Purchasing Energy-Efficient Large Commercial Boilers*. Energy.gov.
<https://www.energy.gov/femp/purchasing-energy-efficient-large-commercial-boilers> (accessed 2024-08-12).

- (22) U.S. Energy Information Administration - EIA - Independent Statistics and Analysis.
https://www.eia.gov/environment/emissions/co2_vol_mass.php (accessed 2024-08-12).
- (23) TRNSYS, 2024.
- (24) Frick. Coolware, 2023.
- (25) Corporation, K. E. *Shell and Tube Heat Exchangers: Best Choice For Liquid-Cooled Oil Coolers*. Medium. <https://medium.com/@kineticengineeringcorporation/shell-and-tube-heat-exchangers-best-choice-for-liquid-cooled-oil-coolers-43c48c7c07c0> (accessed 2024-08-12).
- (26) Nellis, G.; Klein, S. A. *Introduction to Engineering Heat Transfer*; Cambridge University Press: Cambridge, United Kingdom ; New York, NY, 2019.
- (27) Žkauskas, A. Heat Transfer from Tubes in Crossflow. In *Advances in Heat Transfer*; Hartnett, J. P., Irvine, T. F., Eds.; Elsevier, 1987; Vol. 18, pp 87–159.
[https://doi.org/10.1016/S0065-2717\(08\)70118-7](https://doi.org/10.1016/S0065-2717(08)70118-7).
- (28) Carey, V. P. *Liquid-Vapor Phase-Change Phenomena: An Introduction to the Thermophysics of Vaporization and Condensation Processes in Heat Transfer Equipment*; Series in chemical and mechanical engineering; Hemisphere Publ. Corp: Washington, D.C., 1992.
- (29) Nellis, G.; Klein, S. A. *Heat Transfer*; Cambridge University Press: Cambridge ; New York, 2009.

APPENDIX A Frick Coolware Selection Values

Table 6: Frick Coolware selection data for SGC 2313 at 55°F evaporation temperature and 160°F condensing temperature.

Slide valve [%]	Evaporator capacity [tons]	Condenser heat rejection [kBtu/hr]	Oil cooling load [kBtu/hr]	Compressor power [hp]	Evaporation capacity [%]	Discharge temperature [F]
100	591.5	8323	1378	1023	100	231.7
95	536.6	7518	1363	960	90.7	229.1
90	482.9	6728	1337	892.5	81.6	225.8
85	438.8	6083	1307	834.5	74.2	222.7
80	400.6	5526	1273	783	67.7	220
75	372.2	5118	1244	744.7	62.9	218.1
70	349.6	4794	1220	714.4	59.1	216.4
65	327	4470	1195	684.2	55.3	214.8
60	304.8	4154	1170	655.1	51.5	213.1
55	283.9	3858	1147	628.2	48	211.5
50	263.9	3576	1125	603.1	44.6	210
45	243.8	3295	1103	578.5	41.2	208.5
40	224	3019	1081	555.2	37.9	207.1
35	205.1	2758	1062	533.8	34.7	205.7
30	186.6	2503	1043	513.6	31.6	204.5
25	168.1	2249	1026	494.4	28.4	203.3
20	149.5	1996	1009	476.2	25.3	202.2
15	129.9	1732	994	458.3	22	201.1
10	110.3	1467	980	441.7	18.6	200.2
5	90.6	1204	969	426.5	15.3	199.5
0	71	942	961	413	12	199

Table 7: Frick Coolware selection data for SGC 2313 at 55°F evaporation temperature and 150°F condensing temperature.

Slide valve [%]	Evaporator capacity [tons]	Condenser heat rejection [kBtu/hr]	Oil cooling load [kBtu/hr]	Compressor power [hp]	Evaporation capacity [%]	Discharge temperature [F]
100	624.1	8712	1096	911.2	100	221
95	568.8	7913	1090	856	91.1	218.9
90	514.7	7131	1075	797.3	82.5	216.2
85	469.6	6478	1055	746	75.2	213.6
80	430.5	5917	1032	700.6	69	211.3
75	400.1	5483	1010	665	64.1	209.6
70	375.9	5140	991	636.9	60.2	208.2
65	351.7	4798	972	609	56.4	206.8
60	328.1	4464	953	582	52.6	205.3
55	305.2	4143	935	556.5	48.9	203.9
50	283.4	3839	917	532.8	45.4	202.6
45	261.6	3536	900	509.7	41.9	201.3
40	240.2	3239	884	487.7	38.5	200.1
35	219.6	2956	868	467.4	35.2	198.9
30	199.4	2679	854	448.4	31.9	197.9
25	179.2	2404	841	430.2	28.7	196.9
20	159	2129	830	413.1	25.5	196
15	138	1846	819	396.5	22.1	195.3
10	117	1563	811	381.2	18.7	194.7
5	95.9	1281	805	367.2	15.4	194.2
0	74.9	1000	802	354.7	12	194.1

Table 8:Frick Coolware selection data for SGC 2313 at 55°F evaporation temperature and 140°F condensing temperature

Slide valve [%]	Evaporator capacity [tons]	Condenser heat rejection [kBtu/hr]	Oil cooling load [kBtu/hr]	Compressor power [hp]	Evaporation capacity [%]	Discharge temperature [F]
100	656.1	9078	843	804.8	100	209.8
95	600.4	8286	844	756.8	91.5	208.1
90	545.6	7505	838	705.8	83.2	206
85	499.8	6853	827	661.2	76.2	203.8
80	458.7	6270	813	620.3	69.9	201.8
75	428.3	5843	797	589.8	65.3	200.5
70	402.3	5479	784	563.8	61.3	199.4
65	376.5	5118	770	538.2	57.4	198.2
60	351.3	4766	756	513.5	53.5	197
55	326.7	4425	742	489.8	49.8	195.9
50	303.2	4099	729	467.7	46.2	194.8
45	279.6	3774	717	446.2	42.6	193.7
40	256.4	3455	705	425.7	39.1	192.7
35	234.1	3150	694	406.8	35.7	191.8
30	212.2	2852	684	389	32.3	191
25	190.3	2555	676	372.1	29	190.3
20	168.5	2259	669	356.2	25.7	189.7
15	146.1	1958	663	341	22.3	189.3
10	123.7	1656	659	326.9	18.8	189
5	101.2	1355	658	314.2	15.4	189
0	78.7	1055	660	302.8	12	189.2

Table 9: Frick Coolware selection data for SGC 2313 at 55°F ammonia evaporation temperature and 130°F ammonia condensing temperature.

Slide valve [%]	Evaporator capacity [tons]	Condenser heat rejection [kBtu/hr]	Oil cooling load [kBtu/hr]	Compressor power [hp]	Evaporation capacity [%]	Discharge temperature [F]
100	686.5	9403	617	700.6	100	197.7
95	630.3	8619	624	659.5	91.8	196.4
90	574.7	7839	624	615.6	83.7	194.7
85	528.7	7194	620	577.6	77	193.1
80	484.9	6581	613	540.6	70.6	191.4
75	455.9	6180	603	516	66.4	190.5
70	428.1	5796	594	492.4	62.4	189.6
65	400.9	5420	585	469.4	58.4	188.7
60	373.8	5047	575	446.9	54.4	187.8
55	348.1	4694	566	425.8	50.7	187
50	322.6	4346	558	405.5	47	186.2
45	297.3	4000	550	385.8	43.3	185.4
40	272.2	3658	542	366.9	39.6	184.7
35	248.4	3335	535	349.7	36.2	184.1
30	224.8	3016	530	333.4	32.7	183.6
25	201.2	2698	526	317.9	29.3	183.2
20	177.6	2381	523	303.3	25.9	182.9
15	153.8	2062	521	289.6	22.4	182.9
10	130	1743	522	277	18.9	183
5	106.2	1425	526	265.6	15.5	183.4
0	82.4	1106	532	255.4	12	184.1

Table 10: Frick Cookware selection data for SGC 2313 at 55°F ammonia evaporation temperature and 120°F ammonia condensing temperature. ⁽⁶⁾

Slide valve [%]	Evaporator capacity [tons]	Condenser heat rejection [kBtu/hr]	Oil cooling load [kBtu/hr]	Compressor power [hp]	Evaporation capacity [%]	Discharge temperature [F]
100	720.1	9756	421	603.9	100	184.7
95	662.5	8964	430	567.9	92	183.8
90	604.9	8171	435	529.4	84	182.6
85	558.1	7526	436	497	77.5	181.3
80	511.3	6847	469	463.9	71	176.4
75	482.5	6455	463	443.5	67	175.8
70	453.7	6064	457	423.1	63	175.1
65	424.9	5673	451	402.9	59	174.3
60	396.1	5283	444	382.8	55	173.6
55	369.1	4918	438	364.4	51.3	172.9
50	342.1	4554	432	346.4	47.5	172.3
45	315	4190	427	328.8	43.8	171.7
40	288	3828	422	311.8	40	171.1
35	262.8	3490	418	296.6	36.5	170.7
30	237.6	3154	415	281.9	33	170.3
25	212.4	2819	412	268	29.5	170.1
20	187.2	2484	411	254.9	26	170
15	162	2150	411	242.6	22.5	170.1
10	136.8	1816	414	231.2	19	170.4
5	111.6	1483	418	220.8	15.5	171
0	86.4	1150	425	211.5	12	172

Table 11: Frick Cookware selection data for SGC 2313 at 55°F ammonia evaporation temperature and 110°F ammonia condensing temperature.

Slide valve [%]	Evaporator capacity [tons]	Condenser heat rejection [kBtu/hr]	Oil cooling load [kBtu/hr]	Compressor power [hp]	Evaporation capacity [%]	Discharge temperature [F]
100	749.2	9979	324	515.9	100	167.1
95	689.3	9161	335	481.5	92	165.5
90	629.3	8345	343	446.3	84	163.8
85	580.6	7684	346	417.5	77.5	162.3
80	531.9	7025	347	388.7	71	160.9
75	502	6624	343	371.1	67	160.3
70	472	6224	340	353.7	63	159.8
65	442	5825	336	336.4	59	159.2
60	412.1	5426	332	319.4	55	158.7
55	384	5052	328	303.7	51.3	158.2
50	355.9	4679	325	288.3	47.5	157.7
45	327.8	4307	321	273.3	43.8	157.3
40	299.7	3936	318	258.6	40	156.9
35	273.4	3589	316	245.3	36.5	156.6
30	247.2	3244	314	232.5	33	156.3
25	221	2900	312	220.1	29.5	156.1
20	194.8	2555	312	208.1	26	156.1
15	168.6	2212	312	196.7	22.5	156.1
10	142.3	1868	313	185.8	19	156.4
5	116.1	1525	315	175.5	15.5	156.8
0	89.9	1182	319	165.8	12	157.5

Table 12: Frick Cookware selection data for SGC 2313 at 55°F ammonia evaporation temperature and 100°F ammonia condensing temperature. ⁽⁶⁾

Slide valve [%]	Evaporator capacity [tons]	Condenser heat rejection [kBtu/hr]	Oil cooling load [kBtu/hr]	Compressor power [hp]	Evaporation capacity [%]	Discharge temperature [F]
100	772.2	10156	214	433.8	100	152.3
95	710.4	9321	231	403.5	92	150.5
90	648.7	8490	242	372.7	84	148.7
85	598.5	7817	248	347.5	77.5	147.2
80	548.3	7147	252	322.4	71	145.7
75	517.4	6740	249	307	67	145.2
70	486.5	6334	247	291.7	63	144.7
65	455.6	5928	244	276.6	59	144.2
60	424.7	5522	241	261	55	143.6
55	395.8	5142	238	247.7	51.3	143.1
50	366.8	4762	235	234	47.5	142.7
45	337.8	4383	232	220.5	43.8	142.2
40	308.9	4005	229	207.3	40	141.7
35	281.8	3652	227	195.2	36.5	141.3
30	254.8	3300	224	183.4	33	140.9
25	227.8	2949	222	171.9	29.5	140.5
20	200.8	2598	220	160.7	26	140.2
15	173.7	2248	219	149.8	22.5	140
10	146.7	1898	217	139.2	19	139.8
5	119.7	1548	217	129	15.5	139.8
0	92.7	1199	217	119.2	12	139.9

Table 13: Frick Cookware selection data for SGC 2313 at 55°F ammonia evaporation temperature and 90°F ammonia condensing temperature.

Slide valve [%]	Evaporator capacity [tons]	Condenser heat rejection [kBtu/hr]	Oil cooling load [kBtu/hr]	Compressor power [hp]	Evaporation capacity [%]	Discharge temperature [F]
100	794	10322	114	356.7	100	138.1
95	730.5	9466	142	330.8	92	135.6
90	667	8619	160	304.6	84	133.5
85	615.4	7936	169	283.2	77.5	131.9
80	563.8	7255	176	261.8	71	130.3
75	532	6843	174	248.7	67	129.9
70	500.2	6431	172	235.7	63	129.5
65	468.5	6019	170	22.8	59	129
60	436.7	5607	168	209.9	55	128.5
55	406.9	5221	165	197.9	51.3	128
50	377.2	4836	163	186.1	47.5	127.5
45	347.4	4451	161	174.4	43.8	127
40	317.6	4067	159	162.8	40	126.5
35	289.8	3708	156	152.2	36.5	126
30	262	3351	154	141.7	33	125.5
25	234.2	2993	152	131.4	29.5	125
20	206.4	2637	149	121.3	26	124.5
15	178.7	2280	147	111.4	22.5	124
10	150.9	1924	145	101.6	19	123.6
5	123.1	1569	143	92.1	15.5	123.1
0	95.3	1214	140	82.9	12	122.7

Table 14: Frick Cookware selection data for SGC 2313 at 55°F ammonia evaporation temperature and 80°F ammonia condensing temperature. ^[08]

Slide valve [%]	Evaporator capacity [tons]	Condenser heat rejection [kBtu/hr]	Oil cooling load [kBtu/hr]	Compressor power [hp]	Evaporation capacity [%]	Discharge temperature [F]
100	815.4	10462	13	270.9	100	122.5
95	750.2	9592	48	250.6	92	119.7
90	685	8721	84	230.1	84	116.4
85	632	8028	99	213.4	77.5	114.6
80	579	7340	108	196.7	71	113
75	546.3	6923	107	186.4	67	112.7
70	513.7	6507	106	176.2	63	112.4
65	481.1	6092	105	166.1	59	112
60	448.5	5675	103	155.9	55	111.6
55	417.9	5286	102	146.5	51.3	111.2
50	387.3	4896	101	137.1	47.5	110.8
45	356.8	4507	99	127.8	43.8	110.4
40	326.2	4118	98	118.6	40	109.9
35	297.6	3755	96	110	36.5	109.4
30	269.1	3393	94	101.5	33	108.9
25	240.6	3031	92	93.2	29.5	108.4
20	212	2670	91	84.9	26	107.8
15	183.5	2308	88	76.7	22.5	107.2
10	154.9	1948	86	68.6	19	106.6
5	126.4	1587	84	60.6	15.5	105.8
0	97.9	1228	81	52.8	12	105.1

APPENDIX B Daily Hot Water Needs of Facility

Table 15: Load profile of hot water need at subject plant.

Time [min]	Load [gal/min]	Time [min]	Load [gal/min]	Time [min]	Load [gal/min]	Time [min]	Load [gal/min]	Time [min]	Load [gal/min]	Time [min]	Load [gal/min]
10	175	250	101	490	114	730	131	970	410	1210	87
20	110	260	165	500	148	740	146	980	410	1220	190
30	119	270	143	510	102	750	161	990	410	1230	128
40	110	280	141	520	174	760	160	1000	410	1240	80
50	143	290	106	530	124	770	126	1010	410	1250	139
60	101	300	107	540	103	780	161	1020	410	1260	185
70	156	310	162	550	143	790	136	1030	410	1270	187
80	106	320	119	560	167	800	183	1040	410	1280	190
90	123	330	105	570	133	810	164	1050	410	1290	187
100	152	340	175	580	117	820	131	1060	410	1300	188
110	158	350	184	590	144	830	112	1070	405	1310	141
120	133	360	109	600	139	840	154	1080	400	1320	118
130	123	370	178	610	136	850	109	1090	151	1330	173
140	156	380	168	620	112	860	161	1100	157	1340	99
150	149	390	160	630	105	870	186	1110	112	1350	189
160	151	400	129	640	142	880	147	1120	142	1360	89
170	187	410	146	650	136	890	163	1130	144	1370	82
180	138	420	111	660	142	900	400	1140	94	1380	190
190	161	430	125	670	187	910	405	1150	126	1390	189
200	116	440	153	680	104	920	410	1160	160	1400	170
210	138	450	131	690	100	930	410	1170	87	1410	172
220	151	460	179	700	120	940	410	1180	146	1420	120
230	171	470	145	710	144	950	410	1190	94	1430	87
240	119	480	124	720	137	960	410	1200	88	1440	113

APPENDIX C TRNSYS RESULTS RAW DATA

Table 16: TRNSYS raw data: 1 Heat Pump, no storage Compressor Power and Condenser heat rejection.

Time [hours]	Compressor power consumed[btu]	Condenser heat rejection[btu]	Time [hours]	Compressor power consumed[btu]	Condenser heat rejection[btu]
0.17	2185828.73	7391885.85	6.17	1987304.44	6336238.29
0.33	2244946.86	7687845.03	6.33	2202570.87	7476580.04
0.50	1987304.44	6336238.29	6.50	1770148.73	5026834.05
0.67	1871052.45	5660179.51	6.67	2064293.93	6758160.04
0.83	1732015.42	4772894.23	6.83	2010064.09	6463134.17
1.00	1738288.08	4815679.84	7.00	2120129.46	7054062.78
1.17	2040860.85	6631871.50	7.17	1725787.25	4730574.00
1.33	2072186.38	6800903.69	7.33	1942688.65	6082554.34
1.50	2253517.74	7730261.95	7.50	1677295.36	4392999.76
1.67	2279387.15	7856751.16	7.67	2072186.38	6800903.69
1.83	2128242.77	7096680.84	7.83	1783140.49	5111042.24
2.00	1732015.42	4772894.23	8.00	1906430.16	5870775.27
2.17	2104011.65	6969324.43	8.17	2010064.09	6463134.17
2.33	1822979.18	5364118.81	8.33	2104011.65	6969324.43
2.50	1653935.96	4224114.24	8.50	2270738.01	7814708.55
2.67	1695198.36	4519240.46	8.67	1725787.25	4730574.00
2.83	2270738.01	7814708.55	8.83	2010064.09	6463134.17
3.00	1665545.10	4308839.95	9.00	2048643.57	6674141.19
3.17	1829748.60	5406615.43	9.17	1942688.65	6082554.34
3.33	2227911.53	7603546.91	9.33	1713451.39	4646677.60
3.50	2227911.53	7603546.91	9.50	1950047.49	6125148.77
3.67	1913617.92	5913330.56	9.67	2072186.38	6800903.69
3.83	1725787.25	4730574.00	9.83	1836560.19	5449478.54
4.00	2270738.01	7814708.55	10.00	1659718.27	4266219.05
4.17	1864067.14	5617391.12	10.17	2244946.86	7687845.03
4.33	2314297.68	8025531.22	10.33	2227911.53	7603546.91
4.50	2253517.74	7730261.95	10.50	1994838.15	6377697.03
4.67	2056454.64	6716225.18	10.67	1987304.44	6336238.29
4.83	2244946.86	7687845.03	10.83	1964853.31	6209748.81
5.00	1964853.31	6209748.81	11.00	2136357.71	7138201.73
5.17	1659718.27	4266219.05	11.17	2169220.97	7307571.10
5.33	1689198.73	4477495.78	11.33	1892189.28	5787197.41
5.50	1892189.28	5787197.41	11.50	2210982.10	7518724.80
5.67	2120129.46	7054062.78	11.67	2048643.57	6674141.19
5.83	2112069.51	7012257.35	11.83	1671404.16	4351099.78
6.00	1957412.35	6166487.89	12.00	2236402.32	7645307.46

Table 17: TRNSYS raw data: 1 Heat Pump, no storage Compressor Power and Condenser heat rejection.

Time [hours]	Compressor power consumed[btu]	Condenser heat rejection[btu]	Time [hours]	Compressor power consumed[btu]	Condenser heat rejection[btu]
12.17	1750914.78	4899597.70	18.17	2033106.60	6589450.14
12.33	1836560.19	5449478.54	18.33	2314297.68	8025531.22
12.50	1950047.49	6125148.77	18.50	2136357.71	7138201.73
12.67	1653935.96	4224114.24	18.67	2288062.11	7898682.46
12.83	1789689.59	5153119.14	18.83	1770148.73	5026834.05
13.00	2120129.46	7054062.78	19.00	1843380.62	5490957.38
13.17	2244946.86	7687845.03	19.17	2002424.63	6420004.57
13.33	2236402.32	7645307.46	19.33	1757294.81	4942293.80
13.50	1732015.42	4772894.23	19.50	2160970.85	7265684.14
13.67	1763692.94	4983918.79	19.67	1625571.15	4012340.07
13.83	1829748.60	5406615.43	19.83	1546223.16	3379480.00
14.00	1789689.59	5153119.14	20.00	2112069.51	7012257.35
14.17	1899294.83	5829084.80	20.17	1707330.99	4604244.15
14.33	2314297.68	8025531.22	20.33	2048643.57	6674141.19
14.50	2088030.54	6884942.32	20.50	1789689.59	5153119.14
14.67	2305517.38	7983069.93	20.67	2144525.99	7180525.54
14.83	1732015.42	4772894.23	20.83	1994838.15	6377697.03
15.00	4573308.11	16895865.62	21.00	2210982.10	7518724.80
15.17	4629818.25	17107240.58	21.17	2080081.88	6842511.99
15.33	4685978.55	17318201.61	21.33	1546223.16	3379480.00
15.50	4685978.55	17318201.61	21.50	1750914.78	4899597.70
15.67	4685978.55	17318201.61	21.67	2033106.60	6589450.14
15.83	4685978.55	17318201.61	21.83	2296791.03	7941385.09
16.00	4685978.55	17318201.61	22.00	2048643.57	6674141.19
16.17	4685978.55	17318201.61	22.17	1796283.13	5195676.81
16.33	4685978.55	17318201.61	22.33	1857156.04	5575445.38
16.50	4685978.55	17318201.61	22.50	1582172.29	3674464.34
16.67	4685978.55	17318201.61	22.67	1913617.92	5913330.56
16.83	4685978.55	17318201.61	22.83	1950047.49	6125148.77
17.00	4685978.55	17318201.61	23.00	2033106.60	6589450.14
17.17	4685978.55	17318201.61	23.17	1964853.31	6209748.81
17.33	4685978.55	17318201.61	23.33	2219419.94	7560735.31
17.50	4685978.55	17318201.61	23.50	1935359.33	6039756.94
17.67	4685978.55	17318201.61	23.67	1603573.65	3843985.42
17.83	4629818.25	17107240.58	23.83	1642480.53	4139671.72
18.00	4573308.11	16895865.62	24.00	2194186.38	7434298.28

Table 18: TRNSYS raw data: 1 Heat Pump, no storage. Condenser saturation temperature and compressor discharge temperature.

Time [hours]	Condenser Saturation Temperature [F]	Compressor Discharge Temperature [F]	Time [hours]	Condenser Saturation Temperature [F]	Compressor Discharge Temperature [F]
0.17	137.38	191.48	6.17	136.31	189.41
0.33	137.69	192.10	6.33	137.46	191.66
0.50	136.31	189.41	6.50	135.13	187.14
0.67	135.68	188.19	6.67	136.73	190.21
0.83	134.92	186.74	6.83	136.44	189.65
1.00	134.96	186.81	7.00	137.03	190.80
1.17	136.60	189.97	7.17	134.89	186.67
1.33	136.77	190.30	7.33	136.07	188.94
1.50	137.73	192.19	7.50	134.62	186.17
1.67	137.87	192.46	7.67	136.77	190.30
1.83	137.07	190.88	7.83	135.20	187.27
2.00	134.92	186.74	8.00	135.87	188.56
2.17	136.94	190.63	8.17	136.44	189.65
2.33	135.42	187.69	8.33	136.94	190.63
2.50	134.50	185.92	8.50	137.82	192.37
2.67	134.72	186.35	8.67	134.89	186.67
2.83	137.82	192.37	8.83	136.44	189.65
3.00	134.56	186.05	9.00	136.64	190.05
3.17	135.46	187.76	9.17	136.07	188.94
3.33	137.60	191.93	9.33	134.82	186.55
3.50	137.60	191.93	9.50	136.11	189.02
3.67	135.91	188.64	9.67	136.77	190.30
3.83	134.89	186.67	9.83	135.49	187.83
4.00	137.82	192.37	10.00	134.53	185.98
4.17	135.64	188.12	10.17	137.69	192.10
4.33	138.05	192.83	10.33	137.60	191.93
4.50	137.73	192.19	10.50	136.35	189.49
4.67	136.68	190.13	10.67	136.31	189.41
4.83	137.69	192.10	10.83	136.19	189.17
5.00	136.19	189.17	11.00	137.11	190.97
5.17	134.53	185.98	11.17	137.29	191.31
5.33	134.69	186.29	11.33	135.80	188.41
5.50	135.80	188.41	11.50	137.51	191.75
5.67	137.03	190.80	11.67	136.64	190.05
5.83	136.98	190.71	11.83	134.59	186.11
6.00	136.15	189.10	12.00	137.64	192.01

Table 19: TRNSYS raw data: 1 Heat Pump, no storage. Condenser saturation temperature and compressor discharge temperature.

Time [hours]	Condenser Saturation Temperature [F]	Compressor Discharge Temperature [F]	Time [hours]	Condenser Saturation Temperature [F]	Compressor Discharge Temperature [F]
12.17	135.03	186.94	18.17	136.56	189.89
12.33	135.49	187.83	18.33	138.05	192.83
12.50	136.11	189.02	18.50	137.11	190.97
12.67	134.50	185.92	18.67	137.91	192.55
12.83	135.24	187.34	18.83	135.13	187.14
13.00	137.03	190.80	19.00	135.53	187.90
13.17	137.69	192.10	19.17	136.39	189.57
13.33	137.64	192.01	19.33	135.06	187.00
13.50	134.92	186.74	19.50	137.24	191.22
13.67	135.10	187.07	19.67	134.34	185.63
13.83	135.46	187.76	19.83	133.92	184.80
14.00	135.24	187.34	20.00	136.98	190.71
14.17	135.83	188.49	20.17	134.79	186.48
14.33	138.05	192.83	20.33	136.64	190.05
14.50	136.85	190.46	20.50	135.24	187.34
14.67	138.01	192.74	20.67	137.16	191.05
14.83	134.92	186.74	20.83	136.35	189.49
15.00	149.24	218.39	21.00	137.51	191.75
15.17	149.53	219.14	21.17	136.81	190.38
15.33	149.82	219.90	21.33	133.92	184.80
15.50	149.82	219.90	21.50	135.03	186.94
15.67	149.82	219.90	21.67	136.56	189.89
15.83	149.82	219.90	21.83	137.96	192.65
16.00	149.82	219.90	22.00	136.64	190.05
16.17	149.82	219.90	22.17	135.27	187.41
16.33	149.82	219.90	22.33	135.61	188.05
16.50	149.82	219.90	22.50	134.11	185.17
16.67	149.82	219.90	22.67	135.91	188.64
16.83	149.82	219.90	22.83	136.11	189.02
17.00	149.82	219.90	23.00	136.56	189.89
17.17	149.82	219.90	23.17	136.19	189.17
17.33	149.82	219.90	23.33	137.55	191.84
17.50	149.82	219.90	23.50	136.03	188.87
17.67	149.82	219.90	23.67	134.22	185.40
17.83	149.53	219.14	23.83	134.43	185.80
18.00	149.24	218.39	24.00	137.42	191.57

Table 20: TRNSYS raw data: 1 Heat Pump, no storage. PLF.

Time [hours]	PLF	Time [hours]	PLF	Time [hours]	PLF	Time [hours]	PLF
0.17	0.41	6.17	0.35	12.17	0.27	18.17	0.37
0.33	0.43	6.33	0.42	12.33	0.30	18.33	0.45
0.50	0.35	6.50	0.28	12.50	0.34	18.50	0.40
0.67	0.31	6.67	0.37	12.67	0.23	18.67	0.44
0.83	0.26	6.83	0.36	12.83	0.28	18.83	0.28
1.00	0.27	7.00	0.39	13.00	0.39	19.00	0.30
1.17	0.37	7.17	0.26	13.17	0.43	19.17	0.36
1.33	0.38	7.33	0.34	13.33	0.43	19.33	0.27
1.50	0.43	7.50	0.24	13.50	0.26	19.50	0.40
1.67	0.44	7.67	0.38	13.67	0.28	19.67	0.22
1.83	0.39	7.83	0.28	13.83	0.30	19.83	0.19
2.00	0.26	8.00	0.32	14.00	0.28	20.00	0.39
2.17	0.39	8.17	0.36	14.17	0.32	20.17	0.25
2.33	0.30	8.33	0.39	14.33	0.45	20.33	0.37
2.50	0.23	8.50	0.43	14.50	0.38	20.50	0.28
2.67	0.25	8.67	0.26	14.67	0.44	20.67	0.40
2.83	0.43	8.83	0.36	14.83	0.26	20.83	0.35
3.00	0.24	9.00	0.37	15.00	0.97	21.00	0.42
3.17	0.30	9.17	0.34	15.17	0.98	21.17	0.38
3.33	0.42	9.33	0.26	15.33	0.99	21.33	0.19
3.50	0.42	9.50	0.34	15.50	0.99	21.50	0.27
3.67	0.33	9.67	0.38	15.67	0.99	21.67	0.37
3.83	0.26	9.83	0.30	15.83	0.99	21.83	0.44
4.00	0.43	10.00	0.24	16.00	0.99	22.00	0.37
4.17	0.31	10.17	0.43	16.17	0.99	22.17	0.29
4.33	0.45	10.33	0.42	16.33	0.99	22.33	0.31
4.50	0.43	10.50	0.35	16.50	0.99	22.50	0.20
4.67	0.37	10.67	0.35	16.67	0.99	22.67	0.33
4.83	0.43	10.83	0.34	16.83	0.99	22.83	0.34
5.00	0.34	11.00	0.40	17.00	0.99	23.00	0.37
5.17	0.24	11.17	0.41	17.17	0.99	23.17	0.34
5.33	0.25	11.33	0.32	17.33	0.99	23.33	0.42
5.50	0.32	11.50	0.42	17.50	0.99	23.50	0.33
5.67	0.39	11.67	0.37	17.67	0.99	23.67	0.21
5.83	0.39	11.83	0.24	17.83	0.98	23.83	0.23
6.00	0.34	12.00	0.43	18.00	0.97	24.00	0.41

Table 21: TRNSYS raw data: 2 Heat Pumps, no storage Compressor Power and Condenser heat rejection. Low-pressure stage

Time [hours]	Condenser heat rejection[btu]	Compressor power consumed[btu]	Time [hours]	Condenser heat rejection[btu]	Compressor power consumed[btu]
0.17	3044198.70	379356.65	6.17	2609032.72	343592.15
0.33	3166132.34	389913.29	6.33	3078942.65	382348.80
0.50	2609032.72	343592.15	6.50	2069783.04	303879.36
0.67	2330793.43	322416.82	6.67	2783368.60	357524.29
0.83	1965562.45	296839.86	6.83	2661516.26	347719.65
1.00	1983000.59	297998.26	7.00	2905116.91	367576.78
1.17	2730967.98	353289.77	7.17	1948044.32	295687.14
1.33	2800317.45	358941.87	7.33	2505177.73	335491.42
1.50	3183083.50	391434.51	7.50	1809193.13	286697.98
1.67	3235269.35	396040.16	7.67	2800317.45	358941.87
1.83	2922428.34	369032.12	7.83	2105054.26	306278.04
2.00	1965562.45	296839.86	8.00	2417777.41	328882.10
2.17	2870363.68	364679.87	8.17	2661516.26	347719.65
2.33	2208969.83	313602.08	8.33	2870363.68	364679.87
2.50	1739503.37	282351.65	8.50	3217950.00	394500.77
2.67	1861394.31	290022.37	8.67	1948044.32	295687.14
2.83	3217950.00	394500.77	8.83	2661516.26	347719.65
3.00	1774292.78	284510.97	9.00	2748596.04	354698.20
3.17	2226665.00	314847.14	9.17	2505177.73	335491.42
3.33	3131005.36	386872.39	9.33	1913488.45	293403.14
3.50	3131005.36	386872.39	9.50	2522171.89	336825.71
3.67	2435486.53	330195.56	9.67	2800317.45	358941.87
3.83	1948044.32	295687.14	9.83	2243875.34	316093.07
4.00	3217950.00	394500.77	10.00	1756634.37	283426.30
4.17	2313696.65	321144.20	10.17	3166132.34	389913.29
4.33	3305070.21	402244.62	10.33	3131005.36	386872.39
4.50	3183083.50	391434.51	10.50	2626446.65	344961.39
4.67	2765729.40	356106.30	10.67	2609032.72	343592.15
4.83	3166132.34	389913.29	10.83	2557221.18	339519.21
5.00	2557221.18	339519.21	11.00	2939791.46	370492.01
5.17	1756634.37	283426.30	11.17	3009288.34	376382.11
5.33	1844100.06	288908.42	11.33	2383003.79	326280.28
5.50	2383003.79	326280.28	11.50	3096542.57	383854.18
5.67	2905116.91	367576.78	11.67	2748596.04	354698.20
5.83	2887657.03	366126.02	11.83	1791820.55	285601.53
6.00	2539800.80	338169.93	12.00	3148602.79	388390.71

Table 22: TRNSYS raw data: 2 Heat Pumps, no storage Compressor Power and Condenser heat rejection-Low-pressure stage

Time [hours]	Condenser heat rejection[btu]	Compressor power consumed[btu]	Time [hours]	Condenser heat rejection[btu]	Compressor power consumed[btu]
12.17	2017690.44	300332.08	18.17	2713774.56	351891.25
12.33	2243875.34	316093.07	18.33	3305070.21	402244.62
12.50	2522171.89	336825.71	18.50	2939791.46	370492.01
12.67	1739503.37	282351.65	18.67	3252728.14	397583.69
12.83	2122013.24	307481.26	18.83	2069783.04	303879.36
13.00	2905116.91	367576.78	19.00	2261581.90	317348.96
13.17	3166132.34	389913.29	19.17	2643860.58	346335.56
13.33	3148602.79	388390.71	19.33	2035524.64	301511.80
13.50	1965562.45	296839.86	19.50	2992161.07	374904.21
13.67	2052596.60	302692.79	19.67	1650447.18	277051.39
13.83	2226665.00	314847.14	19.83	1391682.97	261735.46
14.00	2122013.24	307481.26	20.00	2887657.03	366126.02
14.17	2400313.06	327578.59	20.17	1895920.46	292267.63
14.33	3305070.21	402244.62	20.33	2748596.04	354698.20
14.50	2835441.25	361801.51	20.50	2122013.24	307481.26
14.67	3287475.57	400683.06	20.67	2957115.50	371956.45
14.83	1965562.45	296839.86	20.83	2626446.65	344961.39
15.00	6958108.96	777781.48	21.00	3096542.57	383854.18
15.17	7045004.91	786584.46	21.17	2817978.48	360369.34
15.33	7132036.57	795313.65	21.33	1391682.97	261735.46
15.50	7132036.57	795313.65	21.50	2017690.44	300332.08
15.67	7132036.57	795313.65	21.67	2713774.56	351891.25
15.83	7132036.57	795313.65	21.83	3270109.78	399131.33
16.00	7132036.57	795313.65	22.00	2748596.04	354698.20
16.17	7132036.57	795313.65	22.17	2139449.61	308694.45
16.33	7132036.57	795313.65	22.33	2296328.45	319872.24
16.50	7132036.57	795313.65	22.50	1513401.81	268676.79
16.67	7132036.57	795313.65	22.67	2435486.53	330195.56
16.83	7132036.57	795313.65	22.83	2522171.89	336825.71
17.00	7132036.57	795313.65	23.00	2713774.56	351891.25
17.17	7132036.57	795313.65	23.17	2557221.18	339519.21
17.33	7132036.57	795313.65	23.33	3113571.13	385358.37
17.50	7132036.57	795313.65	23.50	2487519.69	334157.36
17.67	7132036.57	795313.65	23.67	1582933.39	272785.84
17.83	7045004.91	786584.46	23.83	1704445.20	280216.03
18.00	6958108.96	777781.48	24.00	3061322.13	380847.80

Table 23: TRNSYS raw data: 2 Heat Pumps, no storage Compressor Power and Condenser heat rejection. High-pressure stage.

Time [hours]	Condenser heat rejection[btu]	Compressor power consumed[btu]	Time [hours]	Condenser heat rejection[btu]	Compressor power consumed[btu]
0.17	4347999.50	1329174.13	6.17	3737735.64	1209460.30
0.33	4521532.88	1364403.68	6.33	4397342.70	1339154.11
0.50	3737735.64	1209460.30	6.50	2956474.25	1077880.58
0.67	3328903.37	1139071.39	6.67	3975336.38	1256404.84
0.83	2807252.90	1054597.15	6.83	3801209.53	1223774.26
1.00	2832270.18	1058427.09	7.00	4149067.51	1289885.13
1.17	3900832.40	1242315.48	7.17	2782923.83	1050796.56
1.33	3999924.64	1261129.06	7.33	3577604.96	1182358.19
1.50	4546631.84	1369502.89	7.50	2583706.19	1021091.38
1.67	4620926.83	1384886.29	7.67	3999924.64	1261129.06
1.83	4173795.47	1294732.53	7.83	3006040.09	1085805.59
2.00	2807252.90	1054597.15	8.00	3453315.95	1160480.38
2.17	4099142.87	1280223.65	8.17	3801209.53	1223774.26
2.33	3154994.15	1110066.57	8.33	4099142.87	1280223.65
2.50	2484478.68	1006759.71	8.50	4596184.53	1379744.28
2.67	2658123.49	1032069.71	8.67	2782923.83	1050796.56
2.83	4596184.53	1379744.28	8.83	3801209.53	1223774.26
3.00	2534338.99	1013886.38	9.00	3925630.36	1246991.52
3.17	3180275.25	1114188.78	9.17	3577604.96	1182358.19
3.33	4472229.26	1354262.88	9.33	2733043.23	1043242.15
3.50	4472229.26	1354262.88	9.50	3602237.08	1186789.84
3.67	3478449.11	1164826.23	9.67	3999924.64	1261129.06
3.83	2782923.83	1050796.56	9.83	3204860.01	1118149.82
4.00	4596184.53	1379744.28	10.00	2509053.48	1010308.31
4.17	3304409.49	1134853.81	10.17	4521532.88	1364403.68
4.33	4720556.48	1405624.01	10.33	4472229.26	1354262.88
4.50	4546631.84	1369502.89	10.50	3773076.96	1214217.26
4.67	3950267.61	1251683.68	10.67	3737735.64	1209460.30
4.83	4521532.88	1364403.68	10.83	3652231.77	1195716.08
5.00	3652231.77	1195716.08	11.00	4198887.10	1299608.83
5.17	2509053.48	1010308.31	11.17	4298304.65	1319253.89
5.33	2633738.07	1028394.23	11.33	3403751.84	1151864.30
5.50	3403751.84	1151864.30	11.50	4422511.96	1344180.32
5.67	4149067.51	1289885.13	11.67	3925630.36	1246991.52
5.83	4124443.39	1285053.23	11.83	2558754.99	1017474.17
6.00	3627548.69	1191250.57	12.00	4496636.67	1359318.93

Table 24: TRNSYS raw data: 2 Heat Pumps, no storage Compressor Power and Condenser heat rejection. High-pressure stage

Time [hours]	Condenser heat rejection[btu]	Compressor power consumed[btu]	Time [hours]	Condenser heat rejection[btu]	Compressor power consumed[btu]
12.17	2881628.78	1066143.68	18.17	3875986.22	1237655.66
12.33	3204860.01	1118149.82	18.33	4720556.48	1405624.01
12.50	3602237.08	1186789.84	18.50	4198887.10	1299608.83
12.67	2484478.68	1006759.71	18.67	4645653.92	1390042.40
12.83	3031335.55	1089806.73	18.83	2956474.25	1077880.58
13.00	4149067.51	1289885.13	19.00	3229659.14	1122296.17
13.17	4521532.88	1364403.68	19.17	3766335.60	1218980.30
13.33	4496636.67	1359318.93	19.33	2907060.67	1070040.77
13.50	2807252.90	1054597.15	19.50	4273432.55	1314316.38
13.67	2931390.12	1073946.02	19.67	2360364.42	989332.61
13.83	3180275.25	1114188.78	19.83	1987882.07	940402.06
14.00	3031335.55	1089806.73	20.00	4124443.39	1285053.23
14.17	3428509.70	1156163.65	20.17	2708267.56	1039498.77
14.33	4720556.48	1405624.01	20.33	3925630.36	1246991.52
14.50	4049891.83	1270651.32	20.50	3031335.55	1089806.73
14.67	4695406.11	1400411.28	20.67	4223307.97	1304487.02
14.83	2807252.90	1054597.15	20.83	3773076.96	1214217.26
15.00	9937561.67	2678042.17	21.00	4422511.96	1344180.32
15.17	10062237.15	2708178.80	21.17	4024962.85	1265882.24
15.33	10186156.45	2738016.39	21.33	1987882.07	940402.06
15.50	10186156.45	2738016.39	21.50	2881628.78	1066143.68
15.67	10186156.45	2738016.39	21.67	3875986.22	1237655.66
15.83	10186156.45	2738016.39	21.83	4670838.14	1395227.19
16.00	10186156.45	2738016.39	22.00	3925630.36	1246991.52
16.17	10186156.45	2738016.39	22.17	3055948.11	1093815.50
16.33	10186156.45	2738016.39	22.33	3279182.26	1130642.54
16.50	10186156.45	2738016.39	22.50	2161500.94	962602.53
16.67	10186156.45	2738016.39	22.67	3478449.11	1164826.23
16.83	10186156.45	2738016.39	22.83	3602237.08	1186789.84
17.00	10186156.45	2738016.39	23.00	3875986.22	1237655.66
17.17	10186156.45	2738016.39	23.17	3652231.77	1195716.08
17.33	10186156.45	2738016.39	23.33	4447138.97	1349207.22
17.50	10186156.45	2738016.39	23.50	3552821.76	1177943.57
17.67	10186156.45	2738016.39	23.67	2260458.75	975782.68
17.83	10062237.15	2708178.80	23.83	2434693.86	999721.66
18.00	9937561.67	2678042.17	24.00	4372544.13	1334156.70